UNIVERSITY OF CALIFORNIA, SAN DIEGO

Synthesis of Archaeal-type Lipids and Archaeal-inspired Liposomes

A thesis submitted in partial satisfaction of the requirements for the degree Doctor of Philosophy

in

Chemistry

by Steven Nguyen

Committee in Charge:

Professor Nathan Gianneschi, Chair
Professor Karen Christman
Professor Seth Cohen
Professor Thomas Herman
Professor Emmanuel Theodorakis

2016

The Dissertation of Steven Nguyen is approved, and it is acceptable in quality and form for publication on microfilm and electronically:

Chair

University of California, San Diego

2016

DEDICATION

I dedicate this thesis to my family.

Nguyễn Văn Bằng, Father

Bùi Ngăn Thuần, Mother

Ng Anh Vi, Sister

Ng Michael, Brother-in-law

Ng Emma, Niece

Ng Tyler, Nephew

Nguyễn Vũ Anthony, Brother

Nguyễn Huyền Michelle, Sister-in-law

Nguyễn Duy Nixon, Nephew

Nguyễn Hiếu Hudson, Nephew

Nguyễn Roman, Nephew

EPIGRAPH

"If you lack everything or have lost everything
but still have the Blessed Sacrament, you actually still have everything."

Đức Hồng Y Phanxicô Xaviê Nguyễn Văn Thuận

TABLE OF CONTENTS

LIST OF ABBREVIATIONS

General:

µM	micromolar
µm	micrometer
µL	microliter
^{13}C NMR	carbon-13 nuclear magnetic resonance
CD_2Cl_2	deuterated dichloromethane
CD_3OD	deuterated methanol
DCM	dichloromethane
DLS	dynamic light scattering
DMF	dimethylformamide
DMSO	dimethyl sulfoxide
DNA	deoxyribose nucleic acid
ES-MS	electrospray mass spectrometry
EtOAc	ethyl acetate
g	grams
^{1}H NMR	proton nuclear magnetic resonance
H_2O	water
H_3PO_4	phosphoric acid
HCl	hydrochloric acid
HR-MS	high resolution mass spectrometry
Hz	Hertz
MMPs	matrix metallproteinases
M	molar
MeOH	methanol
mg	milligrams
$MgSO_4$	magnesium sulfate
min	minutes
mL	millileters
mmole	millimoles
m/z	mass per unit charge
$NaHCO_3$	sodium bicarbonate
nM	nanomolar
NMR	nuclear magnetic resonance spectroscopy
PBS	phosphate-buffered saline
PEG	polyethylene glycol
ppm	parts per million
RNA	ribonucleic acid
TEM	transmission electron microscopy
THF	tetrahydrofurane
TLC	thin layer chromatography

For nuclear magnetic resonance spectroscopy:

δ	nuclear magnetic resonance chemical shift in ppm
bs	broad singlet
d	doublet
dd	doublet of doublet

m	multiplet
s	singlet
t	triplet

LIST OF FIGURES

LIST OF TABLES

ACKNOWLEDGEMENTS

I would like to acknowledge my advisor, Professor Nathan Gianneschi, for his support of my graduate studies these long six years. With a biochemistry background and very little chemistry experience, Nathan believed in me and accepted me as a master's student. From the beginning, Nathan was extremely supportive of my goal of becoming a Lecturer at a university. His compassion and understanding has been the backbone towards me being able to achieve my dream.

I would also like to thank my committee members, Professor Emmanuel Theodorakis, Professor Thomas Hermann, Professor Seth Cohen, and Professor Karen Christman for their guidance and support.

I would like to thank the members of the Gianneschi research group both past and present: Lisa Adamiak, Kelsey Alexander, Sarah Barnhill, Nia Bell, Angela Blum, Alex Caldwell, Cassi Callmann, Andrea Carlini, Miao-Ping Chen, Wonmin Choi, Naneki Collins-McCallum, Dustin Crystal, Treffly Ditri, Michael Hahn, Ziying Hu, Yuran Huan, Carrie James, Lizanne Koch, Ti-Hsuan Ku, Joo Hee Lee, Clare LeGuyadar, Kevin Luo, Andrea Luthi, Julia Michaelis, Ben Monson, Lucas Parent, Billy Pistel, Maria Proetto, Lyndsay Randolph, Alexander Roloff, Anthony Rush, Swagat Sahu, Alfred Tam, Matthew Thompson, Mollie Touve, Kate Veccharelli, Zhao Wang, Daniel Wright, Xiujun Yue, and Nanzhi Zang. I would especially like to thank Matthew Thompson for literally everything.

Specifically, I would like to thank my closest friends in the lab for putting up with my rambunctiousness everyday: Lisa Adamiak, Jacqueline Kammeyer, and Sarah Barnhill.

Lastly, I would like to thank my family. Thank you to my parents, Nguyen Van Ban & Bui Ngan Thuan, my brother and his family, and sister and her family.

VITA

2010	Bachelor of Science, University of California, San Diego
2012	Master of Science, University of California, San Diego
2016	Doctor of Philosophy, University of California, San Diego

PUBLICATIONS

Y. V. Shih, Y. Hwang, A. Phadke, H. Kang, N. S. Hwang, E. J. Caro, S. Nguyen, M. Siu, E. Theodorakis, N. C. Gianneschi*, K. S. Vecchio, S. Chien, O. K. Lee and S. Varghese. “Calcium-Phosphate Bearing Matrices induce Osteogenic Differentiation of Stem Cells through Adenosine Signaling.” Proceedings of the National Academy of Sciences, 2014, 3, 990-995.

ABSTRACT OF THE DISSERTATION

Synthesis of Archaeal-type Lipids and Archaea-inspired Liposomes

by

Steven Nguyen

Doctor of Philosophy in Chemistry

University of California, San Diego 2016

Professor Nathan Gianneschi, Chair

Since the discovery of liposomes in the 1960s, lipid-based materials have played a significant role in the development of nanotechnology. Present applications of liposomes range from cosmetics, food, drug formulation, adjuvant carriers, to gene therapy. However, specifically within drug delivery applications, there are major deficiencies concerning the stability of agent carriers with respect to drug loading, controlled release, overcoming biological barriers, and efficient active targeting. Consequently, there is a serious need for the development of stable materials towards improving the delivery of therapeutics. Herein, we

present a strategy for the preparation of robust and stable lipid materials capable of encapsulating small molecules and assembling into well-defined structures as a potential therapeutic delivery system. These systems aim to address the key issues of high permeability of membranes and the subsequent release of encapsulated cargo. Taking inspiration from Archaea organisms, in their ability to withstand extreme environments, archaea-type lipids were synthesized towards generating archaeosomes as an alternative and improved approach for the encapsulation and release of small molecule cargo. These biomimetic materials may potentially serve as stabilizing agents, drug storage, and drug carriers in therapeutics

Chapter 1 : Introduction

1.1 General Overview

In the development of nanomedicine for *in vivo* drug delivery applications, the pharmacokinetics must be taken into account if such materials are to be translatable for clinical use[1–4]. Therapeutic agents should be designed with regard for the safe distribution, metabolism, and therapeutic management of drugs within cancerous or diseased tissues[1,2,5]. Designing materials without such concern can lead to serious problems. Specifically, the inability to deliver effective drug concentrations to diseased tissues for therapeutic value is a main concern[2,5–8]. Additionally, drug-loaded vehicles are unable to selectively target specific sites and cannot accumulate drug at the desired location[9]. Even in cases where drug concentrations are sufficient, the drug is neither bioavailable nor readily accessible[4,6,10]. The bioavailability of the drug is dependent upon the adequate release from the carrier. Drug delivery systems suffer from passive leakage and the inability to release its payload in controlled fashion. An ideal delivery system has a sustained drug release profile that is aligned with the therapeutic window for the drug activity.

To address the many issues towards nanomaterials for treating cancer and diseased tissues, liposomes have long been recognized as the excellent drug-delivery vehicles and are prevalent among clinical applications[6,8,11–14]. The strong interest for liposomal use as a valid platform for drug delivery is attributed to their ability to enhance the pharmacokinetics[1]. Specifically, liposomes are biocompatible nanostructures that enhance the biodistribution within the host. Liposomes enhance blood circulation and increase in the drug half-life to overcome the challenges of narrow therapeutic windows[1]. Moreover, drug-loaded liposomes are known to increase drug efficacy and therapeutic index while reducing drug toxicity and

preventing undesired side effects in comparison to free-form drug[2]. Hence, the emergence of lipid materials, specifically liposomes, has proven to be an effective design strategy for the transport of materials as therapeutic delivery agents.

Given the advantages of liposomes with respect to chemotherapeutics, liposomes have been extensively exploited as drug nanocarriers illustrated in **Figure 1.1**. Their ability to encapsulate both hydrophilic and hydrophobic molecules and interface with biological systems provide an appealing strategy towards drug therapy. Most commonly, liposomes have been used as nanocarriers for the release of anti-cancer drugs such as doxorubicin and paclitaxel[1,6,8]. The advancement of Doxil, a clinically approved doxorubicin-loaded liposome formulation, has given rise towards the utilization of liposomes containing polyethylene glycol (PEG) as a model for cancer treatment. Furthermore, liposomes have been employed for the transport of biomolecules such as proteins, ribonucleic acid (RNA), and deoxyribose nucleic acid (DNA)[12,15,16]. Liposomes, containing genetic material effectively, act as transfection agents transferring genetic information for gene expression. Towards targeting and inducing cell-mediated responses, liposomes have been used as antigen carriers to deliver antigens and target tissues[9,17]. Because of their nature, they are easily recognized by epithelial cells and have high ability for cellular uptake. The ability to modify the liposome surface with various targeting ligands such antibodies, proteins, peptides, carbohydrates, small molecules and drugs has advanced liposomes. Thus, liposomes have served as excellent carriers for drug and cell delivery for the non-specifically encapsulation and transport all types of molecules from ions to biomolecules. Despite the many applications and advantages provided by liposome-based materials, the stability of liposomes remains a major problem with respect to long-term storage, shelf-life, cargo retention, and stability in biological environments[1].

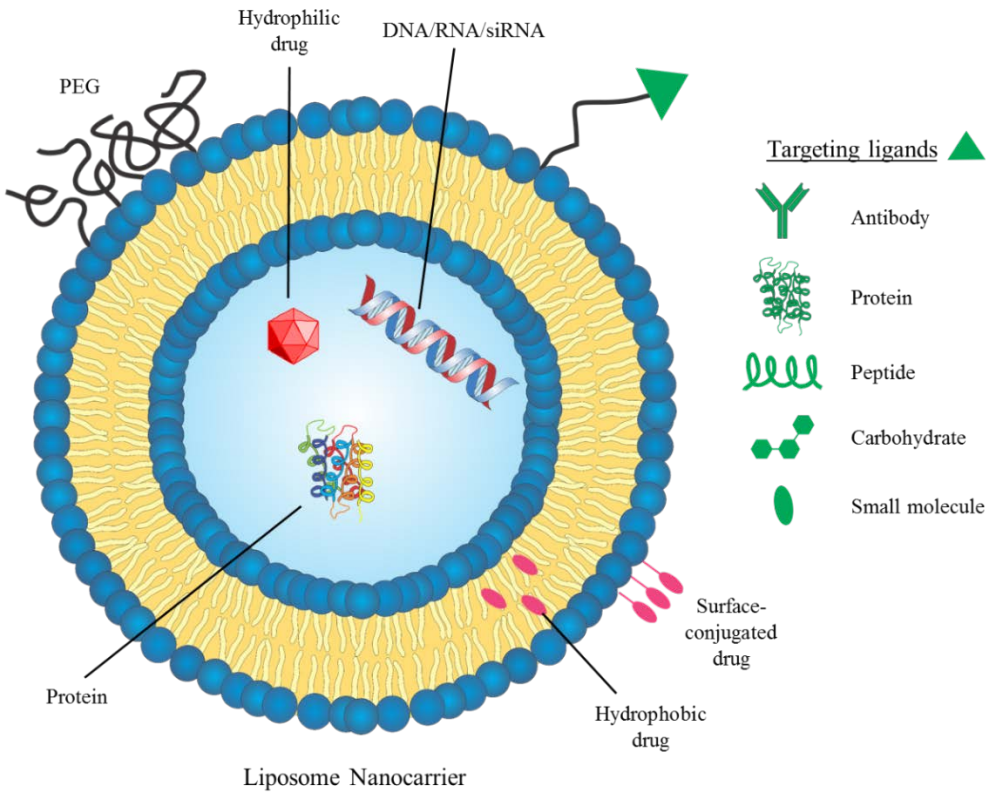

Figure 1.1: Example of encapsulated-liposome nanocarrier with surface modifications for the attachment of ligands.

The focus of this thesis aims to addresses the chief concern of nanomaterial stability with respect to cargo loading and controlled release with an emphasis towards but not limited to biomedical applications. We aspire to develop and improve the preparation of lipid materials capable of maintaining structural membrane integrity and reducing membrane permeability against encapsulated payloads as a potential drug delivery system depicted in **Figure 1.2**. Our goal is two-fold. We aim to 1) design a facile and modular approach towards synthesizing novel archaeal-type lipids with high diversity amenable to liposomal assembly in aqueous media and 2) to increase membrane stability by reducing the permeability of ions and small molecules. Through our efforts, we developed an elective model for the construction of stable liposomes

and artificial membranes to understand more precisely the mechanism & function of biological membranes and to realize the scope of potential biotechnical and nanotechnology applications.

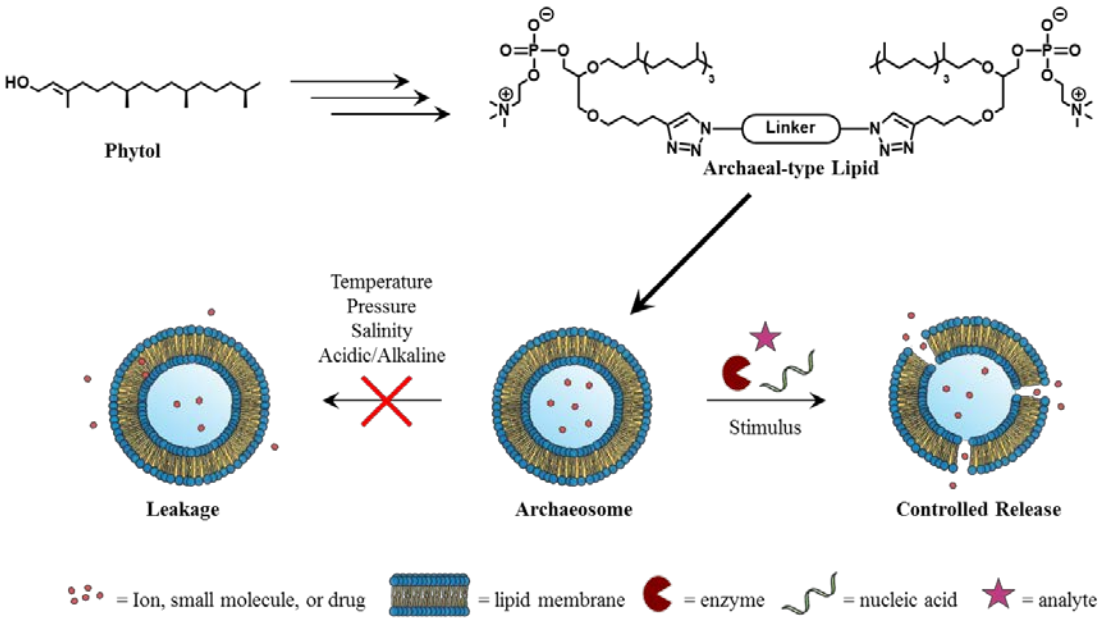

Figure 1.2: Goal towards designing a facile synthesis of archaeal-type lipids for the generation of stable liposomes resistant to leakage upon external stresses.

1.2 Approaches in the Improve Conventional Liposomes

Conventional liposomes are composed of one or more ester phospholipids that self-assemble into colloidal, spherical vesicles in aqueous media. Phospholipids are amphiphilic surfactants containing a polar head group and two acyl fatty tails that aggregate to form a lipid bilayer membrane. Additives such as cholesterol are included during formulation to support the structural integrity and rigidify the bilayer membrane[3]. The assembly of liposomes is driven by the thermodynamic phase properties influenced by entropic confiscation of the hydrophobic regions[18]. The aqueous interior cavity provides a hydrophilic environment while the membrane core is hydrophobic. The amphiphilic nature allows the liposome membrane to serve as a defensive barrier that partitions the encapsulated material from the external environment.

Liposomes provide many advantages towards the advancement of materials, yet several disadvantages remain. Despite their amphiphilic moieties, liposomes have low solubility, short half-life as well as a short shelf-life, and are prone to enzymatic & chemical oxidation & hydrolysis[4]. Overall, all of these issues contribute to membrane leakage which is destructive towards storage and transport of encapsulated cargo. Liposomes suffer greatly from ion and small molecule membrane permeability. This effect is quite undesired as a drug delivery system as encapsulated drugs are subject to diffusing across the lipid membrane. As a delivery agent, the drug is no longer coated/protected and may target undesired tissues[7]. As a step to improve the utility of liposomes as a carrier, several approaches have been taken to address these issues. Here we describe the methods to improve encapsulation and overall membrane stability.

1.2.1 Storage Methods for the Preservation of Liposome Stability

Conventional liposomes dispersed in aqueous solution can undergo physical and chemical instabilities during long-term storage[1]. Typically, lipids of eukaryotic or bacterial nature are prone to ester hydrolysis and oxidation of the unsaturated double bonds. Such vulnerabilities lead to leaky liposomes and unstable materials. To circumvent this inconvenience, the stability of liposomes can be preserved through lyophilizing the lipid-drug conjugate during storage[1]. Freeze-drying the liposome maintains the membranes as dehydrated cakes which, prior to administration, can be reconstituted with water (citation). Consequently, this process also increases the shelf-life of the liposomal formulations in addition to conserving the encapsulate within the membrane structure. Some examples of commercial liposome-based drugs in the lyophilized form are Myocet (Novartis Pharma AG, Basel, Switzerland), Amphotec (Gildead Sciences, Inc)[1]. Furthermore, additives such as carbohydrates are incorporated to maintain particle size distribution. This prevents membranes from fusing

together and encapsulate from escaping the liposome during the lyophilization-rehydration process[19]. Although several techniques have been developed for the storage of liposome-based drugs, these procedures do not address the overall stability of liposomes with respect to biological environments.

1.2.2 Stealth Liposomes for Enhanced Pharmacokinetics

Towards the development of lipid materials for for cancer treatment, Doxil and Myocet were the first clinically-approved liposomal drug products on the market[6]. Both products are liposome-based drug formulations loaded with doxorubicin, an anthracycline used to treat solid and hematological tumors[6]. Both Doxil and Myocet exhibit longer circulation time and higher half-lives in blood compared to the free-form doxorubicin (citation). The use of liposomes as drug carriers demonstrate various therapeutic advantages, however, the stabilization of liposomes require serious improvements. The incorporation of additives that promote physical modifications have been studied to further enhance the stability of liposomes. As mentioned previously, the addition of cholesterol has proven to rigidify the lipid membrane (solid-like phase). Additionally, the presence of cholesterol serves to anchor various molecules such as DNA or PEG[20]. Liposomes containing PEGylated lipids form “stealth” liposomes and have shown substantial benefits in specific regard towards drug delivery. In particular, Doxil is a PEGylated liposomal formulation that has shown longer blood circulation in comparison to the non-PEGylated competitor, Myocet. Although Doxil has shown to reduce drug-related toxicity and have better safety profiles (increase localization), the liposome-drug conjugate is limited by major drawbacks. Patients treated with Doxil suffer from plamar-plantar erythrodysaesthesia (hand-foot syndrome), the accumulation of drug at the fingertips and toes[1]. Consequently, this undesired side effect negatively impacts the quality of life for the patient leading to treatment discontinuation. Contrastingly, free-form doxorubicin and non-PEGylated

liposome-based drugs do not exhibit such side effects. Despite the improvements towards developing liposomes with enhanced pharmacokinetic benefits, liposomes, serious concerns still remain.

1.2.3 Encapsulation Efficiency for Therapeutic Value

To render therapeutic efficacy, sufficient concentrations of drug must be delivered and made bioavailable at diseased-specific sites. Thus, the drug-loading and encapsulation efficiency must be considered to accommodate this concern. The encapsulation is dictated by the solubility of the drug in which, liposomal drug formulations attempt to address. Drugs that are high in hydrophobicity are inserted within the membrane while hydrophilic drugs are present in the aqueous cavity. Although liposomes are suitable for both hydrophilic and hydrophobic drugs, most anti-cancer drugs have intermediate solubility. This most often results in the rapid release of drugs across the lipid membrane, leaking the drug into undesired tissues.

To encapsulate drugs within the liposome, the drug is incorporated during the rehydration step during the lipid-film formulation process. For lipid-film hydration, the drug pre-dissolved in buffer is added to the dried lipid mixture to promote peeling and folding of the lipid to form liposomes in the presence of water. Although this is the most common method for drug encapsulation, the loading efficiency remains low below desired loading concentrations. To achieve highly efficient encapsulation, anti-cancer drugs such as doxorubicin can be driven into pre-formed liposomes by low pH gradients. In the presence of low pH, doxorubicin is forced into the interior of the liposome by enhancing precipitation where the weak base is highly retained (Bozzuto). This loading process allows high loading concentrations above their solubility limits of the drug. Drugs that sparingly soluble in water can be converted to weak-base prodrugs to favor drug-loading (Bozzuto 62). Although this

loading method allows for efficient loading, it does not accommodate for the difficult solubility of certain drugs or requires modification to a prodrug form.

1.3 Archaeal Membranes as a Model for Innovative Liposomes

In our pursuit to develop stable systems, we were inspired from the earliest known living organisms and modeled our design after Archaea. Archaea are single-cell prokaryotes, apart from the three-domain system bacteria & eukaryotes and were initially classified as archaebacterial (part of the bacteria domain). Gene studies, however, reveal that archaea are a domain of their own, and have since been termed archaea. Prokaryotic cell fossils suggest that archaea date approximately 3.5 billion years prior to present day making them the most primitive and ancient lifeforms, as archaea have survived the most extreme environments throughout time. Archaea are considered as a class of extremophiles capable of living in harsh atmospheres such as hot springs, salt lakes, rift vents in the deep sea, anoxic muds of marshes petroleum deposits, and inside the digestive tracts of cows, termites, and marine life giving rise to methogens, halophiles, thermophiles, and pyschorphiles[21,22]. Archaea can withstand extreme conditions such as low and high temperatures, alkaline and acidic environments (pH), variable pressures, oxidative stress, and phospholipases[22]. Their ability to survive and proliferate in such variable environments is attributed to their membrane stabilities. Archaeal membranes are distinct from both bacterial and eukaryotic lipid membranes in their structural features: i) ester linkage, ii) sn-2,3-glycerol carbons, iii) branched phytanyl chains, , iv) dipolar amphiphile as illustrated in **Figure 1.3**.

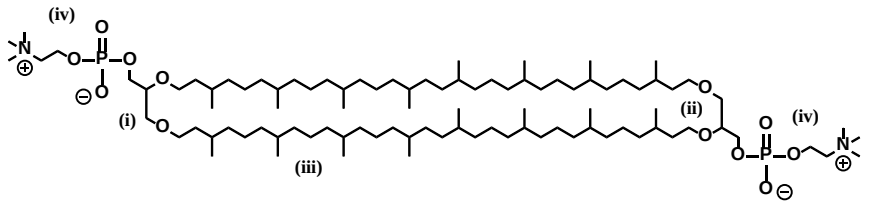

Figure 1.3: Standard archaeal lipid found in archaea. (i) Ester linkage. (ii) sn-2,3-glycerol carbons. (iii) Phytanyl chain. (iv) Dipolar head groups.

The structural characteristics of archaeal membranes provides a plethora of mechanisms to adapt and survive in various environments. The aliphatic tails of archaeal membranes are attached via ether bonds whereas eukaryotes and bacteria are linked by ester bonds. This makes archaea membranes more stable and resistant to acidic and wide ranges of pH in comparison to the facile hydrolysis of ester bonds as observed in non-archaeal lipids. The aliphatic tails consist of phytanyl chains (repeating isoprenoid units) that provide steric hindrance from the branched methyl groups to reduce crystallization and reduce membrane permeability. The fully saturated phytanyl aliphatic chains prevent oxidations and are attached to glycerol at sn-2,3 positions as ether linkages making these lipids resistance from phospholipases shown in **Figure 1.4**. In contrast, eukaryotic and bacterial lipids contain sn-1,2 ester linkages which are easily degraded by enzymes.

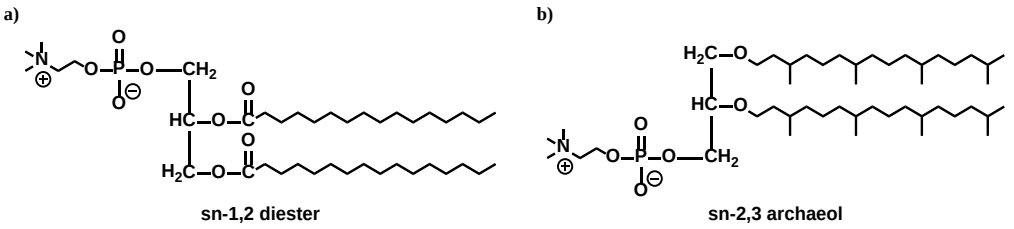

Figure 1.4: Differences between esters and ether linkages within lipids. a) sn-1,2 diester lipid. B) sn-2,3 archaeol lipid.

Furthermore, the aliphatic chains are attached to the glycerol backbone to form archaeol lipids (diether) or caldarchaeol lipids (tetraether) as observed in acyclic and macrocyclic structures as depicted in **Figure 1.5**. Archaeol lipids form a lipid bilayer, while caldarchaeol are transmembrane tetraether lipids that assemble into a single bilayer membrane to generate unilamellar vesicles. Archaea have incorporated cyclic structures (5-membered rings) to enhance membrane packing and reduce membrane fluidity for thermostability properties. Unlike other living organisms, archaeal membranes do not contain cholesterol. Thus, archaeal membranes contain structural and molecular characteristics that allow them to survive and adapt to extreme environments.

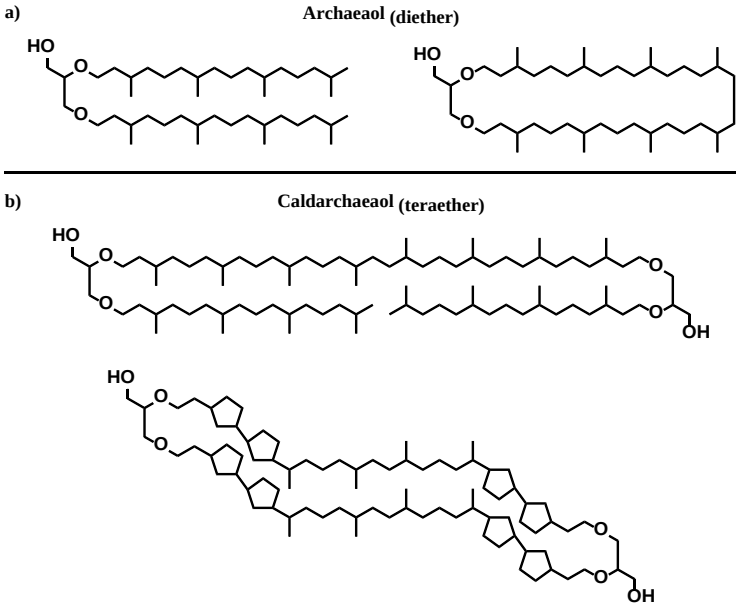

Figure 1.5: Representative examples of lipids from Archaea. a) Archaeol lipids. b) Caldarchaeol lipids.

To improve the stabilities of lipid materials, liposomes composed of natural and/or synthetic polar ether lipids unique to or inspired by archaeal are defined as Archaeosomes. Archaeal lipids can either be obtained by total synthesis or polar lipid extraction from archaea. The lipid membrane of archaeosomes form a bilayer when composed of archaeol, diether lipids, and monolayers when made exclusively from caldarchaeol, tetraether lipids as described

previously. Archaeosomes containing natural archaeal lipids or archaea type lipids contain key molecular features that differentiate themselves from classical lipids that formulate into liposomes. The incorporation of chemical features of archaeal membranes into archaeosomes has been heavily underutilized in the materials field and could elucidate the principles towards generating stable and robust systems.

Towards developing biotechnological applications for drug, gene, and vaccine delivery, archaeosomes have demonstrated its biocompatibility ability to safely interface with biological environments. Similar to conventional liposomes, archaeosomes can also encapsulate small molecule drugs, proteins, and genetic material. The similarities between conventional liposomes and archaeosomes provide analogous benefit, however, archaeosomes have shown to exhibit superior stability towards extreme conditions. The utilization of archaeosomes in this manner presents archaeosomes as a superior nanocarrier as delivery system over conventional liposomes.

1.4 Efforts to Synthesize Archaeal-type Lipids

The utilization of archaeosomes as an alternative to conventional liposomes has directed an increasing interest in obtaining archaeal and/or archaeal-type lipids. Archaeal lipids were first obtained by total lipid extraction yet result in low isolation yields and remain impure. Synthetic lipids have this been reported to obtain archaeal-type lipids and have enabled functionally modified lipids for enhanced properties. Significant contributions have been made towards the reducing the number of synthetic modifications within synthetic schemes, however, these routes only enable the synthesis of one particular lipid. The difficulty in synthesizing archaeal lipids is the reason why this field is seldom studied. For this reason, we designed a facile route for the synthesis of archaeal-type lipids that allow for the generation of

diverse lipids using one synthetic route. Herein, we describe the design of archaeal-type lipids that assemble into archaeosomes as potentially stable systems.

1.5 References

1. Chang, H. I. & Yeh, M. K. Clinical development of liposome-based drugs: Formulation, characterization, and therapeutic efficacy. *Int. J. Nanomedicine* **7,** 49–60 (2012).

2. Puri, A., Loomis, K., Smith, B., Lee, J.-H., Yavlovich, A., Heldman, E. & Blumenthal, R. Lipid-based nanoparticles as pharmaceutical drug carriers: from concepts to clinic. *Crit. Rev. Ther. Drug Carrier Syst.* **26,** 523–80 (2009).

3. Akbarzadeh, A., Rezaei-sadabady, R., Davaran, S., Joo, S. W. & Zarghami, N. Liposome : classification , preparation , and applications. 1–9 (2013). doi:10.1186/1556-276X-8-102

4. Barenholz, Y. Liposome application: Problems and prospects. *Curr. Opin. Colloid Interface Sci.* **6,** 66–77 (2001).

5. Chauhan, V. P. & Jain, R. K. Strategies for advancing cancer nanomedicine. *Nat. Mater.* **12,** 958–62 (2013).

6. Alavi, S. E., Mansouri, H., Esfahani, M. K. M., Movahedi, F., Akbarzadeh, A. & Chiani, M. Archaeosome: As new drug carrier for delivery of paclitaxel to breast cancer. *Indian J. Clin. Biochem.* **29,** 150–153 (2014).

7. Samad, A., Sultana, Y. & Aqil, M. Liposomal drug delivery systems: an update review. *Curr. Drug Deliv.* **4,** 297–305 (2007).

8. Harris, L., Batist, G., Belt, R., Rovira, D., Navari, R., Azarnia, N., Welles, L., Winer, E., Garrett, T., Blayney, D., Elias, L., Mortimer, J., Needles, B., Webb, T., Atiba, J., Bickers, J., Godfrey, T., Love, R., Osborn, D., *et al.* Liposome-encapsulated doxorubicin compared with conventional doxorubicin in a randomized multicenter trial as first-line therapy of metastatic breast carcinoma. *Cancer* **94,** 25–36 (2002).

9. Sprott, D. G., Dicaire, C. J., Côté, J. P. & Whitfield, D. M. Adjuvant potential of archaeal synthetic glycolipid mimetics critically depends on the glyco head group structure. *Glycobiology* **18,** 559–565 (2008).

10. Jakobsche, C. E., Parker, C. G., Tao, R. N., Kolesnikova, M. D., Douglass, E. F. & Spiegel, D. A. Exploring binding and effector functions of natural human antibodies using synthetic immunomodulators. *ACS Chem Biol* **8,** 2404–2411 (2013).

11. Bergstrand, N. *Liposomes for Drug Delivery from Physico-chemical Studies to Application*. *Comprehensive Summaries of Uppsala Dissertation form the Faculty of Science and Technology* (2003).

12. Balazs, D. A., Godbey, W., Balazs, D. A. & Godbey, W. Liposomes for Use in Gene Delivery. *J. Drug Deliv.* **2011,** 1–12 (2011).

13. Kearney, C. J. & Mooney, D. J. Macroscale delivery systems for molecular and cellular payloads. *Nat. Mater.* **12,** 1004–17 (2013).

14. Parmentier, J., Thewes, B., Gropp, F. & Fricker, G. Oral peptide delivery by tetraether lipid liposomes. *Int. J. Pharm.* **415,** 150–157 (2011).

15. Zavec, A. B. edina, Ota, A., Zupancic, T., Komel, R., Ulrih, N. P. & Liovic, M. Archaeosomes can efficiently deliver different types of cargo into epithelial cells grown in vitro. *J. Biotechnol.* **192,** 130–135 (2014).

16. Attar, A., Ogan, A., Yucel, S. & Turan, K. The potential of archaeosomes as carriers of pDNA into mammalian cells. *Artif. cells, nanomedicine, Biotechnol.* **4,** 1–7 (2015).

17. Krishnan, L., Dicaire, C. J., Patel, G. B. & Sprott, G. D. Archaeosome vaccine adjuvants induce strong humoral, cell-mediated, and memory responses: Comparison to conventional liposomes and alum. *Infect. Immun.* **68,** 54–63 (2000).

18. Lasic, D. D. & Martin, F. J. On the mechanism of vesicle formation. *J. Memb. Sci.* **50,** 215–222 (1990).

19. Brard, M., Lainé, C., Réthoré, G., Laurent, I., Neveu, C., Lemiègre, L. & Benvegnu, T. Synthesis of archaeal bipolar lipid analogues: A way to versatile drug/gene delivery systems. *Journal of Organic Chemistry* **72,** 8267–8279 (2007).

20. Barbeau, J., Cammas-Marion, S., Auvray, P. & Benvegnu, T. Preparation and Characterization of Stealth Archaeosomes Based on a Synthetic PEGylated Archaeal Tetraether Lipid. *J. Drug Deliv.* **2011,** 1–11 (2011).

21. Tenchov, B., Vescio, E. M., Sprott, G. D., Zeidel, M. L. & Mathai, J. C. Salt tolerance of archaeal extremely halophilic lipid membranes. *J. Biol. Chem.* **281,** 10016–10023 (2006).

22. Jacquemet, A., Barbeau, J., Lemiegre, L. & Benvegnu, T. Archaeal tetraether bipolar lipids: Structures, functions and applications. *Biochimie* **91,** 711–717 (2009).

Chapter 2 : Synthesis of Archaeal-type Lipids

2.1 Introduction

Towards the synthesis of archaeal-type lipids, we directed our efforts to design a synthetic scheme that would allow for the modulating and the tuning of the hydrophobic lipid core while providing quantitative yields and reducing the number of synthetic modifications. To this end, we exploited click chemistry as a platform to build our lipid systems. Using copper (I)-catalyzed cycloaddition we would be able to attach two compounds together containing an azide and an acetylene functional group. As illustrated in **Figure 2.1**, we utilized click as a means to generate a variety of lipids containing different moieties, to produce dipolar lipids and to tune the membrane thickness[1–4]. Within our design, we envisioned that by designing hydrophobic linkers capable of 1,3-cyclo addition at each end, we could tether the arms of the lipid at both sites to form a hemicycle. This synthetic scheme is a desirable approach because it allows for the control of the construction of countless unique lipids for liposomal assembly varying in structure and function[5]. Essentially, any compound containing two azido functional groups can be clicked into the membrane to tether the lipid hemimacrocycle together. Without having to develop a new synthetic route for each unique lipid, we synthesized a myriad of lipids using one synthetic strategy[5]. Through click chemistry, our design allows for the modular and tunable synthesis of singly tethered bolafoam lipids to achieve stable and diverse materials.

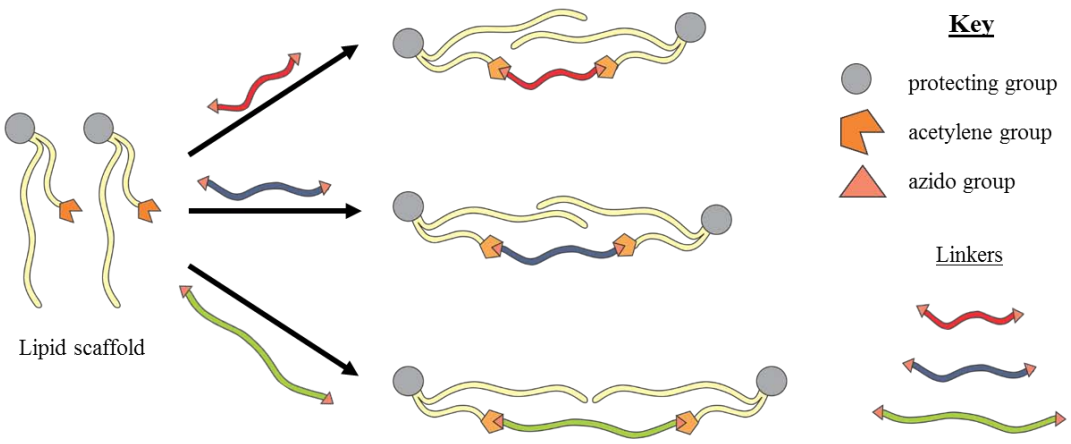

Figure 2.1: Design strategy for generating diverse lipids varying in length and functional moieties.

Towards the synthesis of lipids for the generation of stable materials, we specifically designed novel archaea-inspired lipids that attempt to mimic archaea membrane properties and are capable of withstanding extreme environments. We hypothesized that exploiting the structural characteristics unique to archaeal membranes would enhance the robustness of the archaeosomes and reduce membrane leakage to ions and small molecules[4,6–11]. By synthesizing lipids that contain the following molecular components: 1) ether linkages, (2) repeating isoprenoid units, (3) sn-2,3-glycerol backbone, (3) bolafoam/macrocycle as shown in **Figure 1.3**, we aspired to formulate stable archaeosomes. To generate archaeal-type lipids, we set out to synthesize a diverse library of lipids containing various moieties within the hydrophobic core to further explore the membrane properties. To synthesize a library of archaea-inspired lipids, we designed a facile and modular synthetic route that would allow us to synthesize multiple lipid analogs in a main synthetic route while tuning the lipid core. Thus, we utilized click chemistry as a vital method to synthesize a multitude of lipids that can be formulated into potentially stable and robust materials. Herein, we describe the synthesis of archaeal-type lipids **ATL1-5**.

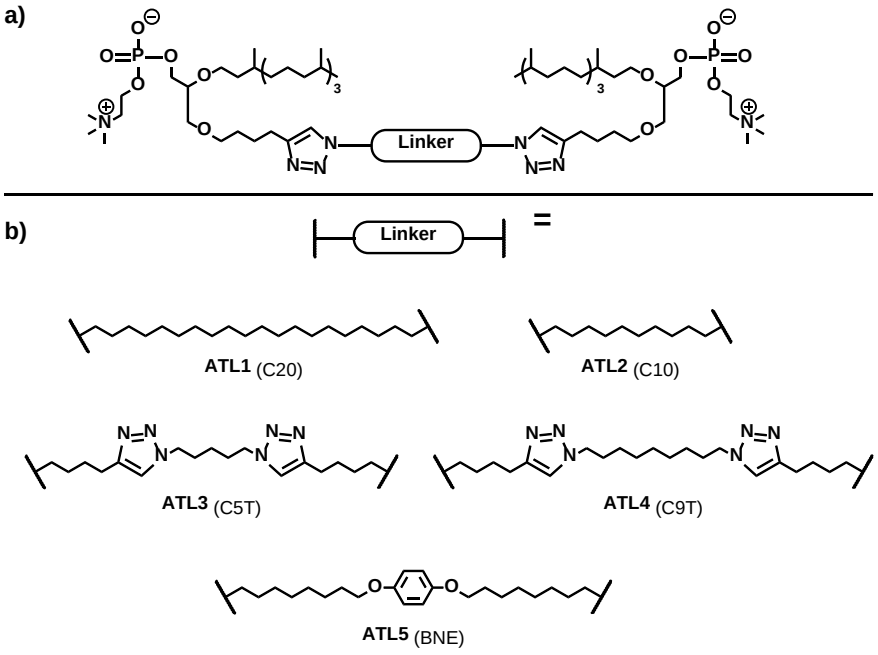

Figure 2.2: Archaeal-type lipids. a) General archaeal-type lipid template. b) Archaeal-type lipids **ATL1-5.**

2.2 Linkers for Singly Tethered Lipids

To design archaea membranes containing dipolar head groups that span the entire lipid membrane and constitute as the hydrophobic core of our archaeosomes, we first had to consider the length of the linker as well as hydrophobicity. The membrane thickness of archaeosomes is strictly governed by the length of each linker. Therefore, we synthesized linkers that when fully clicked form unilayer membranes comparable to archaea lipid membranes consisting 20-40 carbons in length. Our strategy allows us to probe the influence of membrane thickness by tuning the length of our lipids. By synthesizing different diazido linkers varying in length and moieties, we aimed to examine the many variables that contribute towards membrane stability. Thus, we synthesized linkers **K1-5** containing azido functional groups at the terminal ends to

to investigate the properties of our archaea-inspired lipid system and achieve lipid diversity shown in **Figure 2.3**.

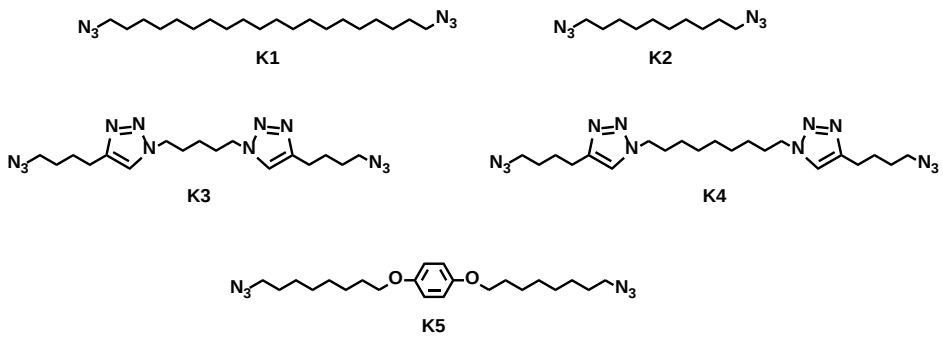

Figure 2.3: Library of linkers K1-5 for the incorporation into archaeal-type lipids.

2.2.1 Tuning Membrane Thickness

To prepare archaeosomes comparable to conventional bilayer forming liposomes, we used 1,2-dipalmitoyl-sn-glycero-3-phosphocholine (DPPC) as our control model to synthesize archaeal-type lipids. DPPC lipids have been extensively studied and used in forming lipid bilayers, liposomes, and biological membranes making DPPC a good standard for comparison. Because bilayer membranes are constituted by two phospholipids that span the entire length of the hydrophobic core, we had to consider the total length in our design. To investigate the control of membrane thickness, we synthesized linkers **K1-2** to study the influence of the length of each lipid. To match the membrane thickness of DPPC liposomes for a head-to-head comparison we specifically synthesized linker **K1**. Linker **K1** consists of 20 carbons and when incorporated into the lipid, in principle, should span the entire liposome membrane analogous to DPPC liposomes. To adjust the membrane thickness, we synthesized linker **K2**, containing 10 carbons, half the length of **K1**, in hopes to reduce the membrane thickness. From these two lipids varying in length, we expected to see stark differences in the membrane thickness of each archaeosome formulation.

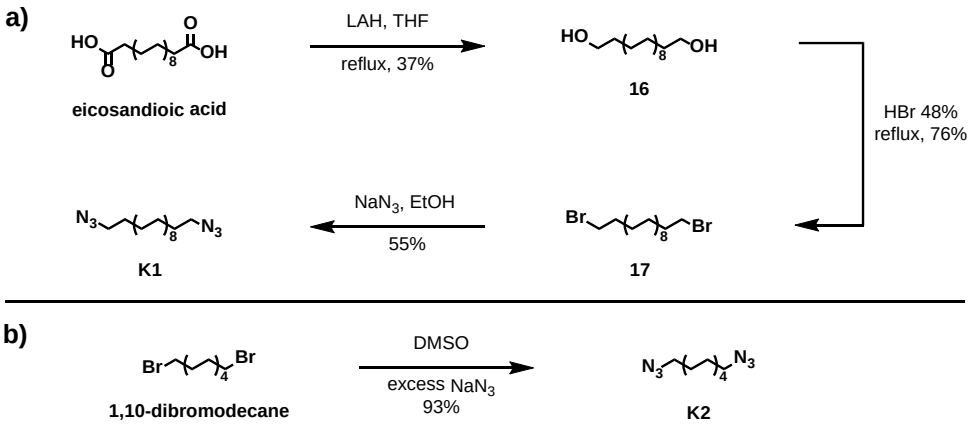

Figure 2.4: Synthesis of alkyl-based linkers. a) Synthesis of 20-carbon based linker **K1**. b) Synthesis of 10-based carbon linker **K2**.

The synthesis of linkers **K1-2** were easily synthesized in a few steps outlined in **Figure 2.4**. Limited by commercial availability, linker **K1** was synthesized from eicosandioic acid. Eicosandioic acid was reduced to compound **16** by lithium aluminum hydride (LAH) in THF to form the diol in 54% yield. The low yield is a result of the insolubililty of eicosandioic acid in organic solvents. To increase the solubility of eicosanioic acid, the reaction was refluxed. Upon the formation compound **16**, the diol was readily soluble in DCM. Compound **16** was then refluxed in hydrobromic acid (48%) to produce the dibromoalkane compound **17**. Compound **17** was treated with excess sodium azide in ethanol/THF (1:1) to displace both terminal bromo groups and afford linker **K2** in 93% yield. To synthesize linker **K2**, 1,10-dibromodecane was treated with excess sodium azide in DMSO obtain the shorter linker in 1 step. Despite initial solubility issues for eicosandioic acid, linkers **K1-2** were easily synthesized in sufficient yields.

To study the effects of triazole rings from click chemistry on the membrane permeability, we synthesized two linkers varying in chain length. Both linkers contain 4 triazole rings in the hydrophobic core when fully synthesized in contrast to the 2 triazole rings from our lipid design. We reasoned that the presence of 5-membered triazole rings may serve

as a simple alternative for cyclopentane rings as found in natural archaeal membranes. Additionally, many reports have demonstrated the importance of incorporating cyclopentane rings as it has shown to increase the gel to liquid phase transition in contrast to lipids without any cyclopentane rings. Therefore, if the presence of triazole rings prove to be as a substitute for cyclopentane rings, then we can significantly improve the thermal stability of the archaeosome given our design. Although, we reasoned that the aromatic triazole would provide stability within membrane core, we reason that the nitrogen heteroatoms could potentially lead to increased leakage. Thus to investigate the effects of triazole rings on membrane permeability, we synthesized linkers **K3-4**.

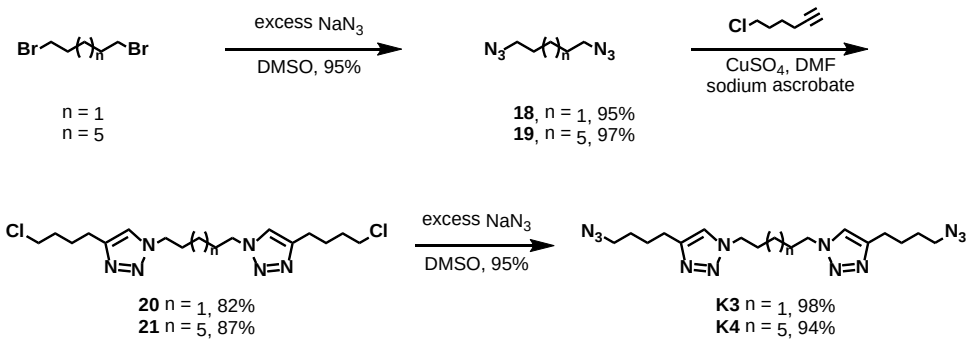

Figure 2.5: Synthesis of triazole-based linkers **K3** and **K4**.

Linkers **K3** and **K4** were synthesized separately using the same synthetic scheme as outline in **Figure 6.1**. 1,5-Dibromopentane and 1,9-dibromooctane were treated with excess sodium azide in DMSO to afford the diazido alkane products **18** and **19** in high yield. Compounds **18** and **19** were then treated with 6-chloro-1-hexyne, $CuSO_4$, and sodium ascorbate in DMF to install the first two triazole rings in compounds **20** and **21**. To incorporate the terminal azido groups for the incorporation of the other triazole rings, compounds **20** and **21** were treated with excess sodium azide in DMSO to afford linkers **K3** and **K4**. In 3 synthetic steps, linkers **K3-4** were each synthesized to provide similar linkers differing in length as a means to study membrane permeability and potential thermostability.

2.2.2 Aromatic Linker for Enhanced Membrane Rigidity

As previously mentioned, cyclopentane rings have been shown to increase the thermostability of archaeal membranes and reduce ion leakage. Similarly, cyclohexane rings have been reported to reduce membrane permeability (citation). To mimic these desired properties within our system, we incorporated an aromatic benzene as a quick synthesis to generate lipids of similar properties. We reasoned that the 6-membered hexane ring would reduce membrane permeability similar to previous reports and that the membrane packing would be strengthen by pi-pi stacking. For ease of synthesis, we synthesized linker **K5**, an aromatic linker containing ether groups, to study the effects of aromatic rings and their potential to increase stability.

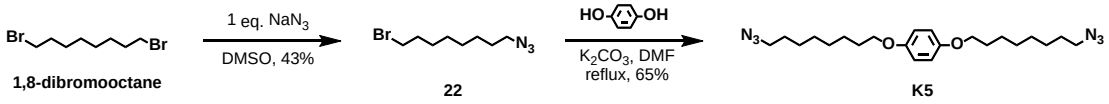

Figure 2.6: Synthesis of aromatic ether linker **K5**.

1,8-Dibromooctane was treated with 1 equivalence of sodium azide in DMSO to yield 45% of the monosubstituted product **22**. Compound **22** was then slowly added dropwise to a refluxing solution containing 1,4-benzenediol, potassium carbonate (K_2CO_3) in DMF to obtain linker **K5**. Linker **K5** was obtained in 2 simple steps. With linkers **K1-5** in hand, we proceeded to tether these linker into our lipid design.

2.3 General Synthetic Scheme

To synthesize archaeal-type lipids, we started with the modification of glycerol, which serves as the backbone and intermediate between the polar head group and aliphatic chains. Glycerol first had to be selectively protected in order to individually modify each hydroxyl in a systematic fashion due to the presence of three hydroxyl groups. To restrict the 1,3-hydroxyl

ends, glycerol was refluxed with freshly distilled benzaldehyde and *p*-Toluenesulfonic acid to form compound **1** as illustrated in **Scheme 2.7**. The driving force for compound **1** is the cyclization of the highly favorable 6-membered acetal ring. We did observe the 5-membered product but obtained compound **1** by recrystallization in diethylether. Upon the synthesis of compound **1**, the protected glycerol only contains a free hydroxyl the C-2 position.

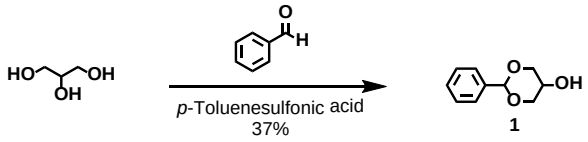

Figure 2.7: Synthesis of compound **1** for the protection of glycerol.

Upon the protection of glycerol, the lipids were synthesized according to the general synthetic scheme in **Figure 2.8**. Before attaching the phytanyl chains to glycerol backbone, phytol was converted to compound **2** to install a good leaving group. Phytol was treated with triphenylphosphine (PPh_3), imidazole, and iodine (I_2) in dichloromethane (DCM) to displace the free hydroxyl and afford compound **2**. To append the phytanyl chain at the 2-position of glycerol, compound **1** was stirred with sodium hydride in dry tetrahydrofuran (THF) to generate the nucleophilic alkoxide and reacted with compound **2** to obtain compound **3**. Compound **3** was then selectively deprotected using stoichiometric equivalence of diisobutylaluminum hydride (DIBAL) to open the acetal ring at one end and expose free hydroxyl in compound **4**. To alkylate the free hydroxyl, compound **4** was treated with sodium hydride in dry THF and 6-chloro-1-hexyne via reflux to incorporate the acetylene to obtain compound **5**. The installation of the acetylene in compound **5** serves as a handle for click chemistry, which is the main precursor for the synthesis of our lipid scheme. Using copper (II) sulfate ($CuSO_4$) and sodium ascorbate in dimethylformamide (DMF), compound **5** was then subjected to copper mediated catalysis with diazido linkers (**K1-5**) to adjoin the glycerol moieties at each end of the lipid.

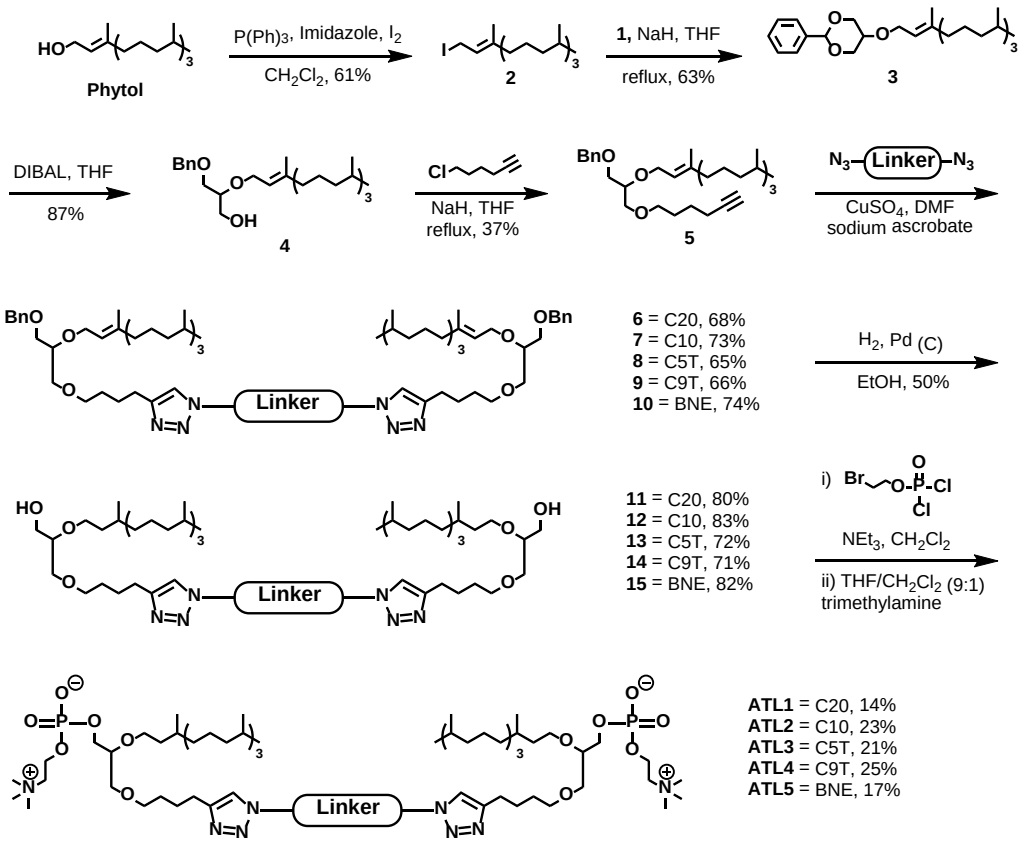

Figure 2.8: Synthetic scheme of archaeal-type lipids **ATL1-5**.

To deprotect the benzyl groups and saturate the alkenes from the phytanyl chains, compounds **6-10** were hydrogenated with excess hydrogen gas and palladium on carbon (10% weight percent loading) in ethanol to obtain the lipid diols **11-15**. Despite the catalytic activity of palladium, 4 equivalence of catalyst was used to overcome any inactivity caused by the chelation of the triazole ring to the metal. Using less than 1 equivalence, we only observed partial hydrogenation. Thus to ensure the complete deprotection and hydrogenation, excess of palladium was used to obtain lipid diols **11-15**.

To install the hydrophilic polar moieties at each end, we incorporated phosphatidylcholine head groups, given their known ability to form stable liposomes. Phosphatidylcholine are zwitterionic groups most commonly found among biological lipid

membranes and serve to form stable lipid dipolar bolafoams within our system. From lipid diols **11-15**, phosphatidylcholine lipids **ATL1-5** were prepared in 2 parts. Lipid diols **11-15** dissolved in trimethylamine and dry THF were added dropwise to a solution of bromoethyldichlorophostphate in dry THF. The intermediate product was dissolved in DCM/THF (9:1) and stirred in a solution of trimethylamine (33% in ethanol) for 5 days to yield diphosphatidylcholine lipids **ATL1-5**. This design allows for the synthesis of membrane spanning lipids for the formation of unilamellar/monolayer vesicles.

2.4 Conclusions

In this chapter, we have reported the synthesis of diazido linkers **K1-5** for the generation of singly tethered archaea-inspired lipids **ATL1-5**. Starting from cheap and simple starting materials accessible from commercial resources, we efficiently synthesized a variety of lipid analogues towards the development of stable archaeosomes. Here we demonstrated that molecular features of archaeal lipids can be synthetically inserted to obtain synthetic lipids similar to archaeal membranes. Using click chemistry, we developed a facile and modular approach to synthesize singly tethered tetraether dipolar lipids using 1 main synthetic route.The synthesis of archaeal-type lipids **ATL1-5** provides us with a tool box as a starting point towards understanding the properties and integrity of archaeal membranes. With lipids **ATL1-5** in hand, we further explore the assembly, encapsulation, and leakage properties as described in the chapters 3 and 4.

2.5 Experimental

2.5.1 General Methods/Instrument Details

All reagents were purchased from Sigma-Aldrich, Alfa Aesar, TCI America and other commercial sources and used without further purification. Dry DCM, THF, diethylether, and

toluene solvents were obtained using a Dow-Grubbs tow-column purification system (Classcontour System, Irvine, CA). Dry DMF and THF were distilled from calcium hydride and sodium hydroxide, respectively. Deuterated solvents were purchased from Cambridge Isotopes Laboratories Inc. All other solvents were used as is without further purification. All glassware was flame dried under vacuum prior to use for water-sensitive reactions. All air-sensitive experiments were carried out under nitrogen atmosphere using standard Schlenk flask procedures. Reactions were monitored by thin-layer chromatography (TLC) performed on 12.1mm pre-coated silica gel plates (plastic backed Baker). Products were purified using flash chromatography on silica gel 60 (230-400 mesh). Low resolution mass spectra analysis was performed on a Micromass Quattro Ultima triple quadrupole mass spectrometer with an electrospray ionization (ESI) source. High resolution mass spectra was confirmed by Agilent 6230 HR-ESI-TOF MS provided by the Molecular Mass Spectrometry Facility (MMSF) at UCSD Department of Chemistry and Biochemistry. All NMR spectra were recorded on Bruker AVA 300MHz, Varian Mercury 300MHz, 400MHz, 500MHz, and Joel 500MHz spectrometers. All NMR spectra were recorded in $CDCl_3$, CD_2Cl_2, CD_3OD and chemical shifts are reported in δ (ppm) relative to the respective residual solvent peak(s).

2.5.2 Synthesis

General Procedure for Diazidoalkanes

Dibromodecane (1.0253g, 3.4407mmol) and sodium azide (670.97 mg, 10.322mmol) dissolved in DMSO (20.0 mL) were stirred for 2 hours. Water (100 mL) was added to dilute the DMSO and the product was extracted with ether (3 x 30mL). The ether layers were combined, dried over $MgSO_4$, and concentrated under reduced pressure. The product was purified via silica plug using hexanes followed by ethylacetate to afford a clear oil (748.16 mg, 3.3375 mmol, 93%).

General Procedure for Clicked Benzyl Protected Lipids

To a glass vial, compound **5** (510.12 mg, 0.94388mmol), copper (II) sulfate (75.326 mg, 0.47194 mmol), sodium ascorbate (186.99 mg, 0.94388 mmol) and linker **K1** (156.31 mg, 0.42903 mmol) were dissolved in DMF (10 mL). The reaction was stirred overnight and quenched with water (50 mL). The mixture was then extracted with DCM (3 x 30 ml). The organic layers were combined and washed with water (1 x 30mL) and brine (1 x 30 mL). The organic mixture was concentrated under reduced under pressure and purified by flash chromatography using eluent DCM/EtOAc (2:1). The product was obtain as a gel-like residue (421.63 mg, 0.29174 mmol, 68%).

General Procedure for Debenzylation and Hydrogenation

To a glass vial, compound **11** (204.73 mg, 0.14166 mmol) and 10% wt. palldium on carbon (56.232 mg) were suspended in ethanol (10 mL). To the septum-sealed reaction, the vessel was evacuated via vacuum and purged with hydrogen gas via balloon for 5 repeated cycles. The reaction was stirred overnight under hydrogen atmosphere. The palladium catalyst was removed via celite filter and the filtrate was concentrated under reduced pressure. The crude product was purified by flash chromatography using eluent mixture 5% methanol in DCM to obtain a gel-like reside (143.86 mg, 0.11333 mmol, 80%).

General Procedure for Installation of Phosphotidylcholine Head Groups (ATL1-5)

Bromodichlorophosphate was first synthesized following a reported procedure (citation). Compound **15** (127.19 mg, 0.10021 mmol) and trimethylamine (155.0 μL, 1.1024 mmol) were dissolved in dry THF (2.5 mL). The diol solution was then added dropwise to a solution of bromodichlorophosphate (192.28 g, 0.80168 mmol) dissolved in dry THF (2.5 mL). The reaction was covered in foil and stirred at room temperature for 3 days. Toluene was added to

the reaction to precipitate triethylammonium chloride and was filtered through a pad of celite. The filtrate was concentrated via reduced pressure and the residue was stirred in a THF/$NaHCO_3$ (saturated) mixture for 16 hours. The mixture was then acidified using 1M HCl and extracted using MeOH/DCM (8:2). The organic layers were combined, dried over anhydrous $MgSO_4$, filtered, and concentrated via reduced pressure. The residue dissolved in THF/chloroform (9:1) was stirred with trimethylamine (33% in EtOH, 180 eq) in a sealed pressure tube for 5 days at room temperature. The crude product was concentrated via reduced pressure and purified via flash chromatography using eluent mixture DCM/MeOH/H_2O (7:3:0.5).

2-phenyl-1,3-dioxan-5-ol (1)

To a round bottom flask, glycerol (103.97 g, 1.1301 mol), *p*-Toluenesulfonic acid (1.7904 g, 10.397 mol), and freshly distilled benzaldehyde (110.0 mL, 1.09 mol) was rigorously stirred under nitrogen atmosphere for ## hours at room temperature. The reaction mixture was placed under reduce pressure at 40^{o}C on the rotavap to remove unreacted benzaldehyde. The crude mixure was then washed with water (3x 100mL) and brine (1x 100mL). The organic layers was collected, diethylether (100mL) was added, and dried with magnesium sulfate ($MgSO_4$). The mixture was filtered and recrystallized overnight in -20^{o}C fridge. The white precipitate was filtered via Buchner funnel and used without further purification (75.298 g, 0.41814 mol, 37%). ^{1}H NMR (400MHz, $CDCl_3$): δ 3.13 (d, 1H), 3.62 (m, 1H), 4.15 (m, 4H), 5.55 (s, 1H), 7.38 (m, 3H), 7.49 (m, 2H), ^{13}C NMR (500MHz, $CDCl_3$): δ 63.9, 72.2, 101.6, 125.8, 128.3, 129.1, 137.8.

*Compounds **2-5** were prepared following a reported protocol.*[5]

(E)-1-iodo-3,7,11,15-tetramethylhexadec-2-ene (2)

^{1}H NMR (400MHz, CD_2Cl_2): δ 0.88 (t, 12 H, CH3); 0.99-1.41 (m, 19H); 1.63 (s, 3 H); 1.98 (t, 2 H); 3.94 (d, 2H); 5.53 (t, 1 H,).; ^{13}C NMR (500MHz, CD2Cl2): 4.10, 15.71, 19.71, 19.77, 22.63, 22.73, 24.47, 24.80, 24.91, 27.98, 32.66, 32.80, 36.43, 37.29, 37.36, 37.44, 39.38, 39.88, 121.67, 142.88. ESI+ MS: m/z (M + H) 461.

(E)-2-phenyl-5-((3,7,11,15-tetramethylhexadec-2-en-1-yl)oxy)-1,3-dioxane (3)

^{1}H NMR (400MHz, CD_2Cl_2): 0.86 (t, 12 H); 1.05-1.57 (m, 19H); 1.65 (s, 3 H); 1.99 (m,2 H), 3.29 (s, 1 H); 4.01 (dd, 2 H); 4.15 (dd, 2 H), 4.31 (dd, 2 H),5.39 (t, 1 H), 5.53 (s, 1 H), 7.32 (dd, 3 H), 7.51 (dd, 2 H); ^{13}C NMR (500MHz, CD_2Cl_2): 16.33, 19.62, 22.53, 22.62, 24.35, 24.69, 24.97,27.85, 32.57, 32.67, 36.58, 37.18, 37.26, 37.32, 39.26, 39.80,64.92, 68.97, 69.16, 101.14, 120.66, 126.10, 127.97, 128.64, 138.04, 140.29. ESI+ MS: m/z (M+) 458.

(E)-3-(benzyloxy)-2-((3,7,11,15-tetramethylhexadec-2-en-1-yl)oxy)propan-1-ol (4)

Figure 2.9: ^{1}H NMR (400MHz, CD_2Cl_2): δ 0.85 (t, 15 H); 1.23 (m, 22 H); 1.56 (m, 2 H); 1.99 (t, 1H), 3.63 (m, 6 H), 4.09 (dd, 2H), 4.53 (s, 2 H), 7.33 (bs, 5H); HRMS (M+Na): calculated:483.3809; found: 483.3803.

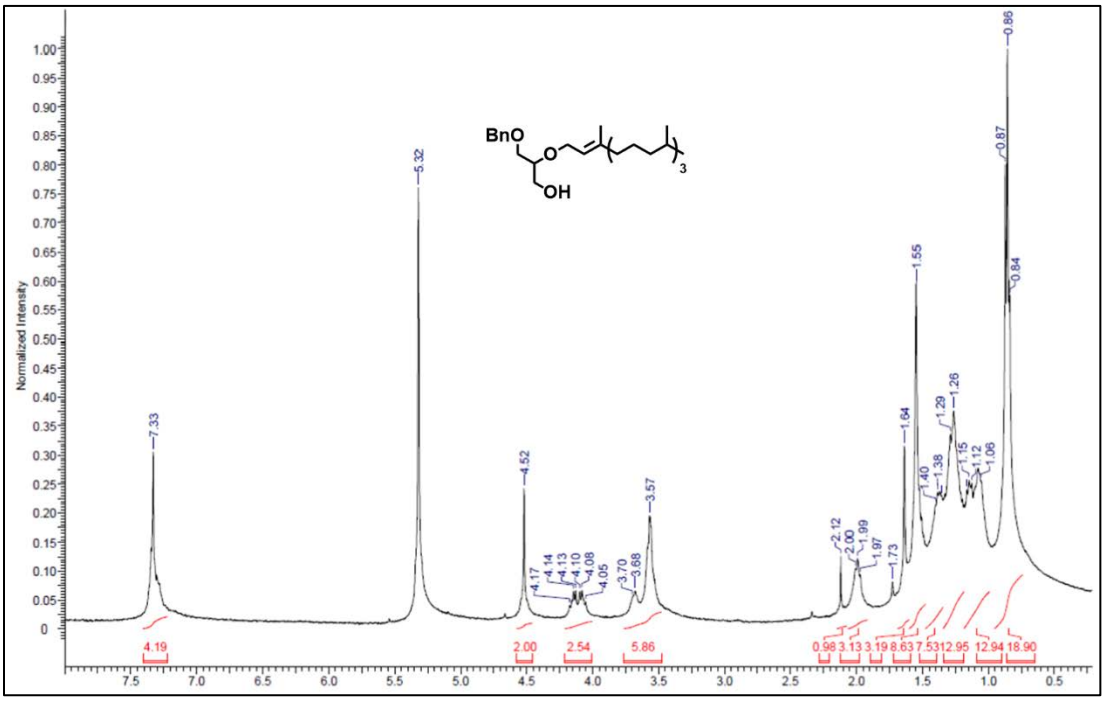

Figure 2.9: ^{1}H NMR of **4**.

(E)-((3-(hex-5-yn-1-yloxy)-2-((3,7,11,15-tetramethylhexadec-2-en-1-yl)oxy)propoxy)methyl)benzene (5)

Figure 2.10: ^{1}H NMR (400MHz, CD_2Cl_2): δ 0.85 (t, 15 H); 1.27 (m, 22 H); 1.97 (m, 3 H); 2.21 (t, 1H), 3.54 (m, 8H), 4.11 (d, 2H), 4.52 (s, 2 H), 7.33 (bs, 5H); HRMS (M+Na): calculated:563.4435; found: 563.4435.

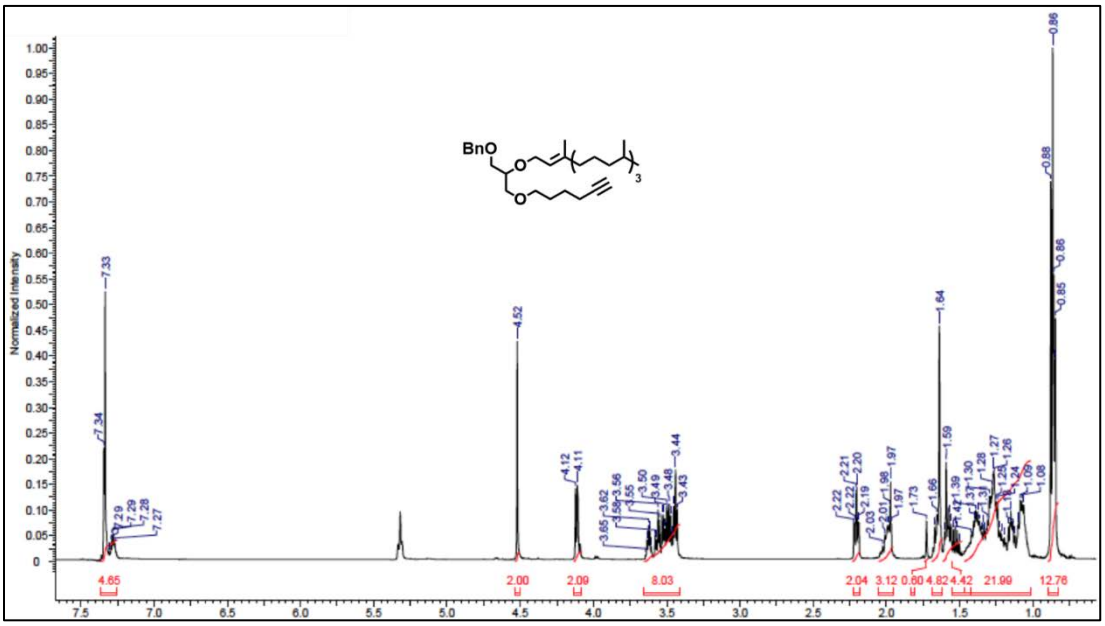

Figure 2.10: ^{1}H NMR of **5**.

1,20-bis(4-(4-(3-(benzyloxy)-2-(((E)-3,7,11,15-tetramethylhexadec-2-en-1-yl)oxy)propoxy)butyl)-1H-1,2,3-triazol-1-yl)icosane (6)

Figure 2.11: ^{1}H NMR (400MHz, CD_2Cl_2): δ 0.85 (t, 30H), 1.25 (m, 175H), 1.62 (s, 3H), 1.72 (t, 4H), 1.84 (t, 4H), 1.97 (t, 4H), 2.69 (t, 4H), 3.54 (m, 14H), 4.11 (d, 4H), 4.26 (t, 2H), 4.51 (s, 4 H), 7.33 (m, 12H); HRMS (M+Na): calculated:1468.2292; found: 1468.2311.

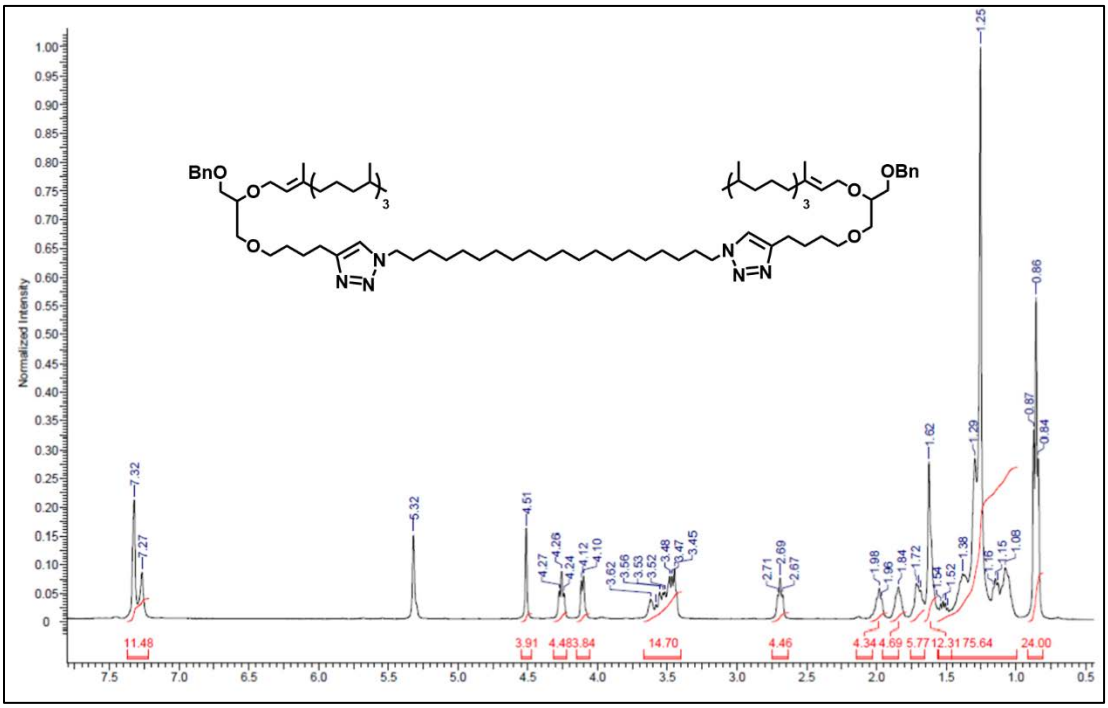

Figure 2.11: ^{1}H NMR of **6**.

1,10-bis(4-(4-(3-(benzyloxy)-2-(((E)-3,7,11,15-tetramethylhexadec-2-en-1-yl)oxy)propoxy)butyl)-1H-1,2,3-triazol-1-yl)decane (7)

Figure 2.12: ^{1}H NMR (400MHz, CD_2Cl_2): δ 0.86 (t, 30 H), 1.25 (m, 126H), 1.85 (t, 10H), 2.01 (m, 9H), 2.70 (t, 4H), 3.54 (m, 21H), 4.11 (d, 4H), 4.26 (t, 4H), 4.51 (s, 4 H), 7.32 (m, 12H);

Figure 2.13: ^{13}C NMR (500MHz, CD_2Cl_2): δ 16.61, 20.03, 22.99, 23.70, 25.32, 26.99 28.52, 30.86, 33.21, 33.32, 37.77, 39.86, 40.38, 50.56, 66.77, 67.07, 70.91, 71.25, 71.62, 73.71, 77.30, 127.94, 128.04, 128.75. HRMS (M+Na): calculated:1328.0727; found: 1328.0696.

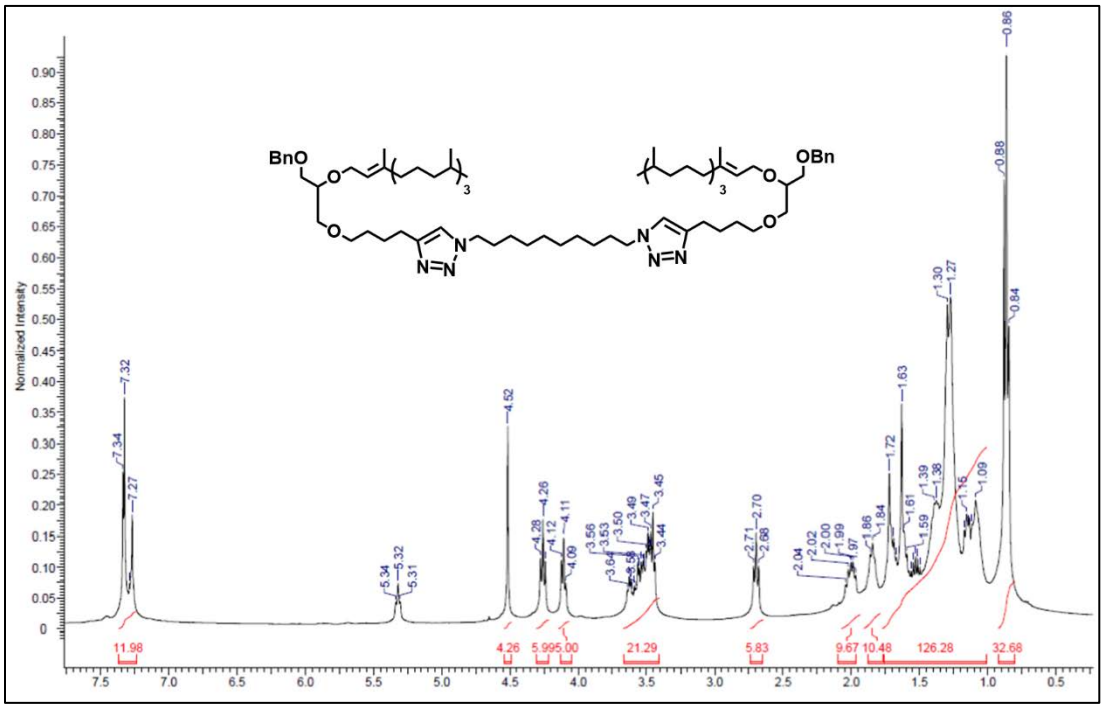

Figure 2.12: ^{1}H NMR of **7**.

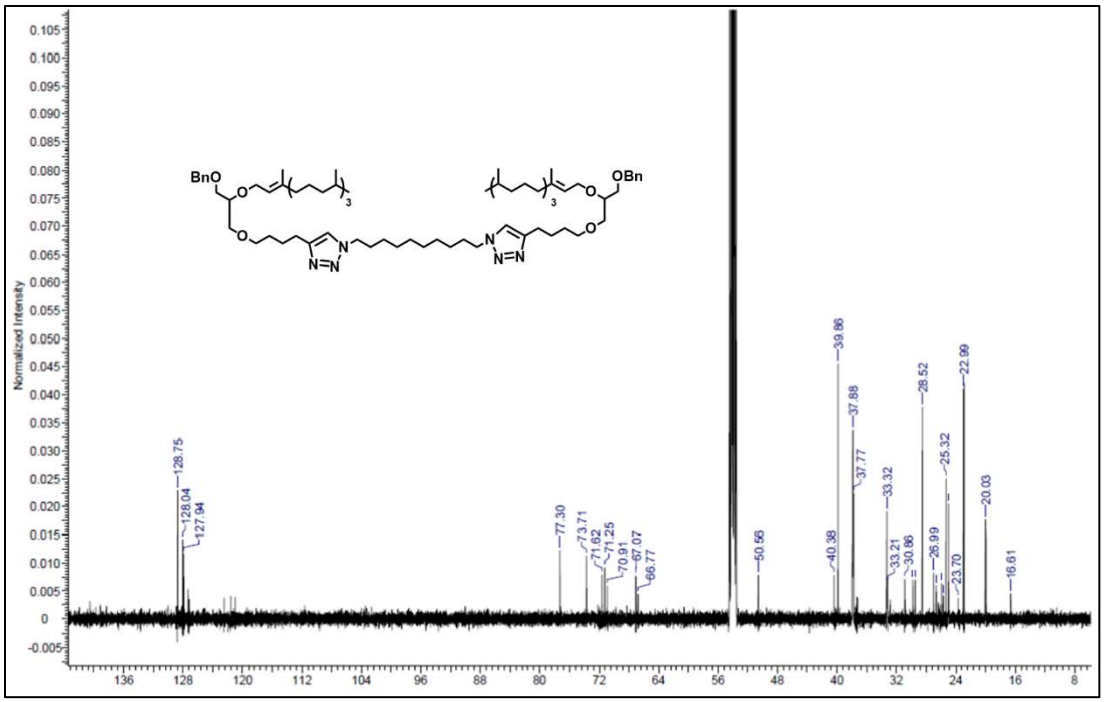

Figure 2.13: ^{13}C NMR of **7**.

1,5-bis(4-(4-(4-(4-(3-(benzyloxy)-2-(((E)-3,7,11,15-tetramethylhexadec-2-en-1-yl)oxy)propoxy)butyl)-1H-1,2,3-triazol-1-yl)butyl)-1H-1,2,3-triazol-1-yl)pentane (8)

Figure 2.14: ^{1}H NMR (400MHz, CD_2Cl_2): δ 0.85 (t, 30H), 1.25 (m, 175H), 1.66 (m, 27H), 1.90 (t, 15H), 2.69 (t, 11H), 3.54 (m, 19H), 4.11 (d, 4H), 4.26 (t, 11H), 4.51 (s, 4 H), 7.32 (m, 12H); **Figure 2.15**: ^{13}C NMR (500MHz, CD_2Cl_2): δ 16.61, 20.03, 22.90, 22.99, 24.96, 25.43, 26.64, 28.52, 28.86, 29.79, 30.18, 30.30, 37.77, 37.87, 39.86, 40.38, 50.20, 66.77, 67.07, 71.24, 73.71, 77.31, 121.13, 121.24, 121.62, 122.49, 127.94, 120.06, 128.75; HRMS (M+H): calculated:1482.1718; found: 1482.1727.

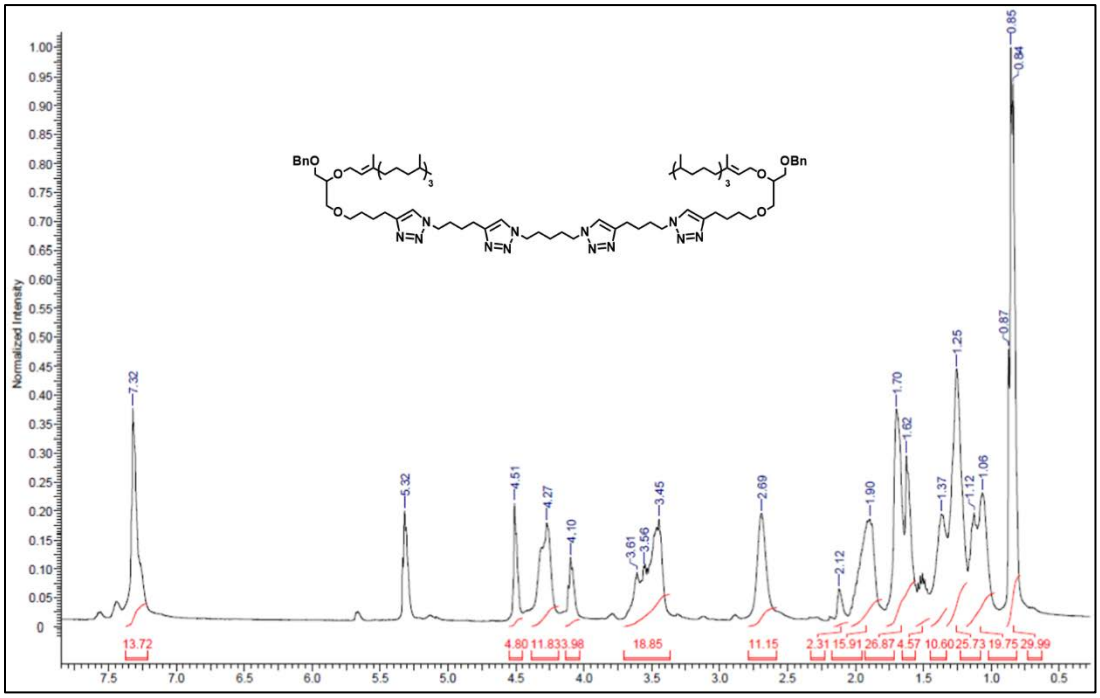

Figure 2.14: ^{1}H NMR of **8**.

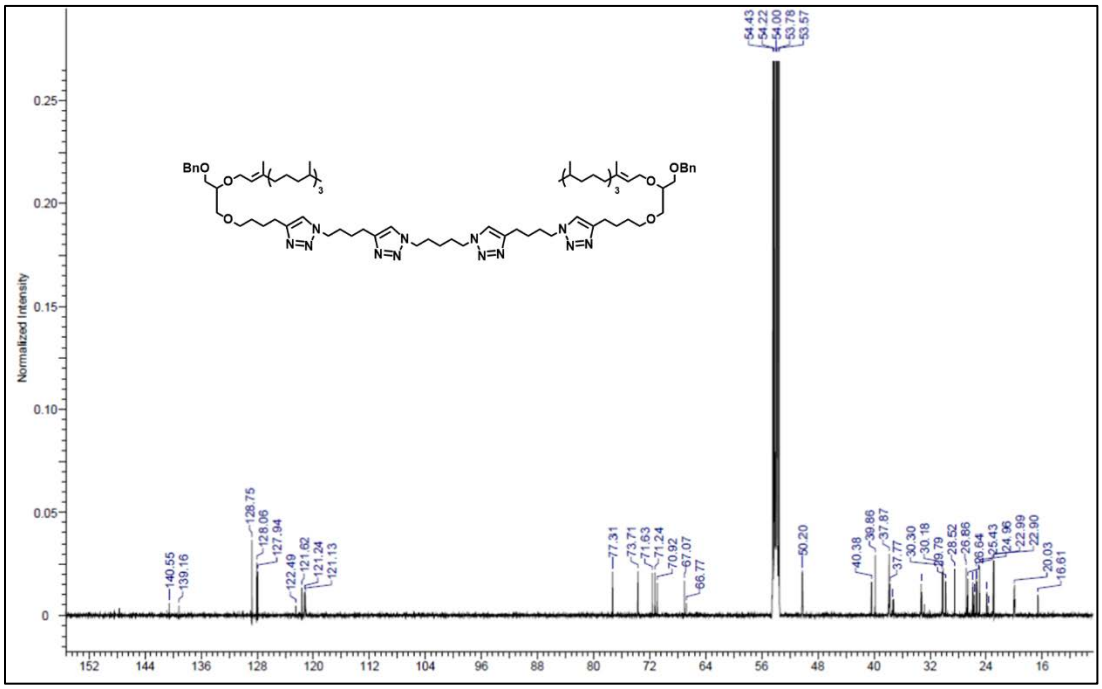

Figure 2.15: ^{13}C NMR of **8**.

1,9-bis(4-(4-(4-(4-(3-(benzyloxy)-2-(((E)-3,7,11,15-tetramethylhexadec-2-en-1-yl)oxy)propoxy)butyl)-1H-1,2,3-triazol-1-yl)butyl)-1H-1,2,3-triazol-1-yl)nonane (9)

Figure 2.16: ^{1}H NMR (400MHz, CD_2Cl_2): δ 0.85 (t, 30H), 1.25 (m, 175H), 1.66 (m, 27H), 1.90 (t, 15H), 2.69 (t, 11H), 3.54 (m, 19H), 4.11 (d, 4H), 4.26 (t, 11H), 4.51 (s, 4 H), 7.32 (m, 12H); **Figure 2.17**: ^{13}C NMR (500MHz, CD_2Cl_2): δ 16.63, 20.03, 22.99, 24.96, 25.31, 27.71, 28.51, 29.79, 32.21, 33.31, 37.21, 37.76, 37.86, 39.85, 40.38, 66.77, 67.07, 70.93, 71.24, 71.64, 73.73, 77.31, 121.61, 122.49, 127.94, 128.04, 128.76, 139.15, 140.54. HRMS (M+Na): calculated:1560.2163; found: 1560.2126.

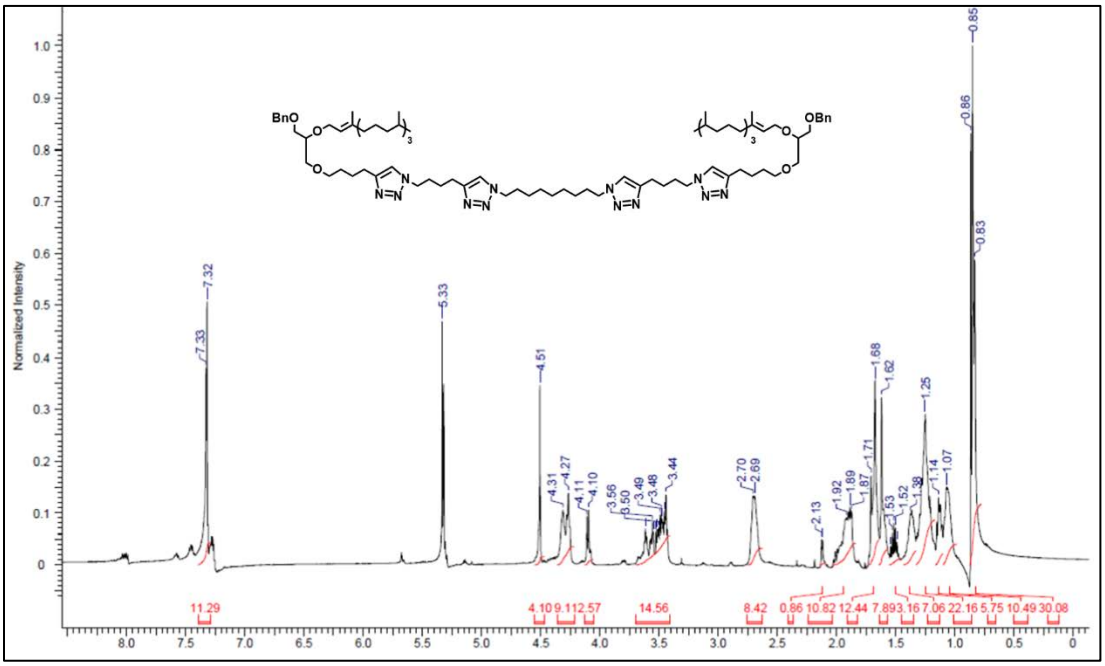

Figure 2.16: ^{1}H NMR of **9**.

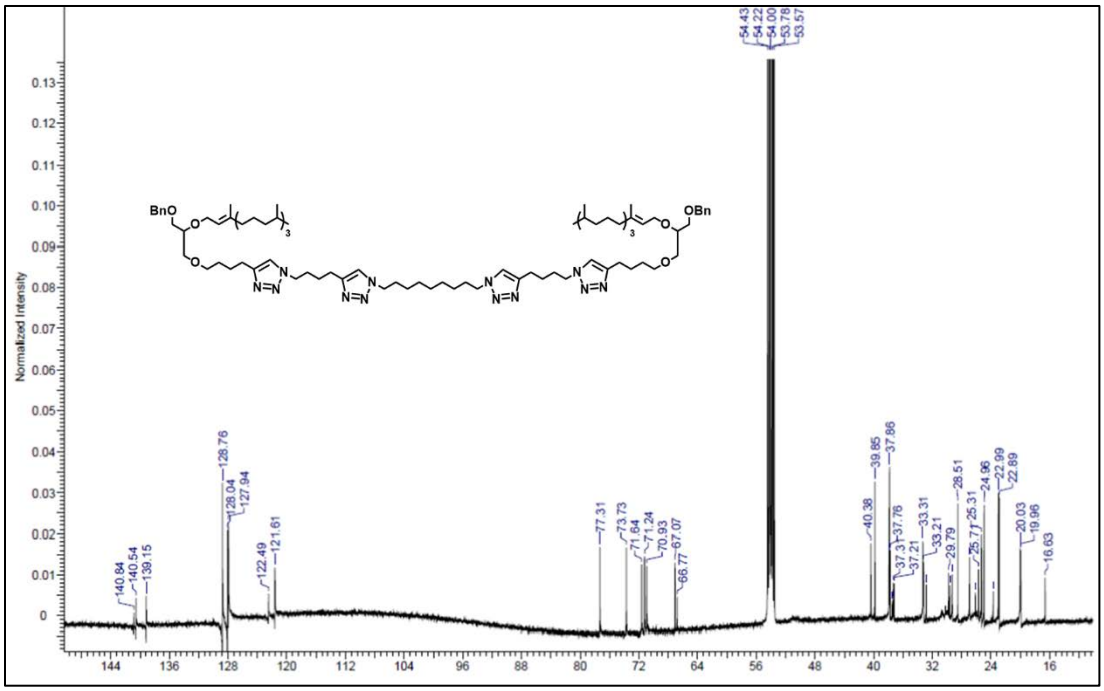

Figure 2.17: ^{13}C NMR of **9**.

1,4-bis((8-(4-(4-(3-(benzyloxy)-2-(((E)-3,7,11,15-tetramethylhexadec-2-en-1-yl)oxy)propoxy)butyl)-1H-1,2,3-triazol-1-yl)octyl)oxy)benzene (10)

Figure 2.18: ^{1}H NMR (400MHz, CD_2Cl_2): δ 0.85 (t, 30H), 1.53 (m, 147H), 1.62 (s, 3H), 1.72 (t, 4H), 1.84 (t, 4H), 2.01 (m, 7H), 2.69 (t, 4H), 3.54 (m, 20H), 3.67 (t, 4H), 4.11 (d, 4H), 4.26 (t, 4H), 4.51 (s, 4 H), 6.78 (s, 4H), 7.32 (m, 12H); **Figure 2.19**: ^{13}C NMR (500MHz, CD_2Cl_2): δ 16.61, 18.63, 19.96, 20.03, 22.99, 24.96, 25.32, 26.16, 28.52, 29.26, 33.31, 37.20, 37.77, 37.87, 39.85, 40.37, 66.79, 67.07, 68.63, 70.88, 71.28, 73.72, 77.27, 84.89, 121.62, 122.48, 127.94, 128.48, 128.75, 139.14, 140.55.

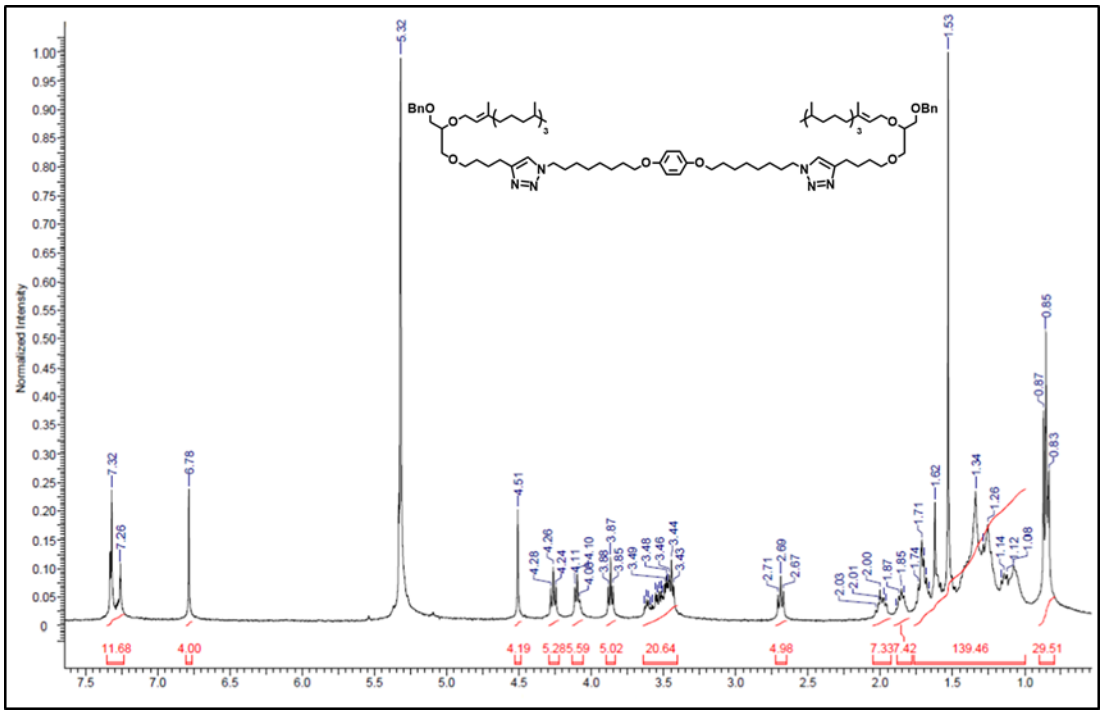

Figure 2.18: ^{1}H NMR of **10**.

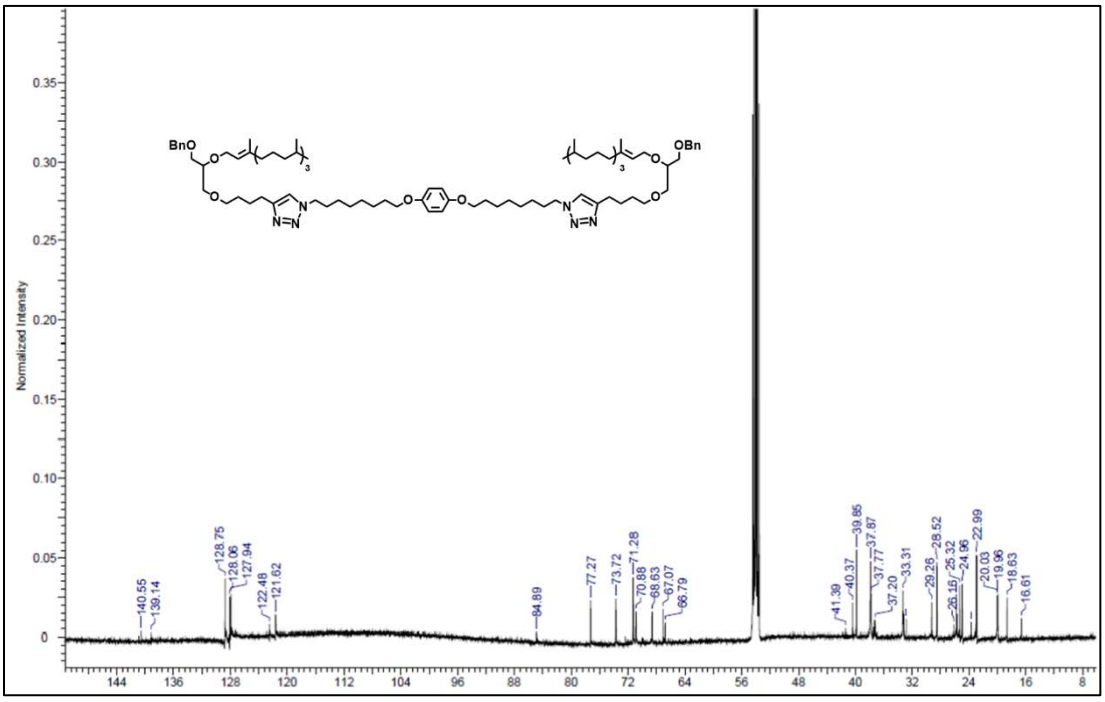

Figure 2.19: ^{13}C NMR of **10**.

3,3'-(((icosane-1,20-diylbis(1H-1,2,3-triazole-1,4-diyl))bis(butane-4,1-diyl))bis(oxy))bis(2-((3,7,11,15-tetramethylhexadecyl)oxy)propan-1-ol) (11)

Figure 2.20: ^{1}H NMR (400MHz, CD_2Cl_2): δ 0.85 (t, 30H), 1.25 (m, 103H), 1.62 (s, 6H), 1.70 (t, 6H), 1.88 (t, 6H), 1.95 (bs, 2H), 2.72 (t, 4H), 3.54 (m, 24H), 4.30 (t, 4H), 7.31 (s, 2H); **Figure 2.21**: ^{13}C NMR (500MHz, CD_2Cl_2): δ 19.94., 19.95, 20.02, 20.04, 20.09, 20.10, 22.94, 25.35, 29.60, 33.37, 37.66, 37.83, 37.99, 50.66, 53.57, 54.00, 63.17, 63.20, 68.96, 68.99, 71.75, 79.05, 79.08, 121.04, 148.30; HRMS (M+Na): calculated:1292.1666; found: 1292.1687.

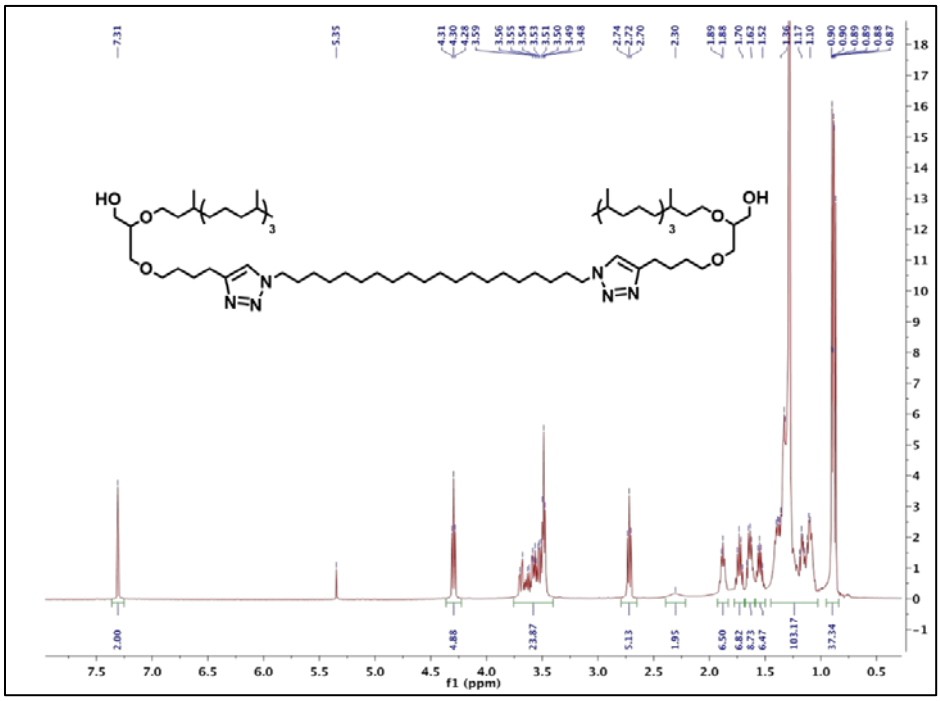

Figure 2.20^{1}H NMR of **11**.

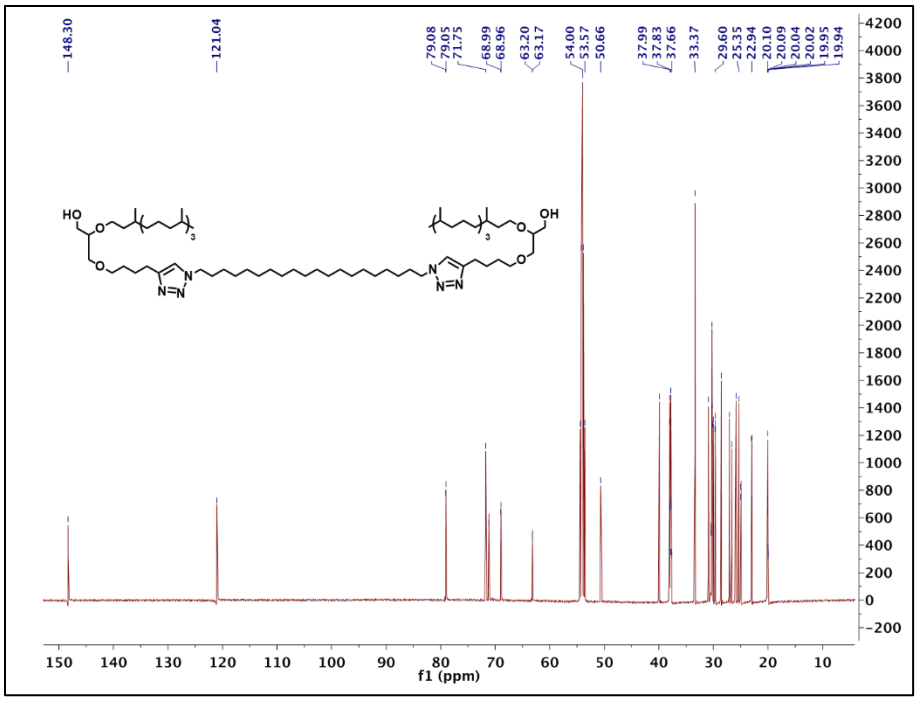

Figure 2.21: ^{13}C NMR of **11**.

3,3'-(((decane-1,10-diylbis(1H-1,2,3-triazole-1,4-diyl))bis(butane-4,1-diyl))bis(oxy))bis(2-((3,7,11,15-tetramethylhexadecyl)oxy)propan-1-ol) (12)

Figure 2.22: ^{1}H NMR (400MHz, CD_2Cl_2): δ 0.86 (t, 30 H), 1.25 (m, 126H), 1.54 (s, 3H), 1.61 (t, 4H), 1.69 (t, 4H), 1.85 (t, 4H), 2.20 (t, 2H), 2.69 (t, 4H), 3.54 (m, 21H), , 4.27 (t, 4H), , 7.28 (m, 2H); **Figure 2.23**: ^{13}C NMR (500MHz, CD_2Cl_2): δ 20.03, 20.09, 22.94, 25.37, 25.90, 27.03, 29.51, 29.82, 30.88, 33.38, 37.85, 38.01, 39.94, 50.64, 63.28, 68.97, 71.19, 71.78,79.03, 121.03, 148.33. HRMS (M+Na): calculated:1152.0101; found: 1152.0091.

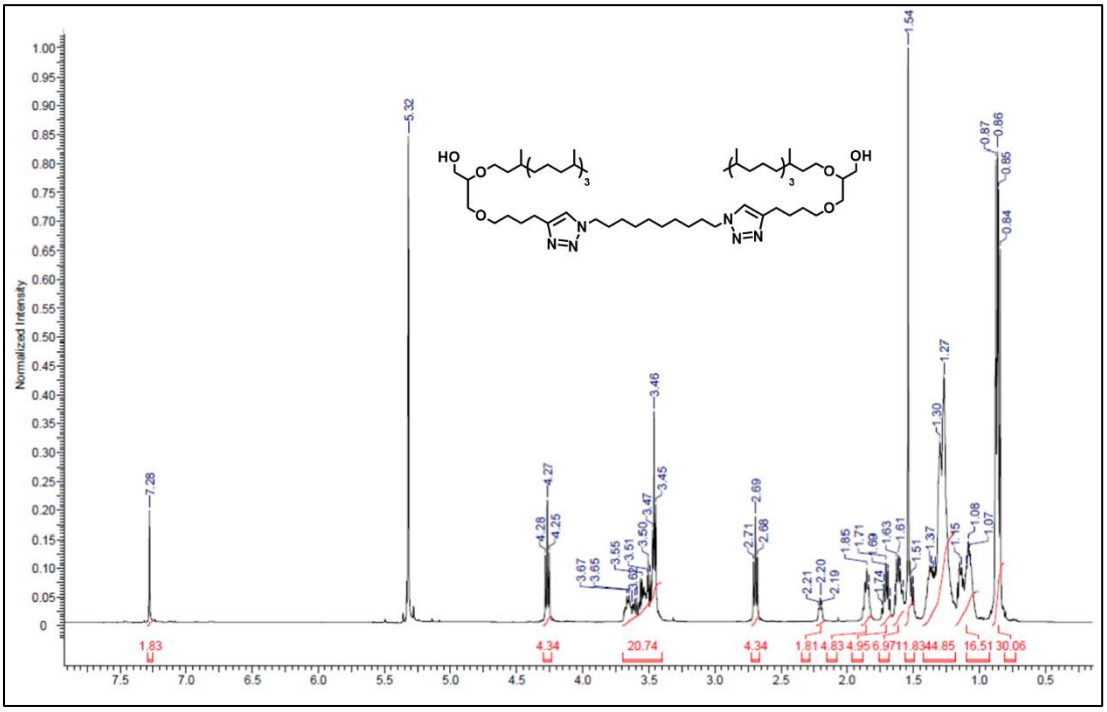

Figure 2.22: ^{1}H NMR of **12**.

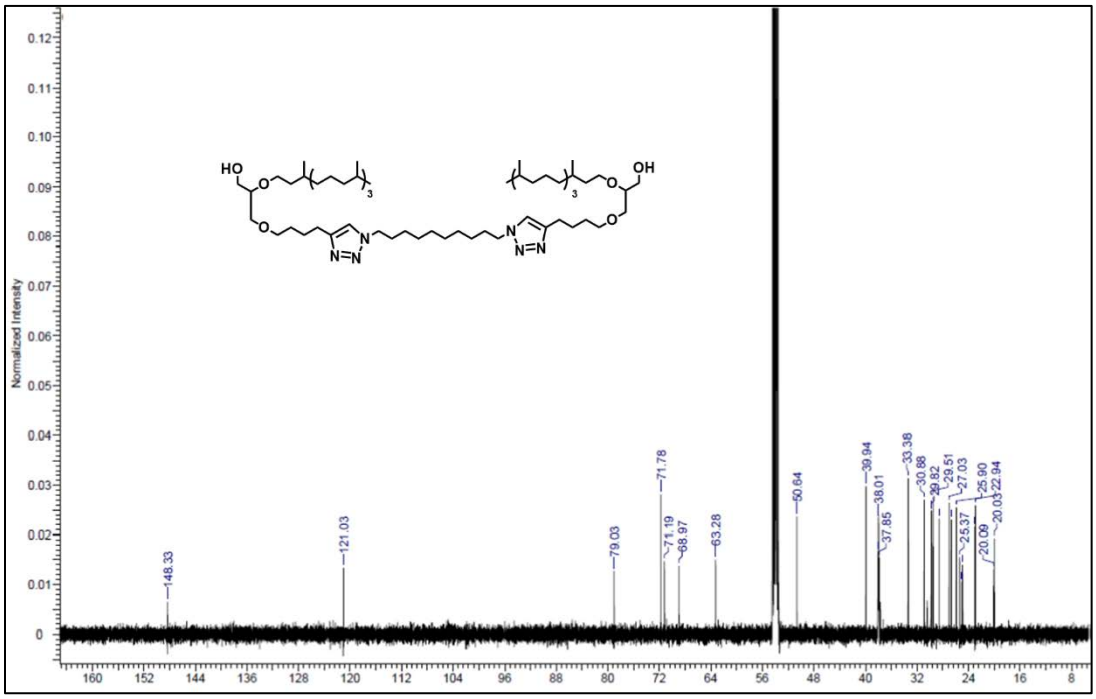

Figure 2.23: ^{1}H NMR of **12**.

3,3'-(((((pentane-1,5-diylbis(1H-1,2,3-triazole-1,4-diyl))bis(butane-4,1-diyl))bis(1H-1,2,3-triazole-1,4-diyl))bis(butane-4,1-diyl))bis(oxy))bis(2-((3,7,11,15-tetramethylhexadecyl)oxy)propan-1-ol) (13)

Figure 2.24: ^{1}H NMR (400MHz, CD_2Cl_2): δ 0.85 (t, 30H), 1.25 (m, 175H), 1.66 (m, 28H), 1.90 (m, 12H), 2.69 (m, 11H), 3.54 (m, 21H), 4.29 (t, 11H), 7.29 (m, 4H); **Figure 2.25**: ^{13}C NMR (500MHz, CD_2Cl_2): δ 94.27, 94.34, 94.42, 97.28, 97.38, 99.35, 99.79, 101.24, 102.90, 104.55, 107.70, 111.99, 112.08, 112.15, 114.24, 124.59, 124.67, 137.49, 143.26, 145.40, 146.05, 153.33, 195.57, 195.66, 203.31, 204.39, 222.06, 222.71.

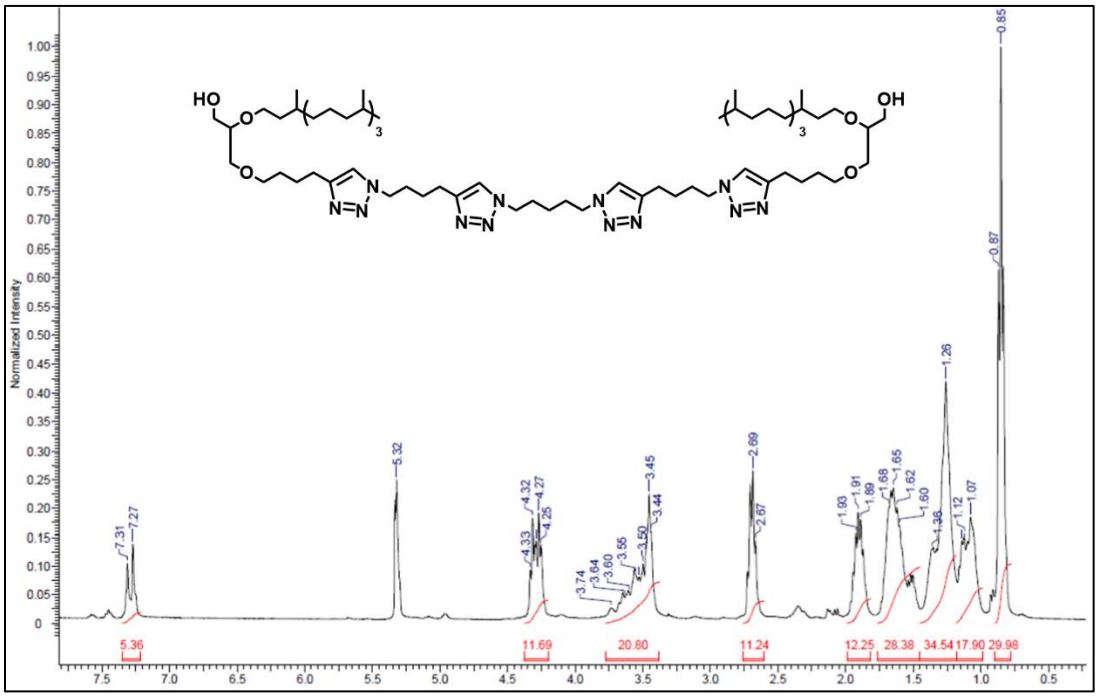

Figure 2.24: ^{1}H NMR of **13**.

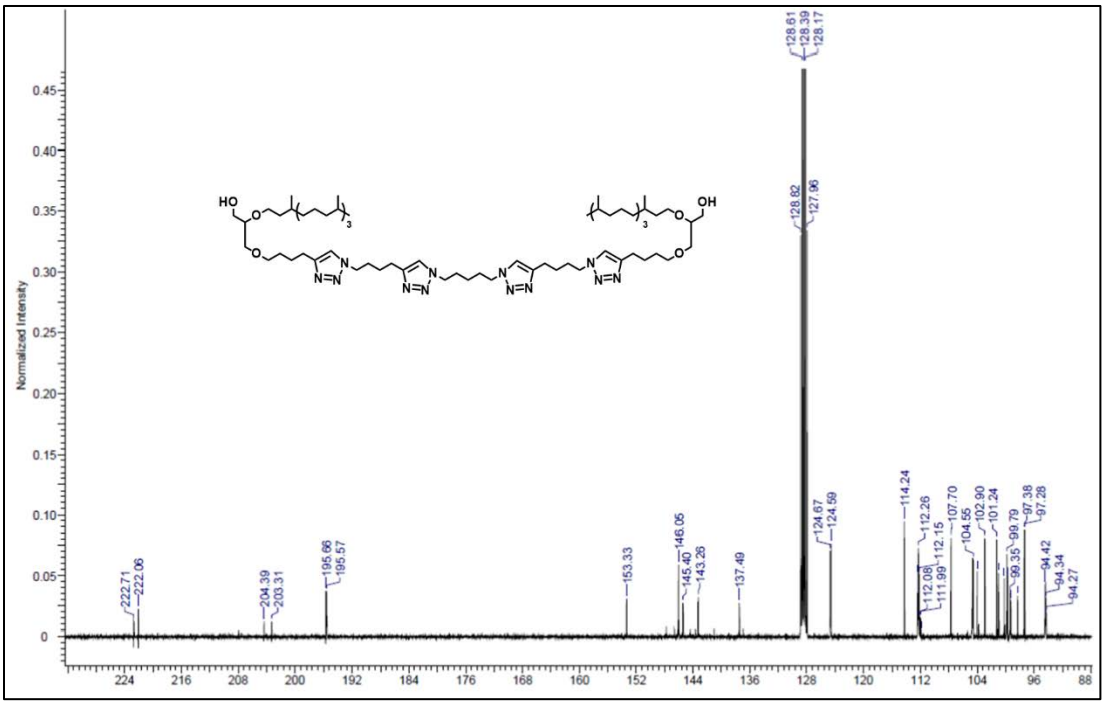

Figure 2.25: ^{13}C NMR of **13**.

3,3'-(((((nonane-1,9-diylbis(1H-1,2,3-triazole-1,4-diyl))bis(butane-4,1-diyl))bis(1H-1,2,3-triazole-1,4-diyl))bis(butane-4,1-diyl))bis(oxy))bis(2-((3,7,11,15-tetramethylhexadecyl)oxy)propan-1-ol) (14)

Figure 2.26: ^{1}H NMR (400MHz, CD_2Cl_2): δ 0.85 (t, 30H), 1.25 (m, 179H), 1.57 (m, 26H), 1.66 (m, 10H), 1.83 (m, 6H), 1.90 (m, 6H), 2.69 (m, 10H), 3.54 (m, 21H), 4.29 (m, 10H), 7.29 (m, 4H); **Figure 2.27**: ^{13}C NMR (500MHz, CD_2Cl_2): δ 42.99, 43.06, 45.91, 46.60, 48.00, 48.53, 49.93, 51.53, 52.65, 3.80, 56.34, 60.80, 60.91, 62.89, 73.30, 73.61, 86.17, 91.91, 94.06, 94.70, 101.98, 144.16, 170.59, 171.36.

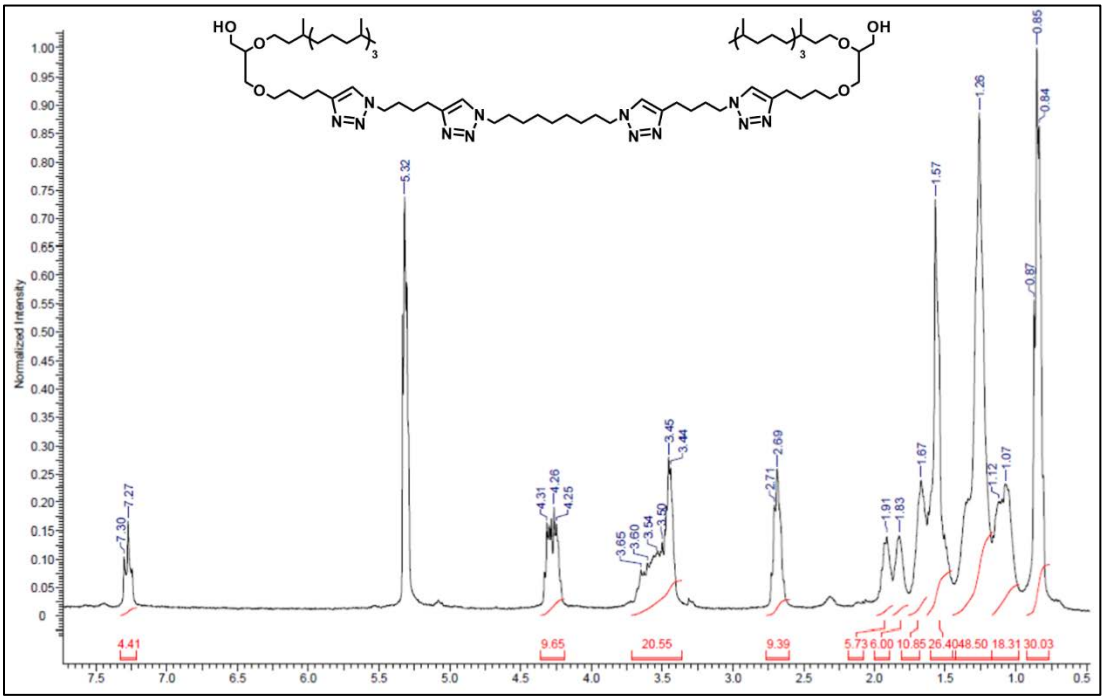

Figure 2.26: ^{1}H NMR of **14**.

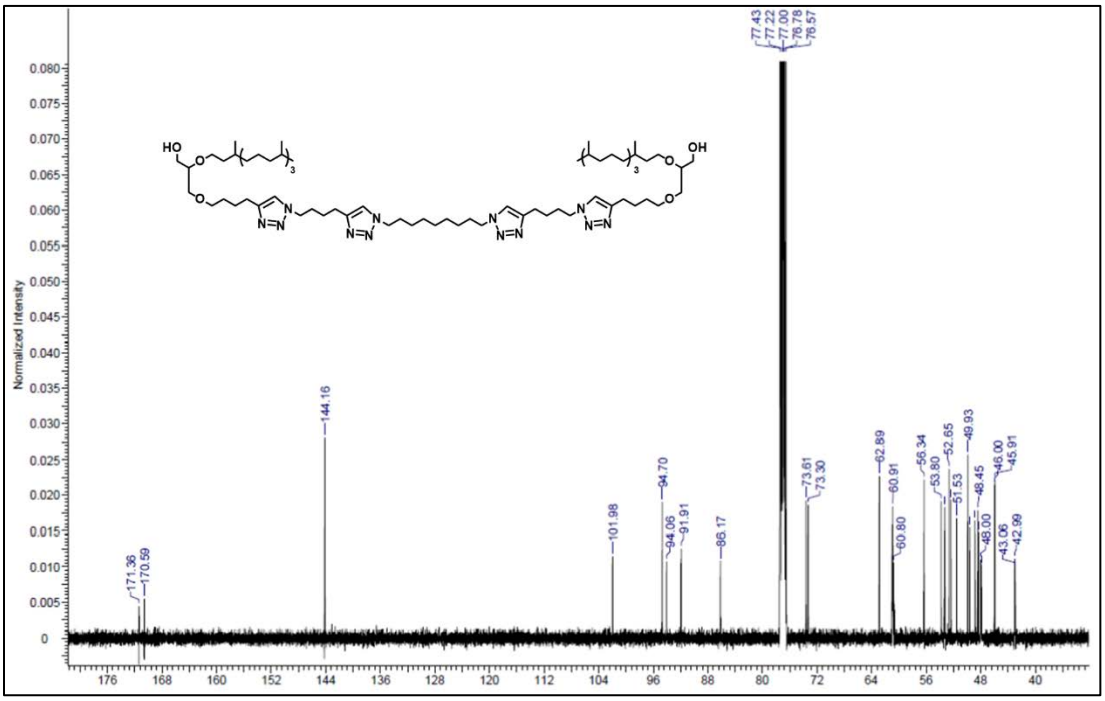

Figure 2.27: ^{13}C NMR of **10**.

3,3'-(((((1,4-phenylenebis(oxy))bis(octane-8,1-diyl))bis(1H-1,2,3-triazole-1,4-diyl))bis(butane-4,1-diyl))bis(oxy))bis(2-((3,7,11,15-tetramethylhexadecyl)oxy)propan-1-ol) (15)

Figure 2.28: ^{1}H NMR (400MHz, CD_2Cl_2): δ 0.85 (t, 30H), 1.33 (m, 118H), 1.84 (t, 6H), 2.21 (bs, 2H), 2.69 (t, 4H), 3.54 (m, 26H), 3.86 (t, 4H), 4.11 (d, 4H), 4.26 (t, 4H), 6.78 (s, 4H), 7.27 (m, 2H); **Figure 2.29**: ^{13}C NMR (500MHz, CD_2Cl_2): δ 19.96, 20.03, 22.84, 23.03, 25.90, 26.50, 26.69, 27.02, 30.88, 33.38, 38.01, 39.93, 50.63, 63.25, 68.97, 69.07, 71.19, 71.78, 79.03,115.80, 121.03, 148.33, 150.58, 153.77.

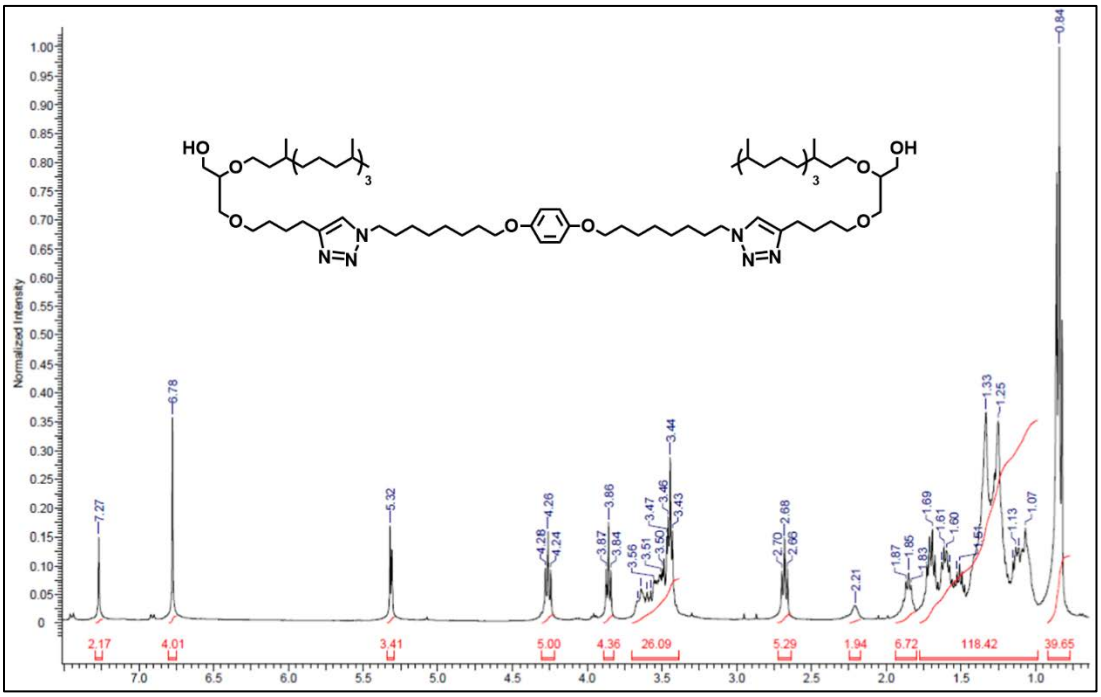

Figure 2.28: ^{1}H NMR of **14**.

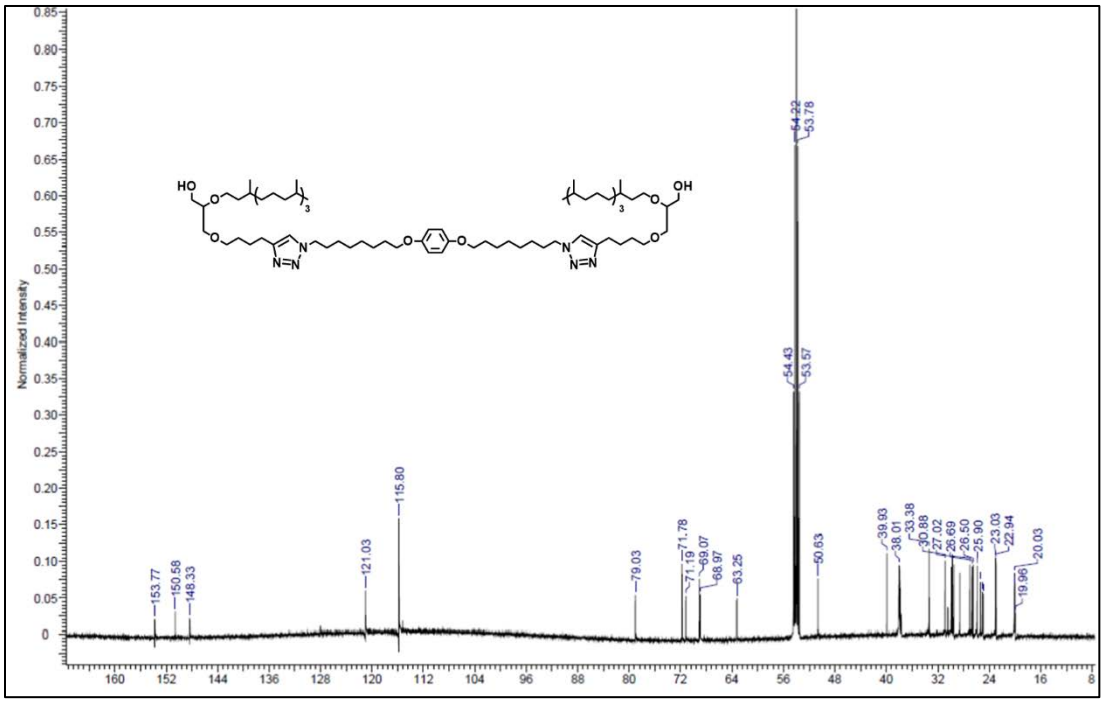

Figure 2.29: ^{13}C NMR of **14**.

Eicosane-1,20-diol (16)

To a flame-dried round bottom flask, eicosanedioic acid (5.7164 g, 16.700 mmol) was suspended in dry THF (500 mL) and refluxed to increase solubility. LAH (1.3943 g, 41.750 mmol) was slowly added and the reaction was refluxed for 4 hours. The reaction cooled over an ice bath and quenched with water until gas formation ceased. The reaction mixture was extracted using chloroform (3x 100 mL). The organic layers were combined, dried over $MgSO_4$, filtered, and concentrated via rotary evaporator. The product was obtained as a white powder (1.9422 g, 6.1790 mmol, 37%). **Figure 2.30**: ^{1}H NMR (400MHz, CD_2Cl_2): δ 1.29 (m, 35H), 1.53 (m, 4H), , 3.54 (t, 4H).

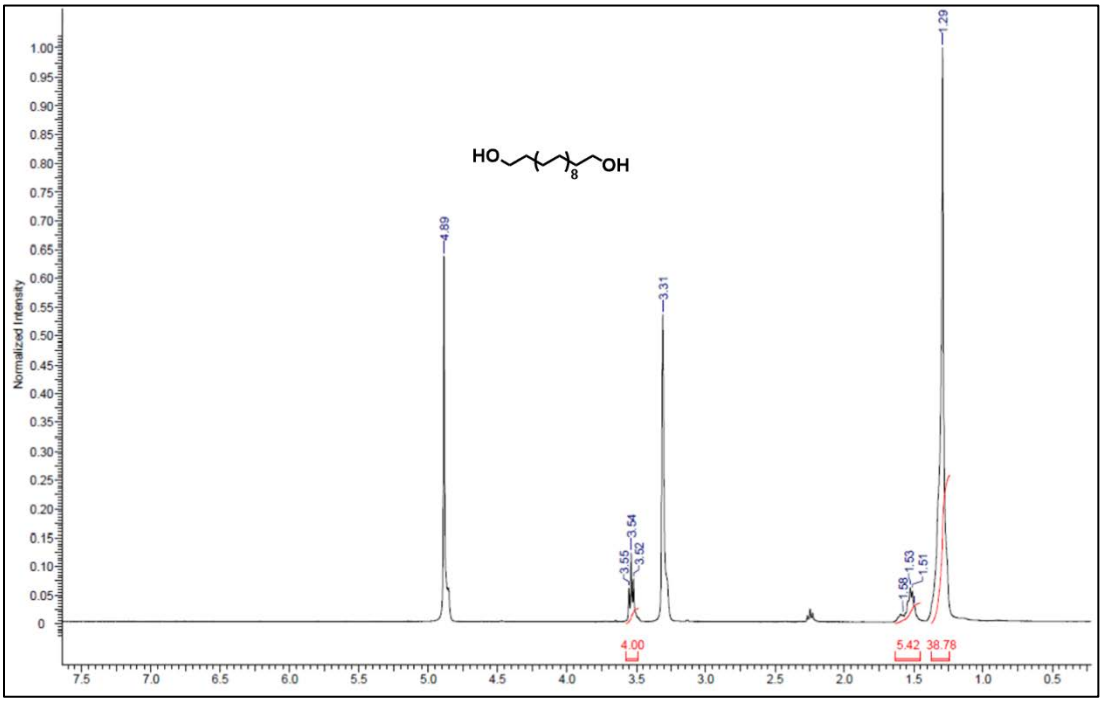

Figure 2.30: ^{1}H NMR of **16**.

1,20-dibromoeicosane (17)

To a round bottom flask, compound **16** (1.0387 g, 3.3045 mmol) was suspended in hydrobromic acid 45% wt. solution (20 mL) and refluxed overnight. The reaction was diluted with water (100 mL) and extracted with chloroform. The organic layers were combined, dried over $MgSO_4$, filtered, and concentrated via rotary evaporator. The product was filtered through 1 inch silica plug using 2:1 hexanes/DCM to afford a white powder (1.1004 g, 2.5115 mmol, 76%). **Figure 2.31**: ^{1}H NMR (400MHz, CD_2Cl_2): δ 1.26 (m, 35H), 1.43 (m, 4H), 1.86 (m, 4H), 3.42 (t, 4H).

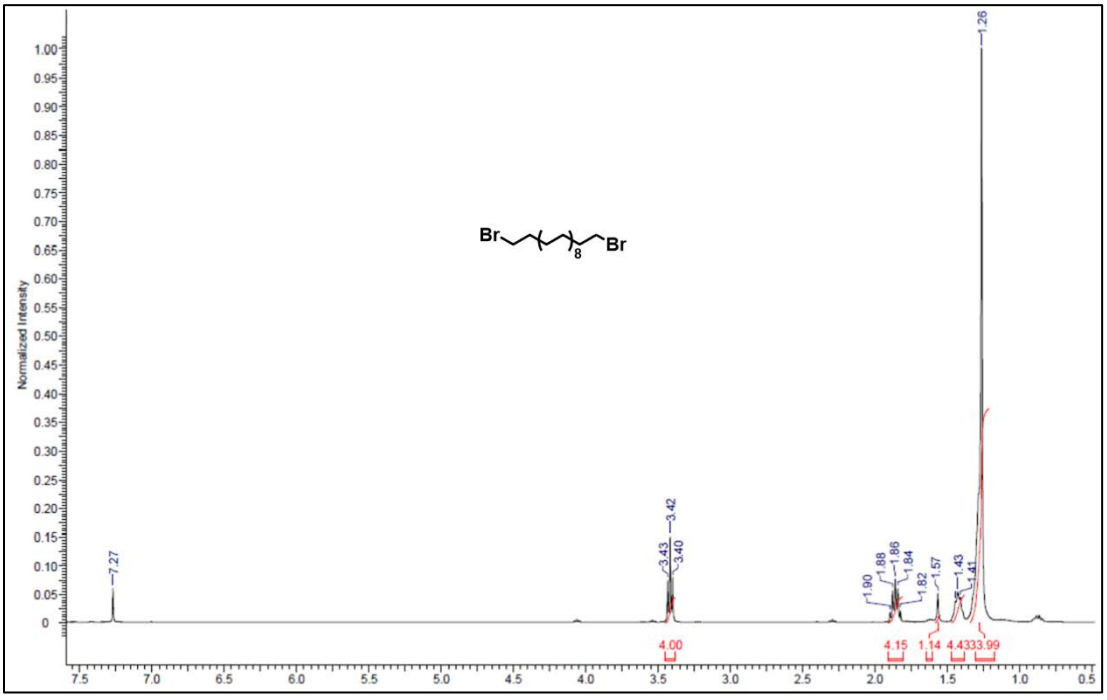

Figure 2.31: ^{1}H NMR of **17**.

1,5-diazidopentane (18)

Figure 2.32: ^{1}H NMR (400MHz, CD_2Cl_2): δ 1.48 (m, 2H), 1.64 (t, 4H) , 3.30 (t, 4H).

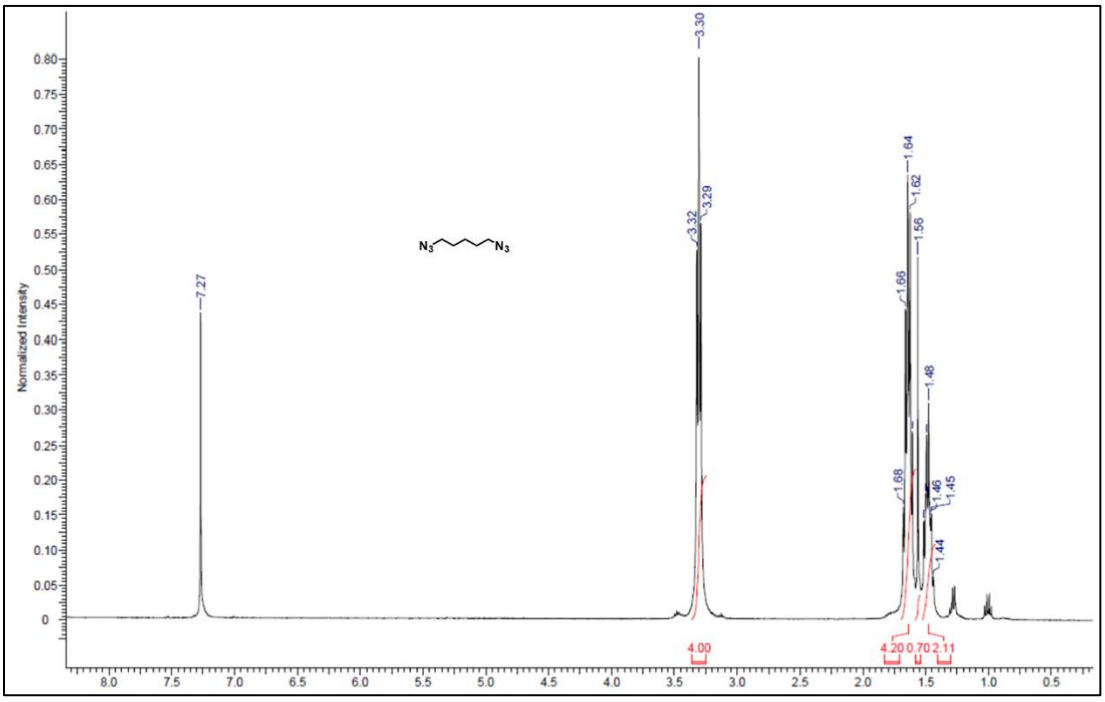

Figure 2.32: ^{1}H NMR of **18**.

1,5-bis(4-(4-chlorobutyl)-1H-1,2,3-triazol-1-yl)pentane (20)

Figure 2.33: ^{1}H NMR (400MHz, CD_2Cl_2): δ 1.29 (m, 4H), 1.54 (m, 4H), 1.85 (m, 18H), 2.70 (t, 4H), 3.57 (t, 4H), 4.27 (t, 4H), 7.27(s, 2H); **Figure 2.34**: ^{13}C NMR (500MHz, CD_2Cl_2): δ 23.93, 25.34, 27.21, 30.19, 32.56, 45.55, 50.22, 121.16, 147.95; ESI-*m*/*z* 387.57 $[M+H]^+$.

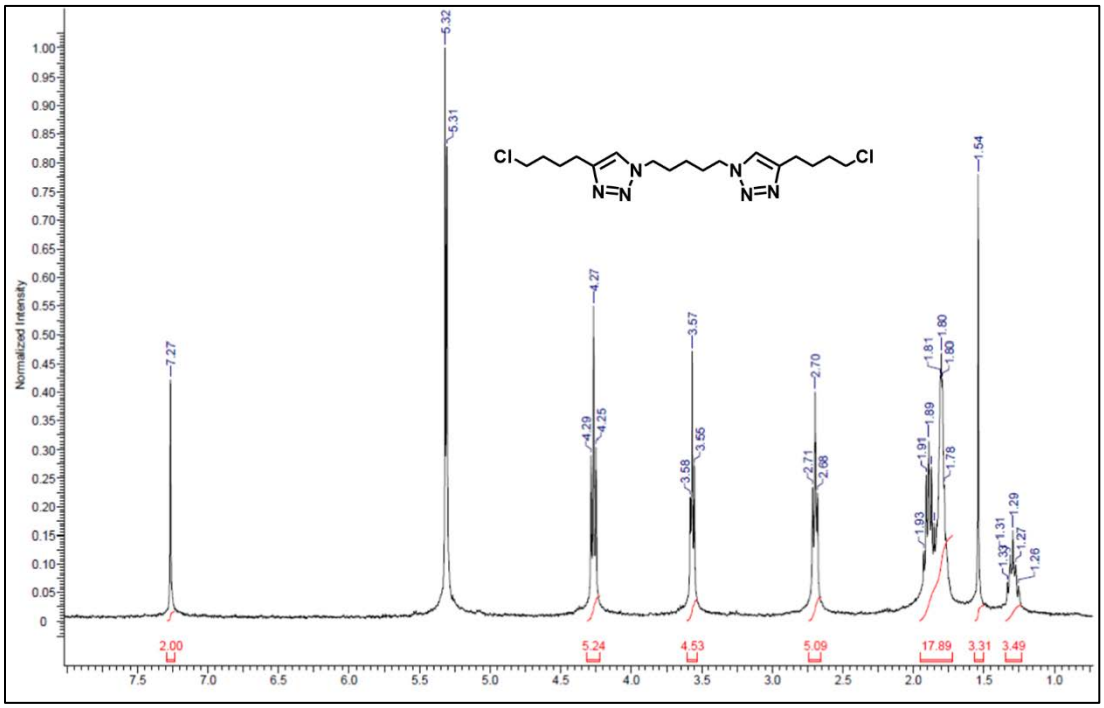

Figure 2.33: ^{1}H NMR of **20**.

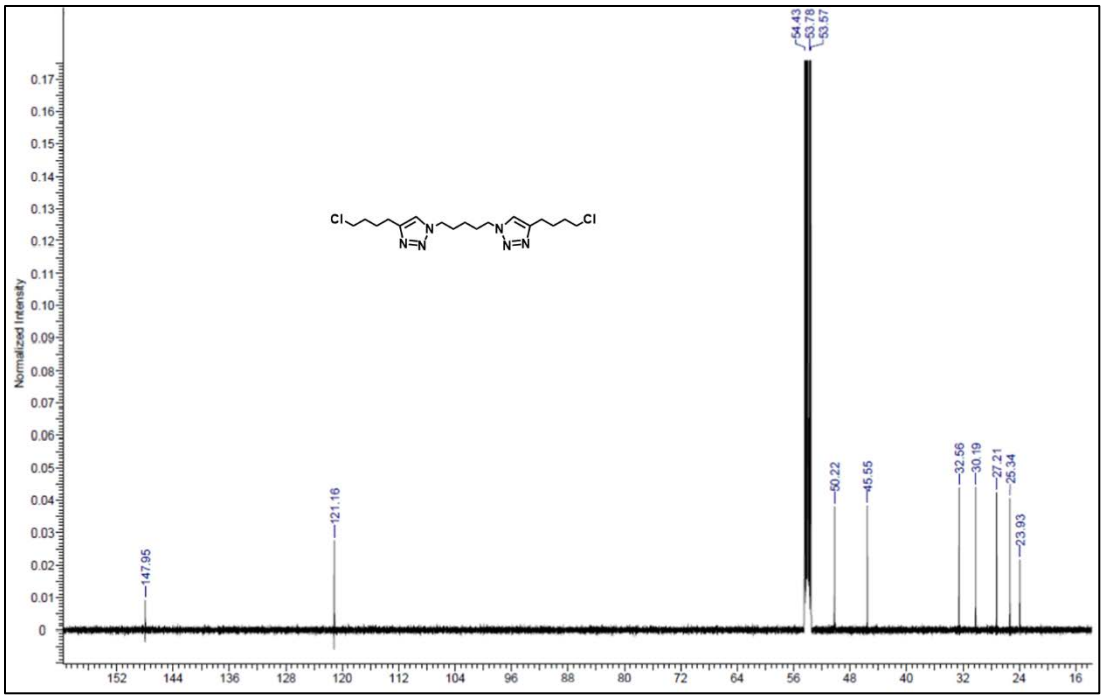

Figure 2.34: ^{13}C NMR of **20**.

1,9-bis(4-(4-chlorobutyl)-1H-1,2,3-triazol-1-yl)nonane (21)

Figure 2.35: ^{1}H NMR (400MHz, CD_2Cl_2): δ 1.41 (m, 6H), 1.62 (m, 9H), 1.85 (t, 11H), 1.94 (t, 6H), 2.77 (t, 4H), 3.29 (t, 4H), 3.58 (t, 4H), 4.34 (t, 4H), 7.27 (s, 1H), 7.29 (s, 1H).

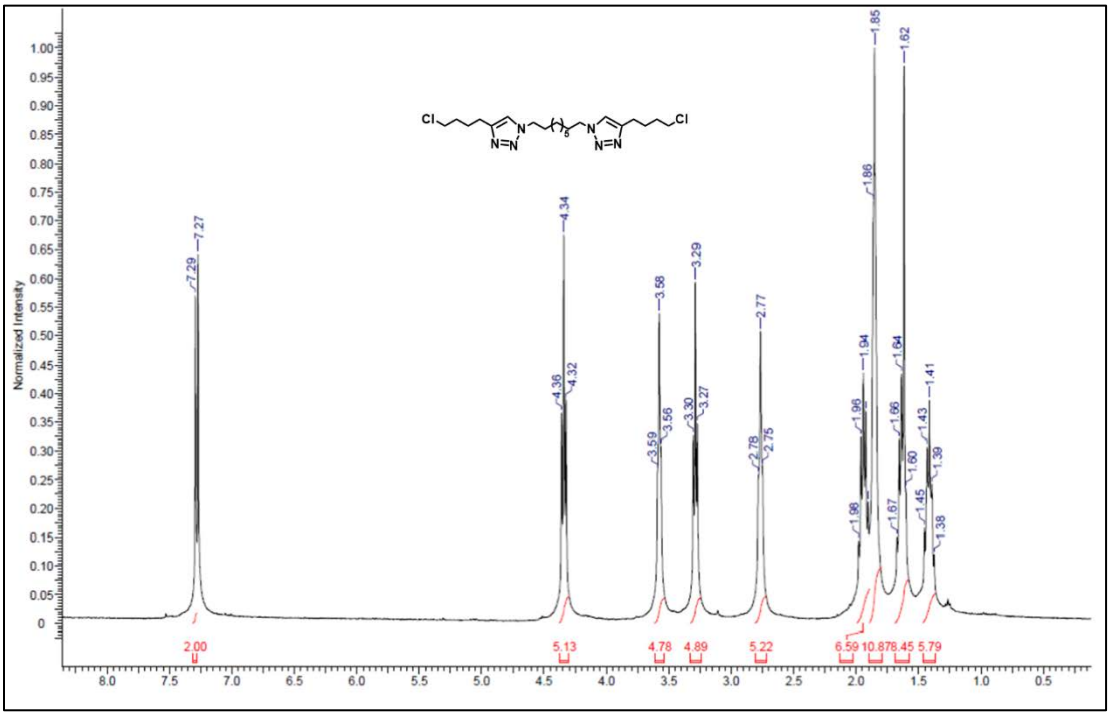

Figure 2.35: ^{1}H NMR of **21**.

1-azido-8-bromo-octane (22)

To a round bottom flask, 1,8-dibromooctane (2.4813 g, 9.1914 mmol) and sodium azide (627.31 mg, 9.6509 mmol) were dissolved in DMSO (25 mL). The reaction was diluted with water (100 mL) after the reaction was stirred for 4 hours. The product was then extracted with ether (3 x 30mL) from the aqueous mixture. The organic layers were combined, dried over $MgSO_4$, filtered, and concentrated under reduced pressure. The product was purified by flash chromatography using hexanes. The product was obtained as a clear oil (921.08 mg, 3.9523

mmol, 43%). **Figure 2.36**: ^{1}H NMR (400MHz, CD_2Cl_2): δ 1.43 (m, 6H), 1.60 (t, 2H), 1.86 (t, 2H), 3.27 (t, 2H), 3.42 (t, 2H).

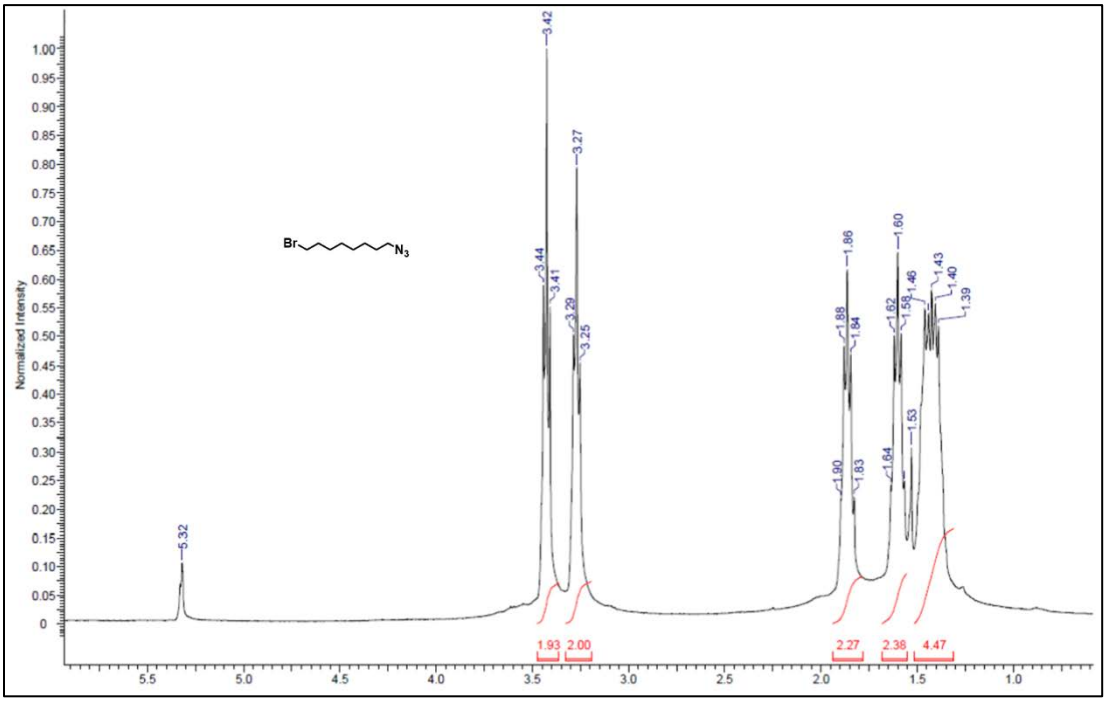

Figure 2.36: ^{1}H NMR of **22**.

1,20-diazidoicosane (**K1)**

Figure 2.37: ^{1}H NMR (400MHz, CD_2Cl_2): δ 1.26 (m, 32H), 1.55 (m, 4H), 3.25 (t, 4H).

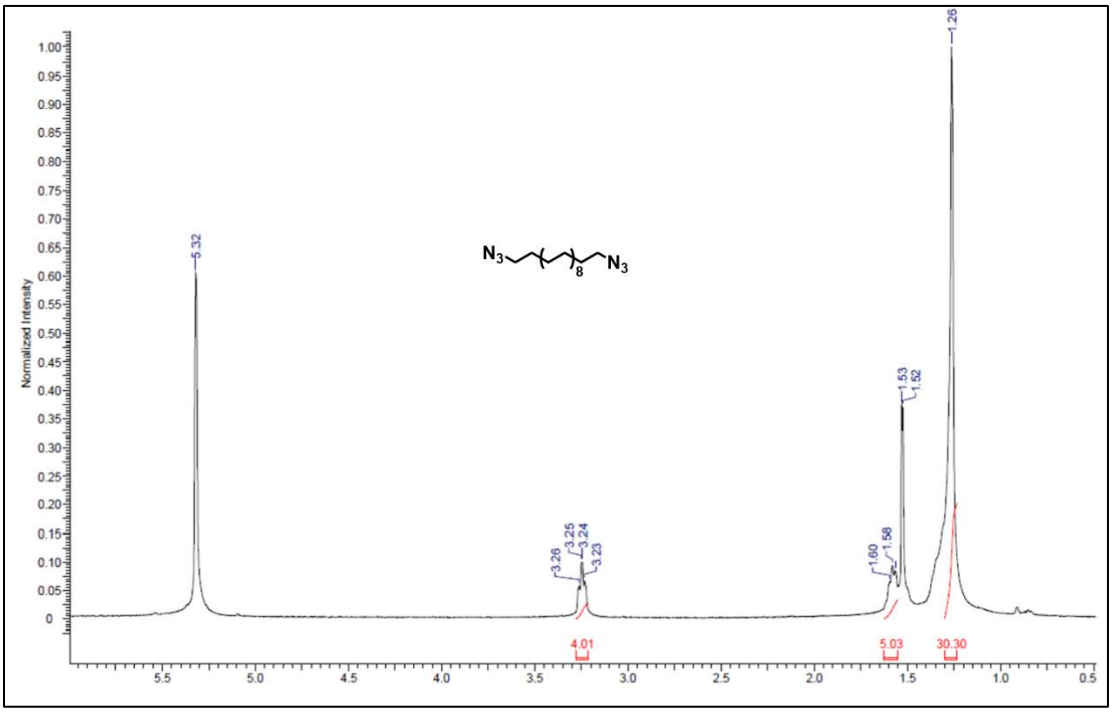

Figure 2.37: ^{1}H NMR of **K1**.

1,10-diazidodecane (**K2)**

Figure 2.38: ^{1}H NMR (400MHz, CD_2Cl_2): δ 1.30 (m, 12H), 1.58 (m, 4H), 3.25 (t, 4H).

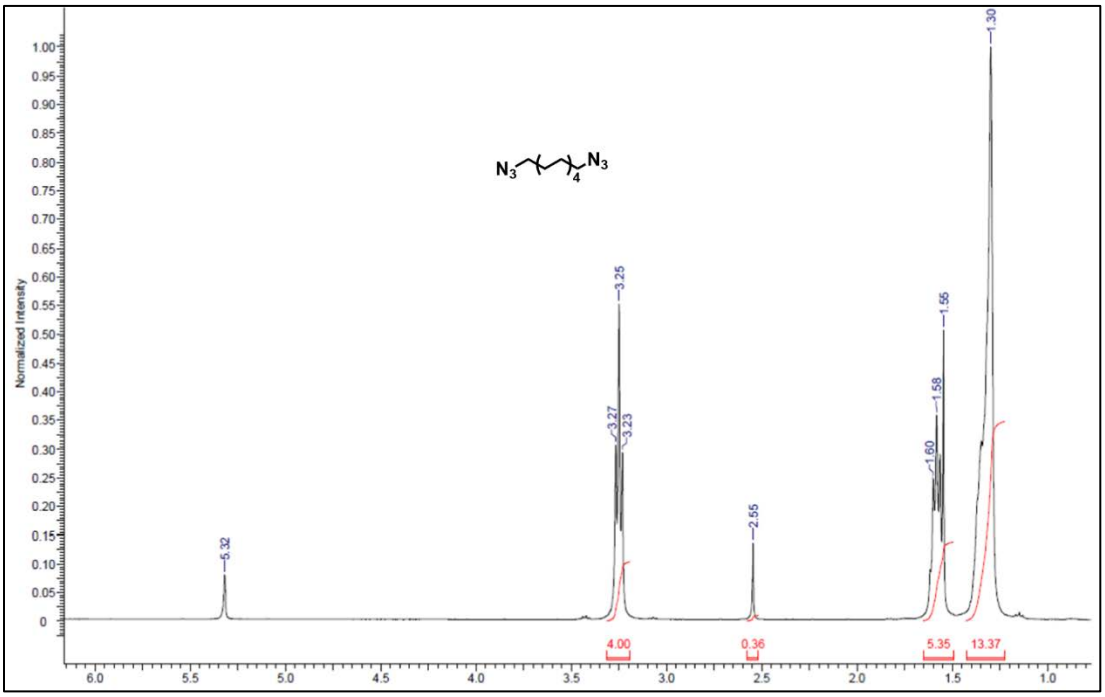

Figure 2.38: ^{1}H NMR of **K2**.

1,5-bis(4-(4-azidobutyl)-1H-1,2,3-triazol-1-yl)pentane (K3)

Figure 2.39: ^{1}H NMR (400MHz, CD_2Cl_2): δ 1.30 (m, 4H), 1.58 (m, 4H), 1.66 (m, 4H), 1.74 (m, 10H), 1.90 (m, 5H), 2.71 (t, 4H), 3.31 (t, 4H), 4.28 (t, 4H), 7.26 (s, 2H).

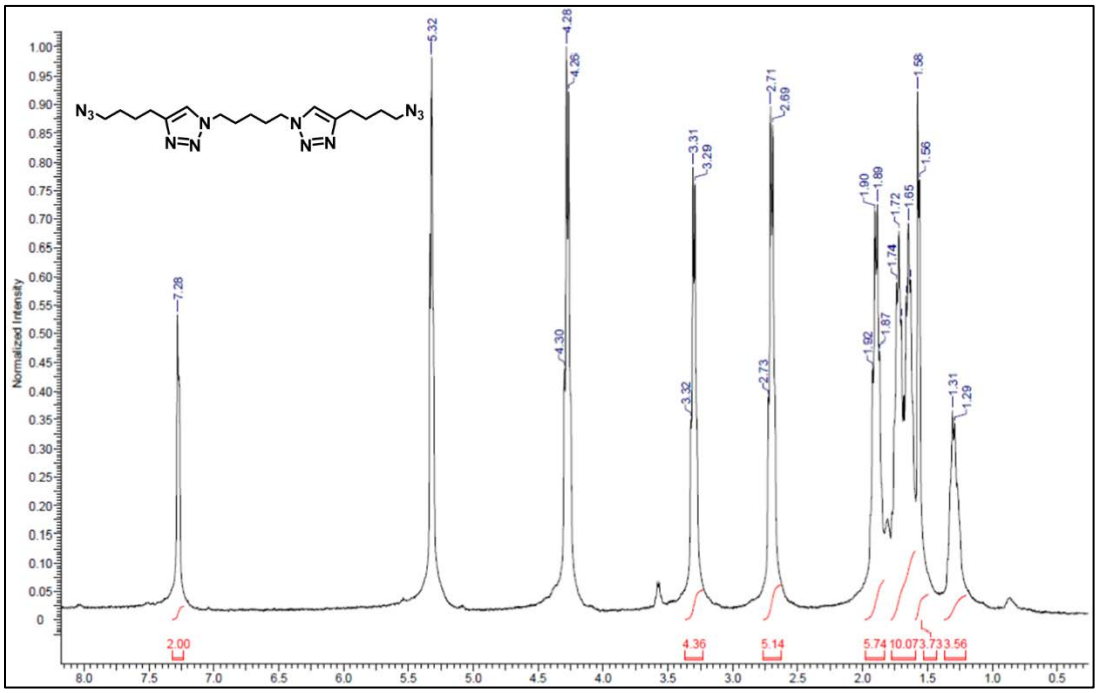

Figure 2.39: ^{1}H NMR of **K3**.

1,9-bis(4-(4-azidobutyl)-1H-1,2,3-triazol-1-yl)nonane (K4)

Figure 2.40: ^{1}H NMR (400MHz, CD_2Cl_2): δ 1.29 (m, 13H), 1.59 (m, 6H), 1.66 (m, 5H), 1.74 (m, 5H), 1.85 (m, 5H), 2.71 (t, 4H), 3.30 (t, 4H), 4.27 (t, 4H), 7.29 (s, 2H).

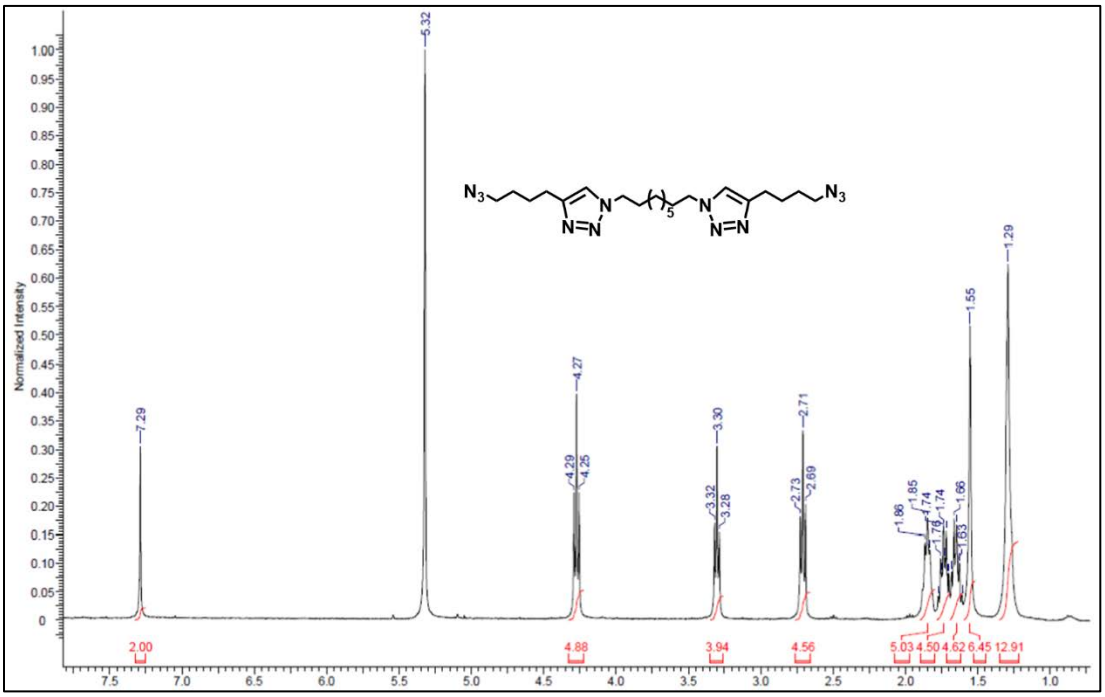

Figure 2.40: ^{1}H NMR of **K4**.

1,4-bis((8-azidooctyl)oxy)benzene (K5)

Figure 2.41: ^{1}H NMR (400MHz, CD_2Cl_2): δ 1.36 (m, 20H), 1.59 (m, 7H), 1.73 (t, 4H), 3.26 (t, 4H), 3.88 (t, 4H), 6.79 (s, 4H).

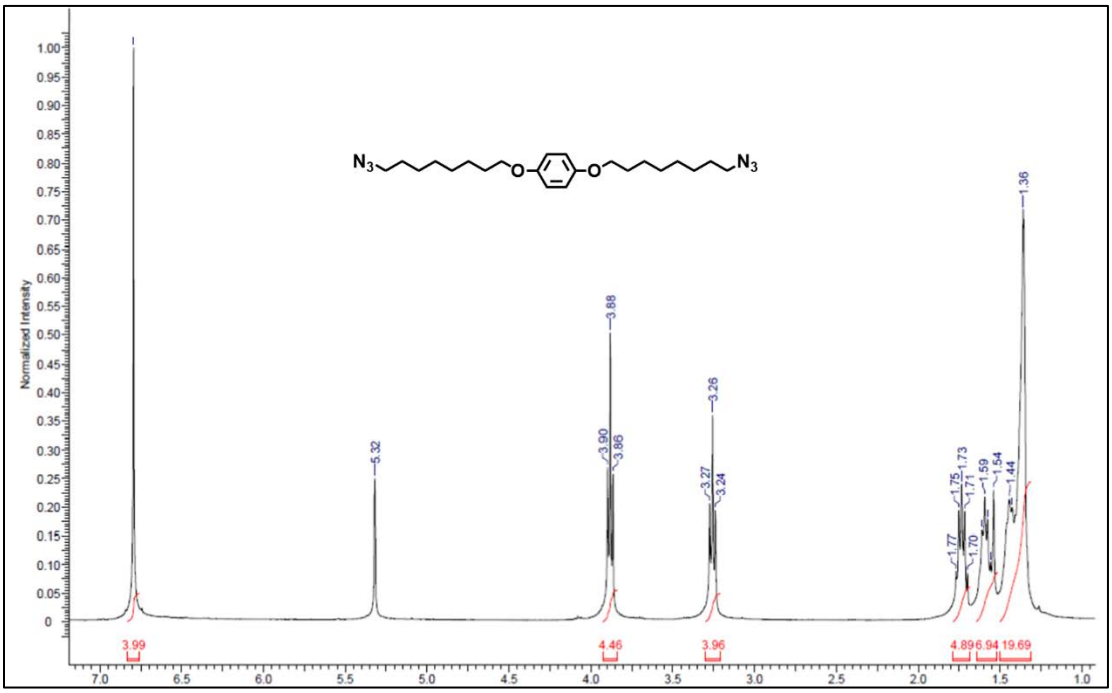

Figure 2.41: ^{1}H NMR of **K5**.

(((icosane-1,20-diylbis(1H-1,2,3-triazole-1,4-diyl))bis(butane-4,1-diyl))bis(oxy))bis(2-((3,7,11,15-tetramethylhexadecyl)oxy)propane-3,1-diyl) bis(2-(trimethylammonio)ethyl) bis(phosphate) (**ATL1)**

Figure 2.42: ^{1}H NMR (400MHz, CD_2Cl_2): δ 0.85 (t, 30H), 1.20 (m, 109H), 1.62 (s, 6H), 1.6 (t, 6H), 1.83 (t, 5H), 2.35 (t, 4H), 3.15 (s, 18H), 3.25 (s, 7H), 3.29 (s, 2H), 3.42 (m, 7H), 3.54 (m, 38H), 3.82 (t, 4H), 4.14 (t, 4H), 4.25 (t, 4H), 4.55 (s, 10H), 7.47 (s, 2H); **Figure 2.43**: ^{13}C NMR (500MHz, CD_2Cl_2): δ 19.75, 19.83, 19.87, 20.02, 25.46, 28.67, 30.24, 33.51, 37.93, 38.09, 38.35, 48.43, 48.78, 49.12, 53.57, 59.65, 59.69, 69.42, 69.54, 71.00, 71.85, 78.71, 122.2, 148.5; HRMS (M+H): calculated: 1600.2956; found: 1600.2991.

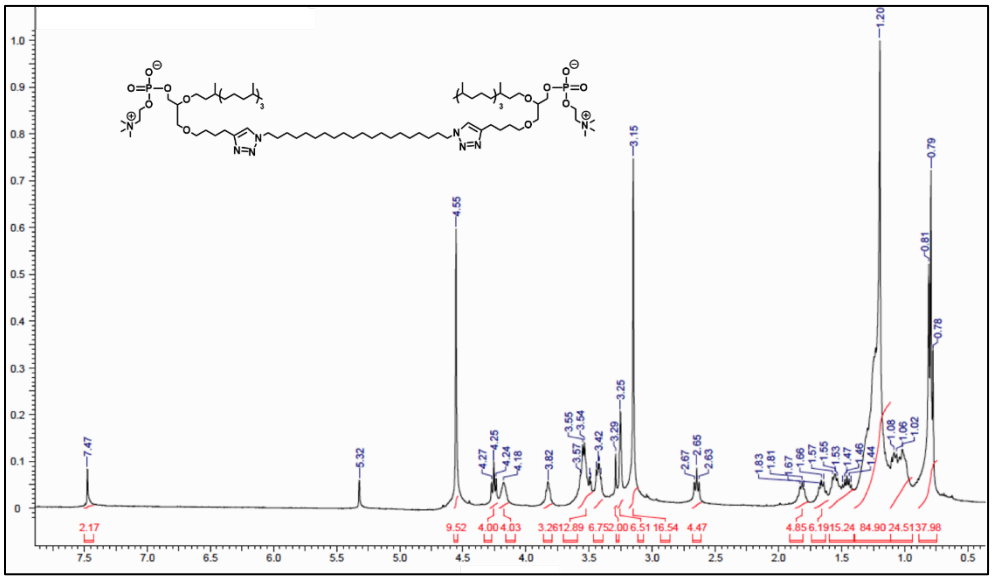

Figure 2.42: ^{1}H NMR of **ATL1**.

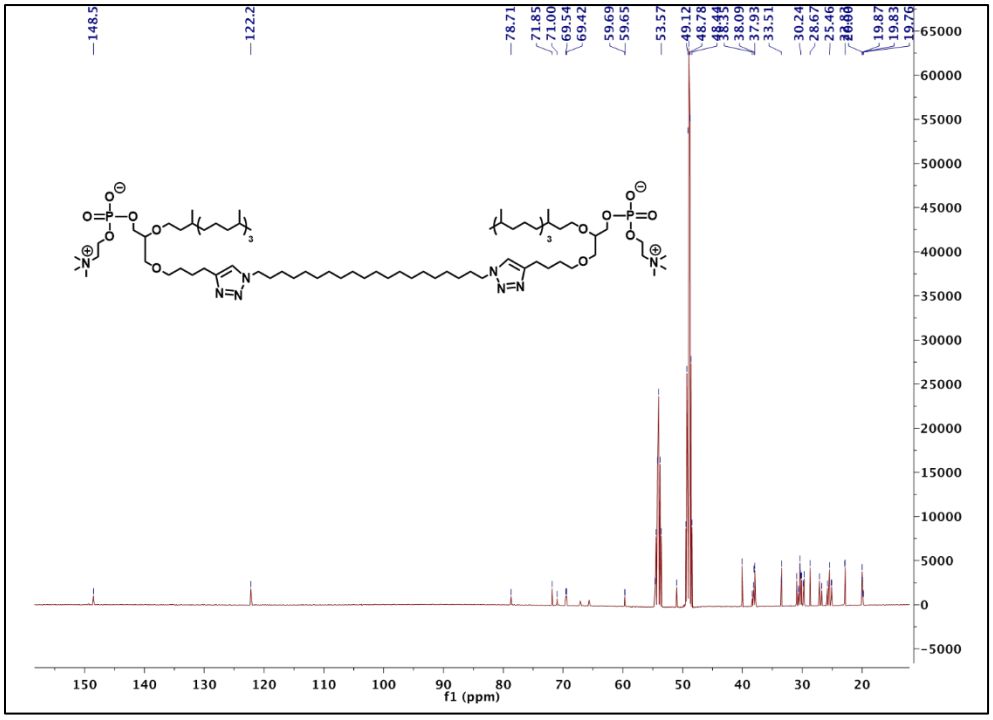

Figure 2.43: ^{13}C NMR of **ATL1**.

(((decane-1,10-diylbis(1H-1,2,3-triazole-1,4-diyl))bis(butane-4,1-diyl))bis(oxy))bis(2-((3,7,11,15-tetramethylhexadecyl)oxy)propane-3,1-diyl) bis(2-(trimethylammonio)ethyl) bis(phosphate) (**ATL 2)**

Figure 2.44: ^{1}H NMR (400MHz, CD_2Cl_2): δ 0.86 (t, 30 H), 1.25 (m, 126H), 1.54 (s, 3H), 1.61 (t, 4H), 1.69 (t, 4H), 1.85 (t, 4H), 2.69 (t, 4H), 3.00 (m, 30H), 3.44 (bs, 9H), 3.54 (m, 5H), 3.60 (m, 8H), 4.02 (m, 8H), 4.30 (m, 5H), 4.50 (t, 2H), 7.42 (m, 2H); **Figure 2.45**: ^{13}C NMR (500MHz, CD_2Cl_2): δ 19.96, 20.05, 22.92, 23.02, 25.03, 25.34, 25.68, 28.51, 29.09, 30.22, 30.64, 33.34, 37.80, 37.87, 38.15, 39.87, 46.40, 55.29.

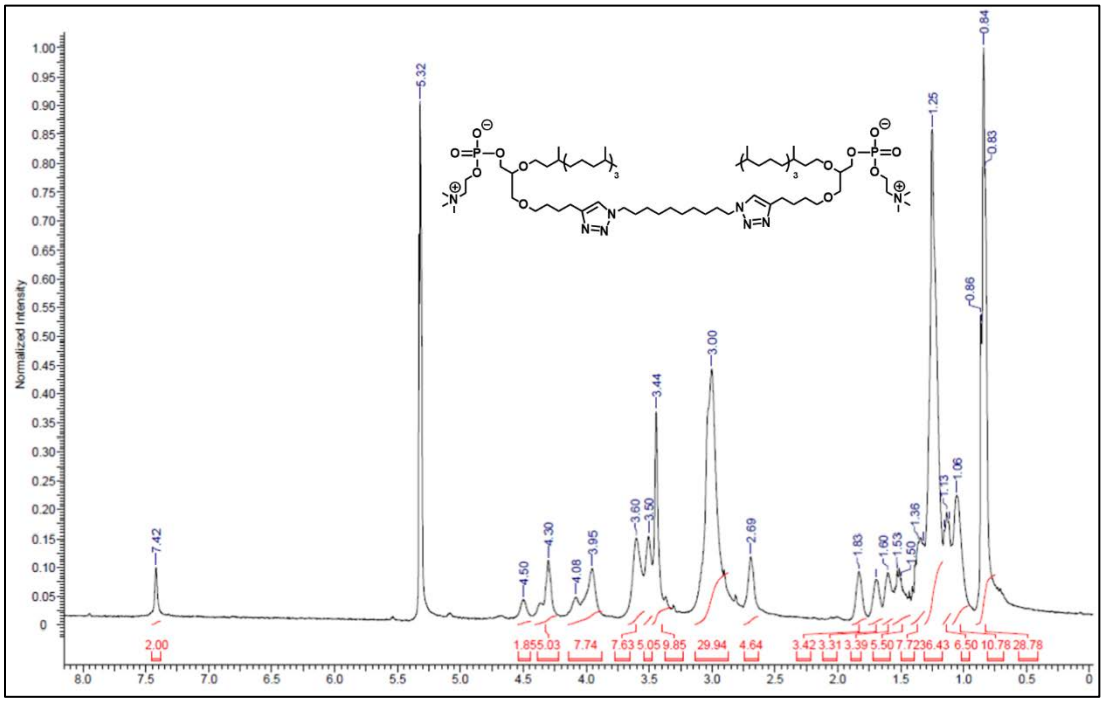

Figure 2.44: ^{1}H NMR of **ATL2**.

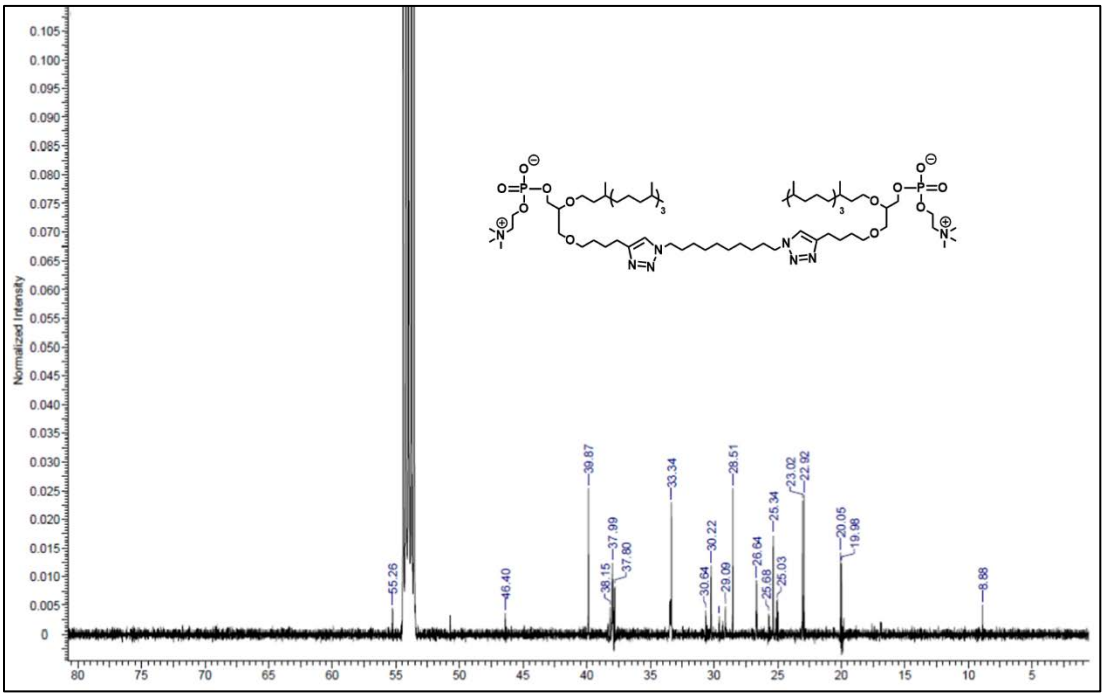

Figure 2.45: ^{13}C NMR of **ATL2**.

(((((pentane-1,5-diylbis(1H-1,2,3-triazole-1,4-diyl))bis(butane-4,1-diyl))bis(1H-1,2,3-triazole-1,4-diyl))bis(butane-4,1-diyl))bis(oxy)) bis(2-((3,7,11,15-tetramethylhexadecyl)oxy)propane-3,1-diyl)bis(2-(trimethylammonio)ethyl) bis(phosphate) (**ATL 3)**

Figure 2.46: ^{1}H NMR (400MHz, CD_2Cl_2): δ 0.85 (t, 30H), 1.25 (m, 135H), 1.63 (m, 13H), 1.85 (m, 8H), 2.66 (m, 16H), 3.29 (m, 76H), 3.81 (m, 11H), 4.33 (t, 11H), 7.52 (m, 4H). HRMS (M+2H): calculated:818.6137; found: 818.6134.

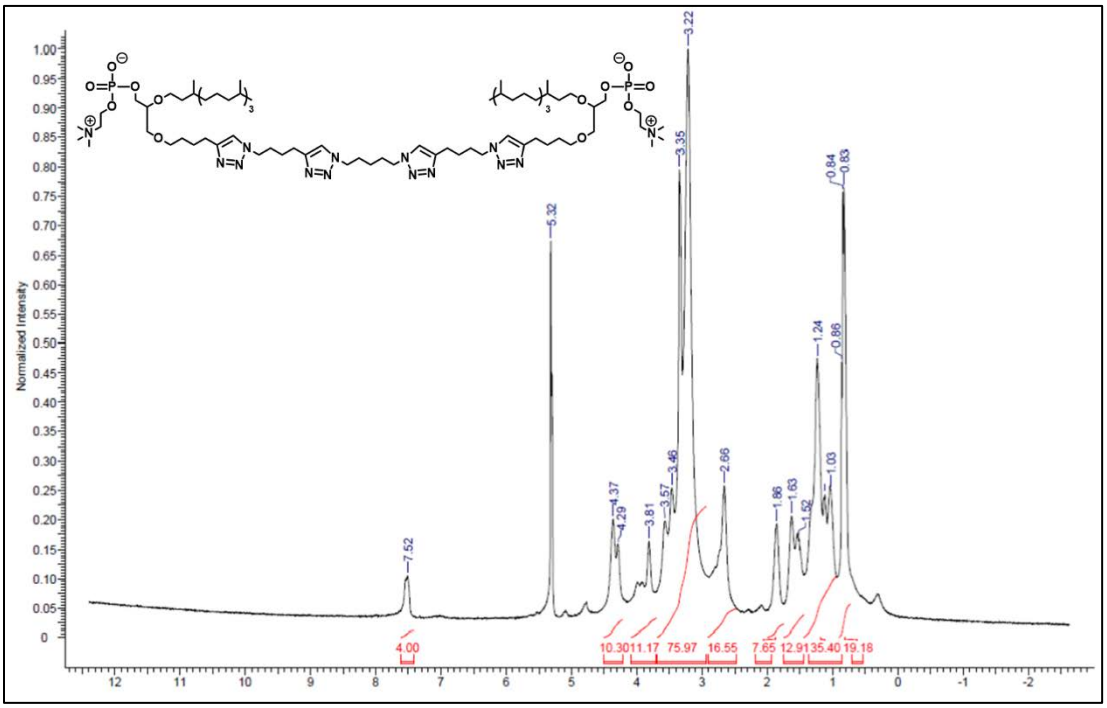

Figure 2.46: ^{1}H NMR of **ATL3**.

(((((nonane-1,9-diylbis(1H-1,2,3-triazole-1,4-diyl))bis(butane-4,1-diyl))bis(1H-1,2,3-triazole-1,4-diyl))bis(butane-4,1-diyl))bis(oxy))bis(2-((3,7,11,15-tetramethylhexadecyl)oxy)propane-3,1-diyl) bis(2-(trimethylammonio)ethyl) bis(phosphate) (**ATL 4)**

Figure 2.47: ^{1}H NMR (400MHz, CD_2Cl_2): δ 0.85 (t, 30H), 1.23 (m, 40H), 1.65 (m, 13H), 1.85 (m, 7H), 2.70 (m, 9H), 3.02 (m, 6H), 3.41 (m, 28H), 4.27 (m, 39H), 4.93 (s, 2H), 7.44 (s, 2H), 7.53 (s, 2H); **Figure 2.48**: ^{13}C NMR (500MHz, CD_2Cl_2): δ 19.83, 19.88, 19.95, 20.03, 20.10, 22.97, 25.00, 25.08, 25.37, 26.52, 26.88, 28.54, 29.54, 29.97, 30.14, 30.57, 33.48, 33.55, 33.39, 37.86, 37.98, 38.06, 38.23, 39.92, 50.37, 50.50, 60.49, 66.75, 71.79; HRMS (M+2Na): calculated: 868.6269; found: 868.6248.

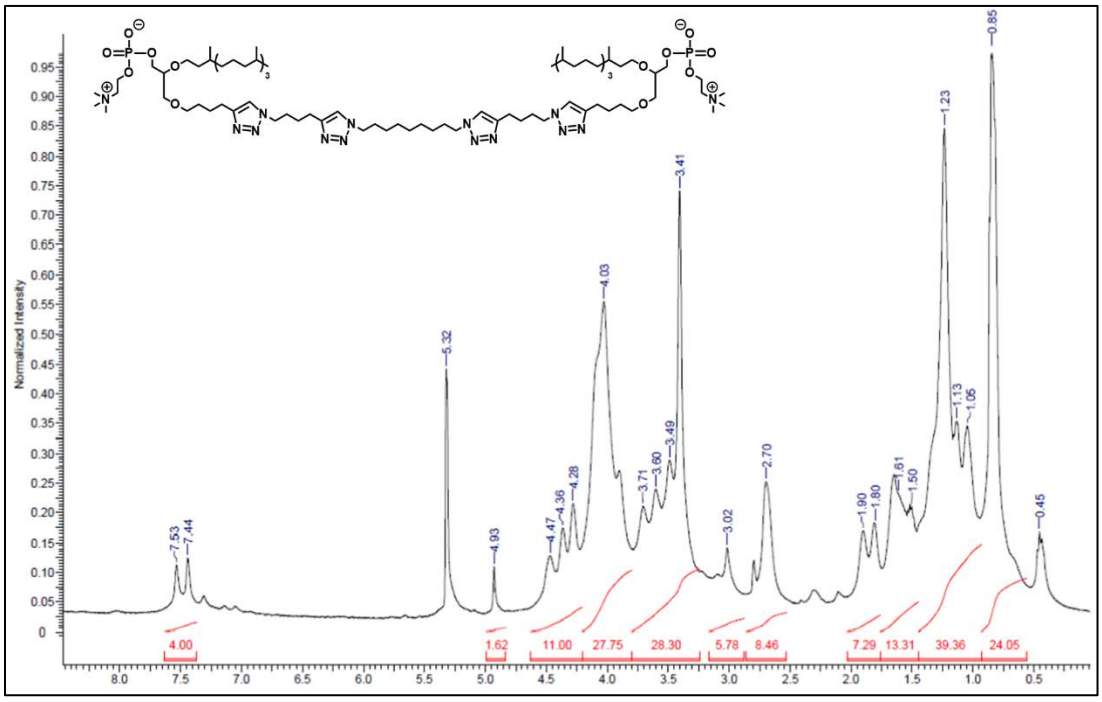

Figure 2.47: ^{1}H NMR of **ATL4**.

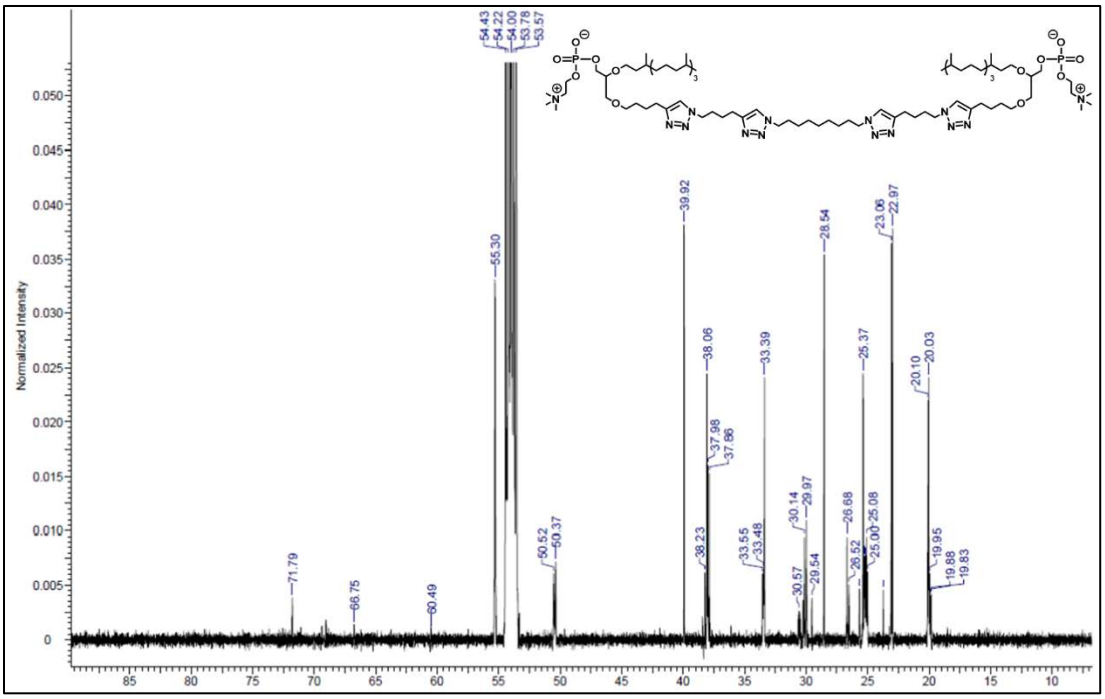

Figure 2.48: ^{13}C NMR of **ATL4**.

(((((1,4-phenylenebis(oxy))bis(octane-8,1-diyl))bis(1H-1,2,3-triazole-1,4-diyl))bis(butane-4,1-diyl))bis(oxy))bis(2-((3,7,11,15-tetramethylhexadecyl)oxy)propane-3,1-diyl) bis(2-(trimethylammonio)ethyl) bis(phosphate) (**ATL 5)**

Figure 2.49: ^{1}H NMR (400MHz, CD_2Cl_2): δ 0.85 (t, 30H), 1.26 (m, 138H), 1.74 (m, 75H), 2.67 (t, 4H), 3.30 (s, 15H), 3.54 (m, 26H), 3.88 (t, 8H), 4.11 (d, 4H), 4.26 (t, 4H), 4.37 (m, 4H), 6.78 (s, 4H), 7.32 (s, 2H); **Figure 2.50**: ^{13}C NMR (500MHz, CD_2Cl_2): δ 14.45, 20.02, 22.95, 23.04, 25.06, 25.37, 28.56, 30.25, 30.79, 33.38, 38.03, 39.92, 50.62, 68.89, 115.93;

HRMS (M+2Na): calculated: 848.6126; found: 848.6117.

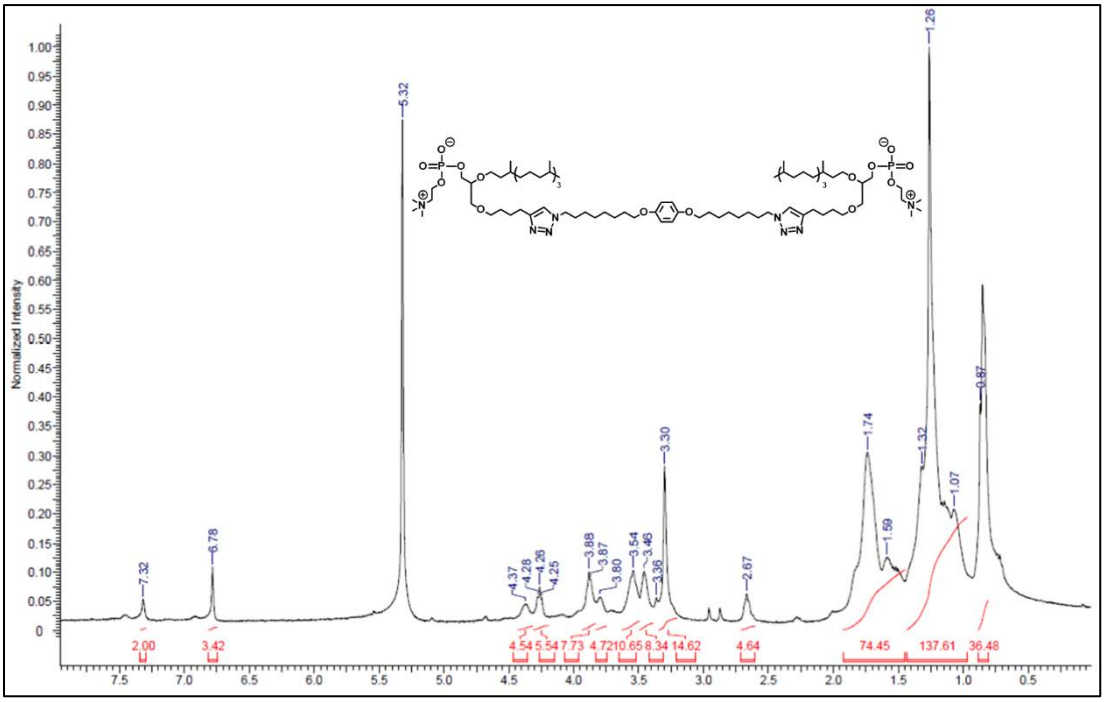

Figure 2.49: ^{1}H NMR of **ATL5**.

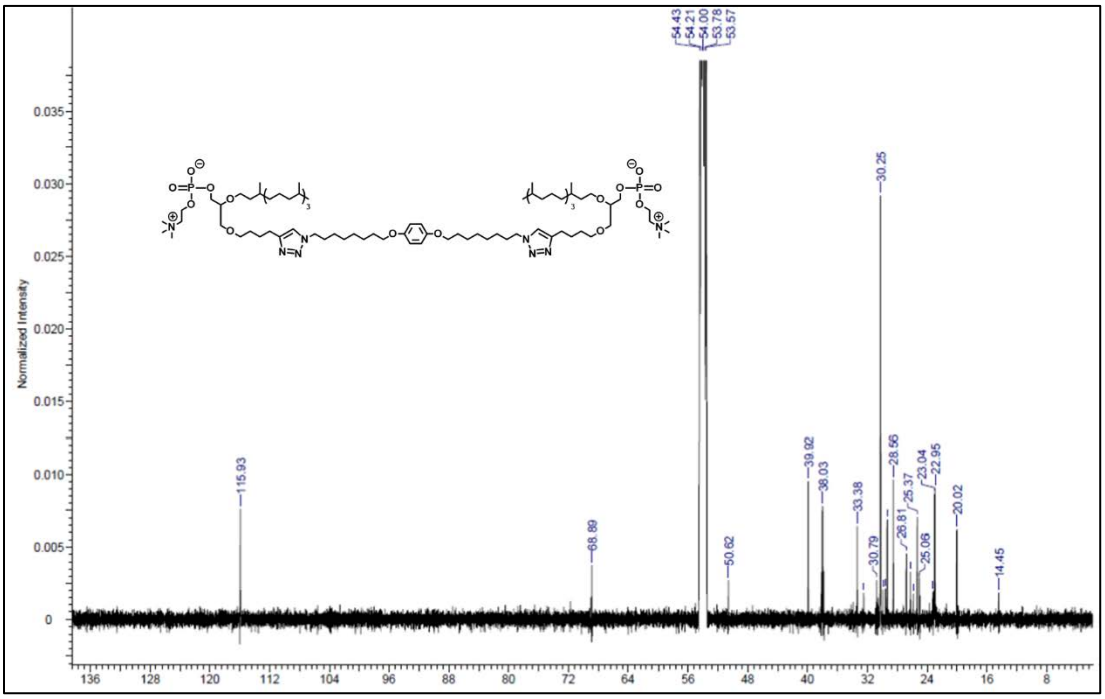

Figure 2.50: ^{1}H NMR of **ATL5**.

2.6 References

1. Peanasky, J., Schneider, H. M., Granick, S. & Kessel, C. R. Self-Assembled Monolayers on Mica for Experiments Utilizing the Surface Forces Apparatus. *Langmuir* **11,** 953–962 (1995).

2. Chang Chung, Y., Hong Chiu, Y., Wei Wu, Y. & Tai Tao, Y. Self-assembled biomimetic monolayers using phospholipid-containing disulfides. *Biomaterials* **26,** 2313–2324 (2005).

3. Zhai, Y., Lee-Gau Chong, P., Taylor, L. J. A., Erlkamp, M., Grobelny, S., Czeslik, C., Watkins, E. & Winter, R. Physical properties of archaeal tetraether lipid membranes as revealed by differential scanning and pressure perturbation calorimetry, molecular acoustics, and neutron reflectometry: Effects of pressure and cell growth temperature. *Langmuir* **28,** 5211–5217 (2012).

4. Gliozzi, A., Relini, A. & Chong, P. L. G. Structure and permeability properties of biomimetic membranes of bolaform archaeal tetraether lipids. *J. Memb. Sci.* **206,** 131–147 (2002).

5. Febo-Ayala, W., Morera-Félix, S. L., Hrycyna, C. A. & Thompson, D. H. Functional reconstitution of the integral membrane enzyme, isoprenylcysteine carboxyl methyltransferase, in synthetic bolalipid membrane vesicles. *Biochemistry* **45,** 14683–

14694 (2006).

6. Raguse, B., Culshaw, P. N., Prashar, J. K. & Raval, K. The synthesis of archaebacterial lipid analogues. *Tetrahedron Lett.* **41,** 2971–2974 (2000).

7. Kim, J. M. & Thompson, D. H. Tetraether Bolaform Amphiphiles as Models of Archaebacterial Membrane-Lipids - Synthesis, Differential Scanning Calorimetry, and Monolayer Studies. *Langmuir* **8,** 637–644 ST – Tetraether Bolaform Amphiphiles as M (1992).

8. Brard, M., Lainé, C., Réthoré, G., Laurent, I., Neveu, C., Lemiègre, L. & Benvegnu, T. Synthesis of archaeal bipolar lipid analogues: A way to versatile drug/gene delivery systems. *Journal of Organic Chemistry* **72,** 8267–8279 (2007).

9. Barbeau, J., Cammas-Marion, S., Auvray, P. & Benvegnu, T. Preparation and Characterization of Stealth Archaeosomes Based on a Synthetic PEGylated Archaeal Tetraether Lipid. *J. Drug Deliv.* **2011,** 1–11 (2011).

10. Réthoré, G., Montier, T., Le Gall, T., Delépine, P., Cammas-Marion, S., Lemiègre, L., Lehn, P. & Benvegnu, T. Archaeosomes based on synthetic tetraether-like lipids as novel versatile gene delivery systems. *Chem. Commun. (Camb).* 2054–6 (2007). doi:10.1039/b618568a

11. Benvegnu, T., Réthoré, G., Brard, M., Richter, W. & Plusquellec, D. Archaeosomes based on novel synthetic tetraether-type lipids for the development of oral delivery systems. *Chem. Commun. (Cambridge, U. K.)* 5536–5538 (2005). doi:10.1039/b511440c

Chapter 3 : Preparation of Lipid Materials

3.1 Introduction

In the development of nanomaterials, there has been a strong effort to control the structure, size, and morphology of liposomes[1–4]. The methods of preparation greatly influence how the lipids assemble to form spherical vesicles. Multilamellar vesicles (MLVs) are formed using the lipid hydration method while unilamellar vesicles (ULVs) are formed by extrusion by filtering liposomes through defined pore sizes[1,2]. Furthermore, liposomes can also be achieved through repeated freeze-thaw cycles to produce large vesicles great than 1μm. Each of these methods contribute to the assembly of liposomes and by taking advantage of these techniques, we can formulate liposomes to study membranes. Although there are many reported methods for the preparation of liposomes, our main focus was to demonstrate the assemblies of well-defined arcaheosomes. This chapter discusses the preparation and characterization of conventional liposomes and archaeosomes formulated from commercially available lipids and archaeal-type lipids described in chapter 2.

3.2 Conventional Liposomes

Conventional liposomes were prepared from DPPC and 1,2-Dioleoyl-sn-glycero-3-phosphocholine (DOPC) lipids as models for comparison against archaeosomes[1,2,5–7]. DPPC lipids are fully saturated while DOPC have unsaturated bonds. These two lipids serve a great control for studying the difference in liposome stability between saturated and unsaturated fatty acyl chains. Moreover, to study the influence of supplemental additives, we formulated liposomes with or without the presence of cholesterol. Liposomes **L1-4** hydrated in water, pH

7.4, were prepared by extrusion, and were analyzed by DLS and TEM. Here we discuss the liposome formulations and characterization of of **L1-4** as listed in **Table 3.1**.

Table 3.1: Liposome formulations from DPPC and DOPC lipids.

Liposome Entry	Lipid	Lipid (mM)	Cholesterol (mM)
L1[a]	DPPC	6	-
L2[a]	DPPC	6	2
L3[a]	DOPC	6	-
L4[a]	DOPC	6	2
L5[b]	DPPC	6	2

a) Liposomes were hydrated with H_2O, pH 7.4.
b) Liposomes were hydrated with 100mM calcein, 100mM NaCl, pH 7.4.

3.2.1 DPPC-based Liposome Formulations

To study the assembly of conventional liposomes, DPPC-based liposome formulations were prepared to study fully saturated membranes. In the preparation of liposome **L1**, our findings were inconsistent with our expectations. Because **L1** liposomes were extruded through a 200 nm polycarbonate membrane filter, we expected to observe liposomes within the range of 200 nm. By DLS, the particle characterization of **L1** shows small particles of averaging hydrodynamic diameter of 35 nm as shown in **Figure 3.1a**. We observed much smaller liposomes than we had anticipated. Furthermore, **L1** liposomes were examined by TEM to confirm the data obtained by DLS and to obtain a more accurate representation of the morphologies of **L1** as depicted in **Figure 3.1b & c**. TEM images show small liposomes that are about 50 nm in diameter, which is somewhat consistent with the DLS data. Very few particles seem to appear as spherical vesicles while a majority of the particles are amorphous structures. Although we clearly observe particles by TEM, the liposomes do not seem to be as well-defined in the case of **L2** liposomes.

To better understand the assembly of conventional liposomes, liposome **L2** was formulated in the presence of cholesterol to highlight the importance of additives shown in **Figure 3.1d-e**. **L2** liposomes were prepared using the same procedure as **L1** yet there were stark differences in their hydrodynamic radius. As expected, by DLS, **L2** liposomes showed a high population of particles averaging in 150 nm in hydrodynamic diameter. Confirmed by TEM images, we see that **L2** is consistent with DLS and are larger than **L1** liposomes. Moreover, we clearly observe well-defined particles as depicted in **Figure 3.1f**. This suggests and confirms that cholesterol does contribute in the assembly of liposomes and it is evident in the images obtained by TEM.

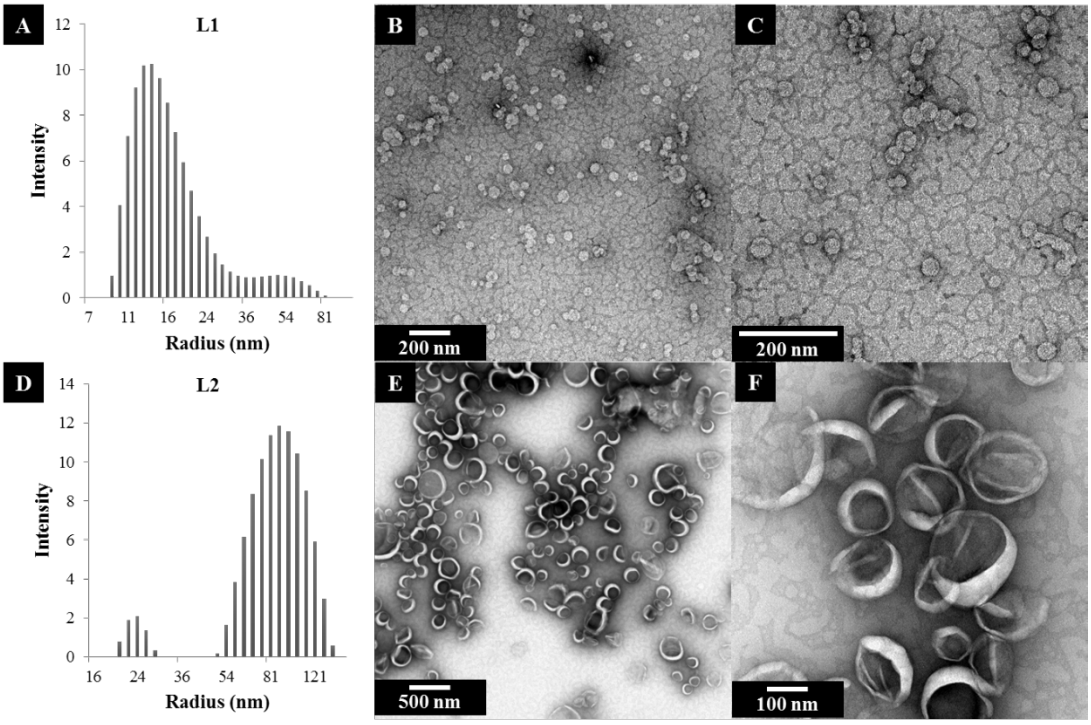

Figure 3.1: Characterization of Liposomes **L1** & **L2**. a) Hydrodynamic radius of **L1**. b) TEM image of **L1**. c) TEM image of **L1**. d) Hydrodynamic radius of **L2**. e) TEM image of **L2**. f) Zoom in image of e.

3.2.2 DOPC-based Liposome Formulations

To study the influence of unsaturated fatty chains within liposomes membranes, we prepared liposomes **L3** and **L4** as characterized by **Figure 3.2**. **L3** liposomes were prepared from DOPC lipids without cholesterol. By DLS, we observe a wide distribution of particle sizes with two main populations sizes of 50 nm and 180 nm particles. Again, we analyzed **L3** by TEM, however, were unable to observe any particle formation. Despite obtaining data from DLS, **L3** liposomes could not be observed. In the case of liposome **L4** containing cholesterol, we also observe two main population sizes of particles on average from 30-80 nm. Similarly, when analyzed by TEM, liposomes could not be found anywhere on the TEM grid. We hypothesize that during the preparation of TEM grids, the dry state exerts high sheer forces that destroy the liposomes. We believe that both **L3** and **L4** liposomes are not mechanically and physically stable compared to DPPC-based liposomes. Despite the inability to visualize **L3** & **L4** liposomes by dry state TEM, **L4** liposomes were observed by cryo-TEM shown in **Figure 3.2f**. The inability to observed **L3** and **L4** liposomes by TEM suggests that DOPC-based liposomes are not as mechanically stable and robust as DPPC-based liposomes.

Overall, the formation of conventional liposomes using DPPC and DOPC is greatly improved with cholesterol. Despite being unable to observe **L3** and **L4** liposomes by TEM, we were able to view liposomes by cryo-TEM. This suggests that unsaturated lipids are much more unstable in liposome formation and that cholesterol improves the formation of well-defined particles as seen in **L3**.

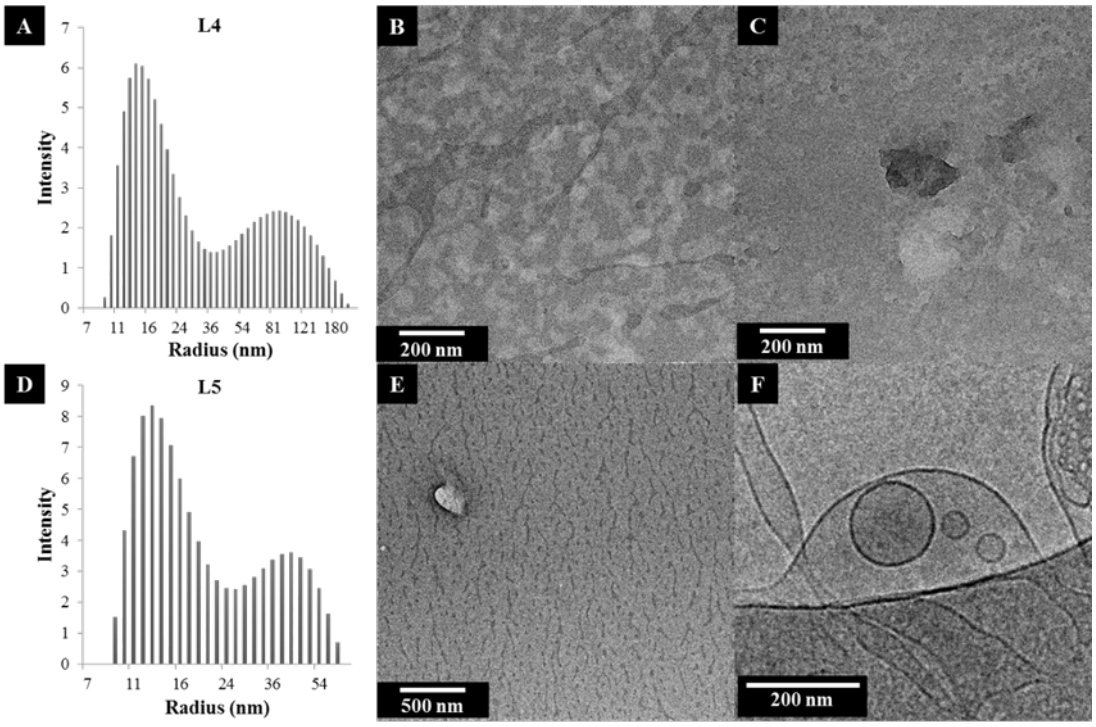

Figure 3.2 : Characterization of Liposomes **L3** & **L4**. a) Hydrodynamic radius of **L3**. b) TEM image of **L3**. c) TEM image of **L3**. d) Hydrodynamic radius of **L4**. e) TEM image of **L4**. f) Cryo-TEM image of **L4**

3.3 Archaeosomes

To examine archaeal-type lipids in the assembly of liposomes, we prepared archaeosome formulations listed in **Table 3.2** consisting of archaeal-type lipids. To understand the importance of attaching zwitterionic phosphatidylcholine head groups, we prepared an archaeosome formulation using compound **12** in the diol form. Moreover, we surveyed several lipid formulations using lipid **ATL1** with and without additives to demonstrate the ability to assemble into liposomes. Lastly, we studied archaeosome membrane stability through several cycles of lyophilization and rehydration to study their ability to maintain their initial morphologies. Here we discuss this preparation and assembly of archaeosomes.

Table 3.2: Archaeosome formulations from archaeal-type lipids.

Liposome Entry	Lipid(s)	Lipid (mM)	Cholesterol (mM)
A1[a]	Compound 12	5	-
A2[a]	ATL1	5	-
A3[a]	ATL1	3	2
A4[a]	ATL1/DSPE-PEG	2.75/0.25	2
A5[b]	ATL1	4.5	0.5
A6[b]	ATL1	4	1
A7[b]	ATL1	3.5	1.5
A8[b]	ATL1	3	2
A9[b]	ATL1	2.5	2.5

a) Liposomes were hydrated with H_2O, pH 7.4.
b) Liposomes were hydrated with 100mM calcein, 100mM NaCl, pH 7.4.

3.3.1 The Importance of Polar Head Groups

To study the significance of the polar head groups of archaeal-type lipids for particle assembly, we attempted to formulate archaeosomes from lipid diols. Compound **17** is an archaeal-type lipid precursor that lacks the phosphatidylcholine zwitterionic head groups and has free hydroxyl ends. To investigate whether archaeosomes can be generated from the diol form, we prepared archaeosome **A1** from compound **17** using standard lipid film hydration methods. The sample was analyzed by DLS but could not be defined within the parameters of the instrument. This suggests that liposomes could not be formed simply from the diol form. The samples were further examined by TEM to observe any archaeosome assembly. It is clear that we do not observe well-defined archaeosomes from **A1** as shown in **Figure 3.3**. Despite observing well-defined liposomes, we see small aggregated clusters of materials possibly resembling oil droplets. Ultimately, this suggests that polar head groups are necessary to drive the formation of well-defined archaeosomes.

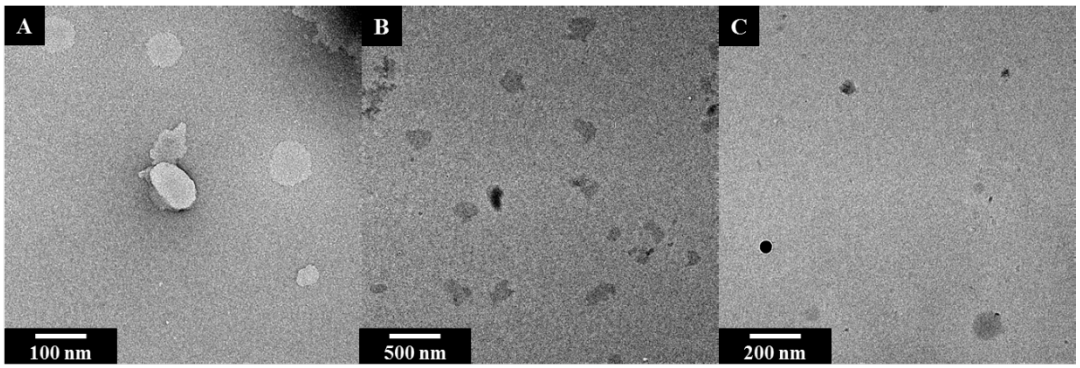

Figure 3.3: TEM images of **A1**. a) TEM image of **A1**. b) TEM image of **A1**. c) TEM image of **A1**.

3.3.2 PEGylated Archaeosomes

Prior to forming archaeosomes purely from archaeal-type lipids, we first prepared liposome formulations using additives to drive assembly of our materials. As a proof-of-concept, archaeosomes were prepared from lipid **ATL1** and cholesterol with or without DPSE-PEG to generate archaeosomes **A2** and **A3** shown in **Figure 3.4**. Archaeosomes were prepared using additives to ensure that archaeal-type lipids could in fact assemble into liposomes. Analyzing the formulations by TEM, we observed liposomes for both **A2** and **A3** with and without the presence of cholesterol depicted in **Figure 3.4a-b**. **A2** showed a wide size distribution among the population with mainly small liposomes around 50 nm. Similarly, **A3** archaeosomes were around 50 nm, however, not as abundant on the TEM grid. Further examining these samples by cryo-TEM, we observed polydisperced, well-defined unilemellar liposomes for both **A3** and **A4** exhibited in **Figure 3.4c-d**. Regardless of the presence of DPSE-PEG, we observe archaeosomes that are comparable in size and morphology.

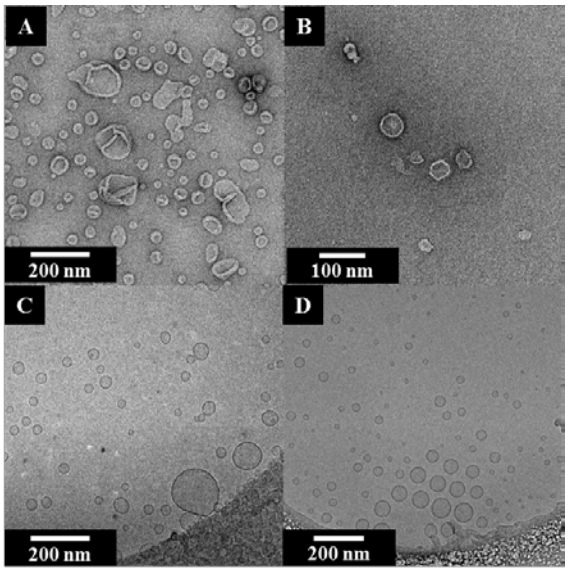

Figure 3.4: Electron microscopy characterization of **A2** & **A3**. a) TEM image of **A2**. b) TEM image of **A2**. c) Cryo-TEM image of **A2**. d) Cryo-TEM image of **A3**.

3.3.3 Pure Archaeosomes

To investigate archaeal-type lipids within the context of their own structure for the formulation of archaeosomes, we prepared formulations without any additives such as DPSE-PEG or cholesterol. Archaeosome **A4** were prepared from lipid **AL1** in water, pH 7.4 shown in **Figure 3.5**. DLS shows uniform size distrubtion of particles consisting of 200nm in hydrodynamic diameter **Figure 3.5a**. **A4** was further examined by TEM observing spherical particles larger than 200 nm. **Figure 3.5c** shows cryo-TEM of large multilamellar vesicles with many liposomes entrapped within one another. The size distribution of these liposomes vary from 100 – 500 nm as observed by cyro-TEM. Again, this finding was inconsistent with our expectation as we expected unilamellar liposomes. Despite using DSPE-PEG for **A2**, archeosomes **A2** and **A3** formed unilemellar liposomes. This suggests that cholesterol may play a significant role in the formation of unilemellar vesicles over multilamellar vesicles. Despite

the multilamellar vesicles, we have shown that lipid **AL1** is capable of assembling into archaeosomes of well-defined nature.

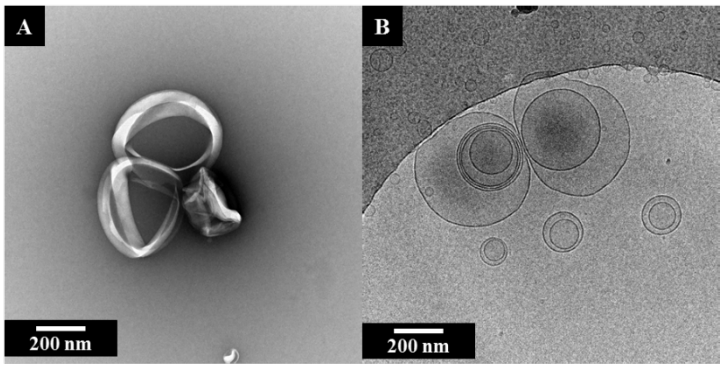

Figure 3.5: Electron microscopy characterization of **A4** archaeosomes. a) TEM image of **A4** archaeosomes. b) Cryo-TEM image of **A4** archaeosomes.

3.3.4 Lyophilization & Rehydration Cycles

Upon characterizing both conventional liposomes and archaeosomes, we further investigated their membrane stability. Specifically, we examined their ability to maintain their structural morphologies within multiple lyophilization and rehydration cycles. Liposomes **L1** and **A4**, both lacking cholesterol, were lyophilized and rehydrated with water for five repeated cycles. DLS measurements were taken before and after each cycle shown in **Figure 3.6**. Liposomes **L1** had an initial hydrodynamic diameter of 220 nm and after the first cycle the diameter increased to 550 nm. During the repeated cycles, **L1** liposomes fluctuated in size. No trend was observed. This suggests that after lyophilization, the liposomes reassemble into vesicles when rehydrated and do not maintain their initial size and structure. In contrast, archaeosome **A4**, shows an initial hydrodynamic diameter of two population sizes around 200 nm and 1000 nm by DLS. It is clear that **A4** has a wide distribution of particles sizes and upon the lyophilization rehydration cycle, we continue to a wide distribution of sizes. Despite the

measurements obtained by DLS, we furthered our study to visualize these liposomes by electron microscopy.

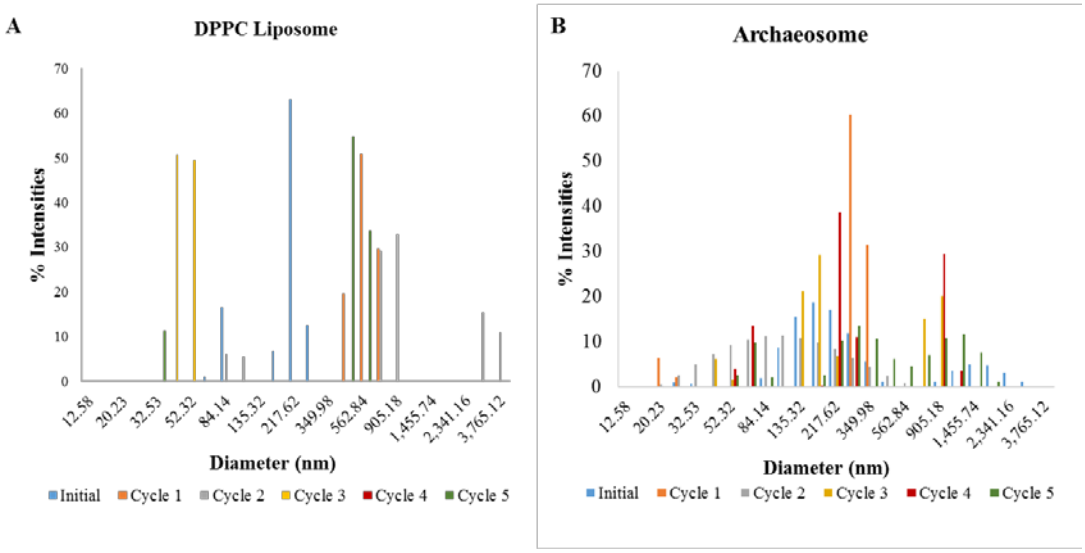

Figure 3.6: DLS measurements of liposomes. a) Hydrodynamic diameter of **L1**. b) Hydrodynamic diameter of **A4**.

To obtain an accurate representation of the morphology of liposomes **L1** and **A4**, we obtained electron microscopy images of the initial and final state of both materials shown in **Figure 3.7**. In **Figure 3.7a**, the initial diameter of **L1** liposomes were roughly 200 nm in diameter, which was consistent with DLS. Analyzing the initial morphology of **L1** liposomes by cryo-TEM, we observed well-defined and monodispersed liposomes also around 200 nm represented in **Figure 3.7b**. Additionally, we observed few multilamellar liposomes, which could not be resolved by dry state TEM. After five repeated lyophilization and rehydration cycles, **L1** liposomes showed a significant increase in diameter as shown by cryo-TEM in **Figure 3.7c**. Moreover, we observe more multilamellar vesicles with liposomes entrapped inside other liposomes. Again, this suggests that the lipids are not maintaining their membrane structures and are reforming liposomes upon rehydration.

In the case for **A4** archaeosomes, we observe 250 nm liposomes that are polydisperse in the initial state shown in **Figure 3.7d**. Similar to **L1** liposomes, we also observed multilamellar liposomes by cryo-TEM depicted in **Figure 3.7e**. This is consistent with our observations with the liposome formulations lacking cholesterol. After the A4 archaeosoems were subjected to five cyles of lyophilization and rehydration, we see clusters of aggregates rather than well-defined liposomes shown in **Figure 3.7f**. These archaeosomes do not seem to be polydisperse throughout the cryo-TEM grid and suggests that these lipids are reassembling to form archaeosomes. From both **L1** and **A4** studies, we have shown that vesicles are reformed after various lyophilization and rehydration cycles. Despite their ability to assemble into liposomes, we observe an increase in multilamellar vesicles compared to unilamellar vesicles. Additionally, for **A4**, we see aggregated materials in contrast to well-defined archaeosomes.

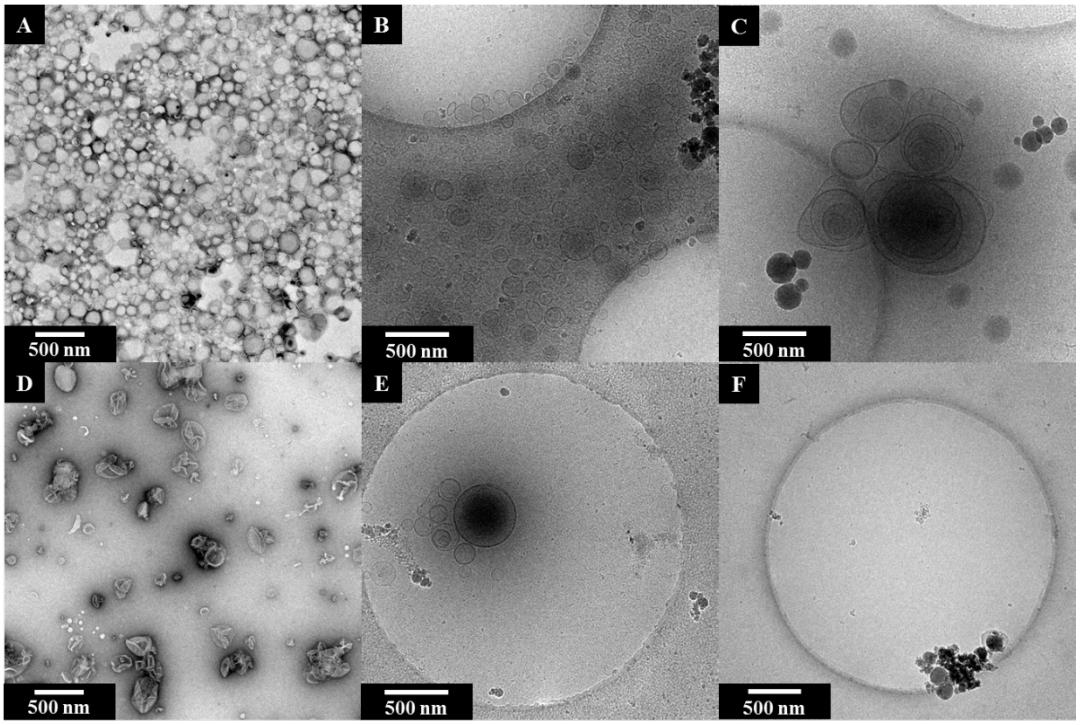

Figure 3.7: Electron microscopy images of liposomes **L1** & **A4**. a) TEM image of **L1** prior to first lyophilization cycle. b) Cryo-TEM image of **L1** prior to first lyophilization cycle. c) Cryo-TEM image

of **L1** after 5th lyophilization/rehydration cycle. d) TEM image of **A4** prior to first lyophilization cycle. e) Cryo-TEM image of **A4** prior to first lyophilization cycle. f) Cryo-TEM image of **A4** after 5th lyophilization/rehydration cycle.

3.4 Conclusions

In this chapter, we have discussed the morphological characterization of conventional liposomes and archaeosomes by DLS and electron microscopy techniques. Visualizing our materials by TEM and cryo-TEM, we observed well-defined liposomes for DPPC-based liposomes and archaeal-type-based archaeosomes. Using commercially available lipids, we were able to fully characterize **L1-2**, however, we were unable to visualize **L3-4** by TEM. We believe that the unsaturated fatty tails of DOPC-based liposomes are less rigid and less stable in regards to the TEM grid preparation procedures. However, we demonstrate that **L4** can be visualized by cryo-TEM. Furthermore, we demonstrated the necessity to install polar head groups towards the assembly of liposomes within archeal-type lipids. Using **ATL1** we demonstrated the assembly of archaeosomes from archaeal-type lipids. Lastly, we have shown that both **L1** and **A4** liposomes are capable of reassembling into vesicular structures after many lyophilization and rehydration cycles. These experiments help explain the preparation of liposomes with respect to stability as drug nanocarriers.

3.5 Experimental

3.5.1 General Methods/Instrument Details

All regents were purchased from commercial sources. Calcein was specifically purchased from Avanti Polar Lipids, Inc. Water was purified by MiliQ water filter (Irvine, CA) and autoclaved prior to use. Sonication was achieved using a Branson ultrasonic ¾ Benchtop Cleaner bath or probe sonicator. Liposomes were extruded using a mini-extruder using 0.8μm,

0.4μm, and 0.2μm polycarbonate membranes filters (). The hydrodynamic radius was determined by DLS on a DynaStarPro Nanostar provided by Wyatt Technologies. Electron electron microscopy images were obtained by Spherea for dry stain TEM and Polara for cryo-em.

3.5.2 General Procedure for Lipid Extrusion

Liposomes were prepared by standard lipid film hydration procedures as reported in the literature (citation). Lipids and (+/-) cholesterol dissolved in a solution mixture of DCM/MeOH (2:1) were transferred to glass vial. The solvent mixtures were evaporated either by rotary evaporator or under nitrogen atmosphere via vortexing to achieve a thin lipid film adhering to the walls of the glass vial. The dried lipid film was further dried under hi-vacuum pump for 4 hours. The lipid film was then hydrated in buffer solution followed by vortexing the solution for 30 seconds and sonication for 30 minutes in a water bath sonicator. Early liposomes samples were prepared by probe sonication via 300 probe cycles. The liposome solution was then extruded through 0.8μm, 0.4μm, and 0.2μm polycarbonate membrane filters 21 times respectively. The liposome solutions were stored in HPLC glass vials at 10^{o}C.

3.5.3 Lyophilization and Rehydration Procedures

Liposomes samples (200μL) placed in 1.5 mL centrifuge tubes were freeze-dried by liquid nitrogen and lyophilized until dry. Samples were dissolved in filtered water (200μL). The procedure was repeated for a total of 5 cycles. DLS measurements were taken before and after each cycle. Initial and final images were obtained by both TEM and cryo-TEM.

3.6 References

1. Akbarzadeh, A., Rezaei-sadabady, R., Davaran, S., Joo, S. W. & Zarghami, N. Liposome : classification , preparation , and applications. 1–9 (2013). doi:10.1186/1556-276X-8-102

2. Lasic, D. D. & Martin, F. J. On the mechanism of vesicle formation. *J. Memb. Sci.* **50,** 215–222 (1990).

3. Barbeau, J., Cammas-Marion, S., Auvray, P. & Benvegnu, T. Preparation and Characterization of Stealth Archaeosomes Based on a Synthetic PEGylated Archaeal Tetraether Lipid. *J. Drug Deliv.* **2011,** 1–11 (2011).

4. Laouini, A., Jaafar-Maalej, C., Limayem-Blouza, I., Sfar, S., Charcosset, C. & Fessi, H. Preparation, Characterization and Applications of Liposomes: State of the Art. *J. Colloid Sci. Biotechnol.* **1,** 147–168 (2012).

5. Raguse, B., Culshaw, P. N., Prashar, J. K. & Raval, K. The synthesis of archaebacterial lipid analogues. *Tetrahedron Lett.* **41,** 2971–2974 (2000).

6. Kim, J. M. & Thompson, D. H. Tetraether Bolaform Amphiphiles as Models of Archaebacterial Membrane-Lipids - Synthesis, Differential Scanning Calorimetry, and Monolayer Studies. *Langmuir* **8,** 637–644 ST – Tetraether Bolaform Amphiphiles as M (1992).

7. Gliozzi, A., Relini, A. & Chong, P. L. G. Structure and permeability properties of biomimetic membranes of bolaform archaeal tetraether lipids. *J. Memb. Sci.* **206,** 131–147 (2002).

Chapter 4 : Exploring Membrane Stability

4.1 Introduction

Different from conventional liposomes, archaeosomes do not require cholesterol in the formulation to enhanced membrane stability[1–3]. Archaeosomes exhibit high membrane stabilities against extreme conditions, especially, acidic pH, high temperatures, high pressures, oxidative stresses, and phospholipase degradation[1,4–7]. Specifically, archaeosomes have proven to reduce the leakage of encapsulated carboxyfluorescein at pH 1 and at temperatures above 90^{o}C[4]. Moreover, archaeosomes remain stable and resistant to enzymatic degradation under biological environments further demonstrating the utility for *in vivo* applications[8–10]. Thus, the stability of archaeal membranes has prompted an interested towards the use of archaeosomes as an alternative to conventional liposomes. This chapter attempts to addresses the leakage properties of archaeosomes with respect to temperature, salinity, and blood serum. Here, we describe the membrane stability of archaoesomes **A5-9** in contrast towards conventional liposomes **L2** & **L5**.

4.2 Encapsulation and Release Studies

In order for liposomes to serve as promising nanocarriers, liposomes must be able to encapsulate efficiently and retain their cargo. The passive leakage of ions and small molecules is a problem that needs to be addressed within drug delivery applications. To address this issue, cholesterol additives have been incorporated to prepare more stable liposomes[10]. The amount of cholesterol varies with the type of lipid. Additionally, to render utility, liposomes must be stable under physiological conditions[11]. Herein, we discuss the encapsulation and release studies archaeosomes and control liposomes.

4.2.1 The Effects of Osmolarity

To test the leakage of archaeosomes, calcein-loaded liposomes **A2** and **L5** were incubated with hypotonic, weakly hypertonic, and strongly hypertonic solutions shown in **Figure 4.1**. The release of calein was monitored by fluorescence for over 2 hours. **Figure 4.3a** depicts the high calcein permeability of archaeosome **A2** in all three solutions. In the hypotonic solutions, containing less salt and less osmotic pressure, **A2** showed calcein leakage from the initial time plot. All of the calcein was leaked before the experiment had begun. In weakly and strongly hypertonic solutions, we observed initial leakage for **A2**, however over the course of 60 minutes, we saw an increase in fluorescence that were comparable. This suggests that calcein was slowly leaking across the membrane. Despite the hypertonic solutions exerting osmotic pressure on the archeal-type membrane, **A2** was susceptible to calcein permeability.

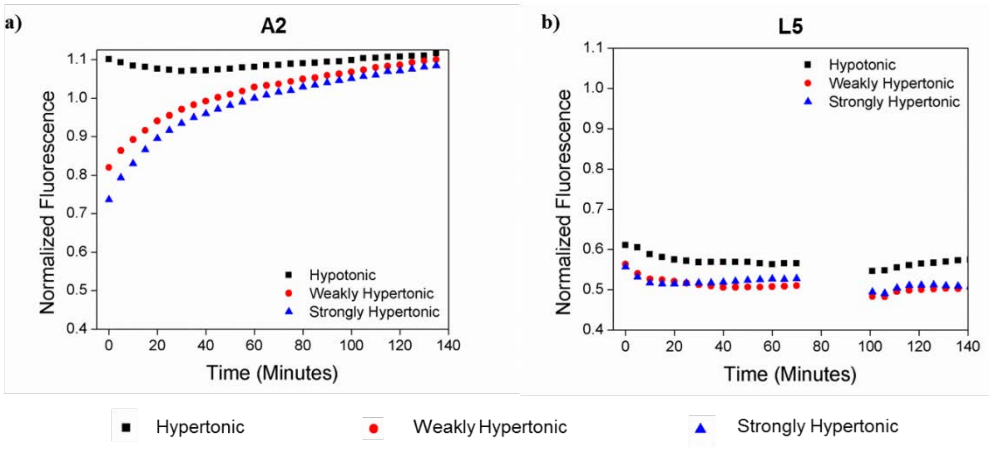

Figure 4.1: Calcein leakage of liposomes by fluorescence.

Contrastingly, **L5** liposomes demonstrated significant membrane stability shown in **Figure 4.1b**. In all conditions, **L5** liposomes proved to be stable showing no increase in fluorescence. This suggests that calcein was not passively leaking across the membrane and that **L5** proved to me more stable than **A2**. We questioned whether cholesterol was the result

in the stability of L5. Because of this result, we explored further archaeosome stability by surveying various cholesterol formulation mixtures described in next section.

4.2.2 Archaeosome Cholesterol Formulation Screen

Our previous experiments demonstrate that **A2** archaeosomes exhibit high calcein leakage compared to **L2** liposomes possibly due to the lack of cholesterol. To investigate the influence of cholesterol within archaeosomes, we prepared archaeosomes **A5-9**, each containing different mole percentages of cholesterol increasing from 10-50%. **Figure 4.2** displays the calcein release profile over the course of 13 hours at room temperature. Because calcein beings to leak from the membranes immediately after eluting through Sephadex G-100, each sample has a different starting time.

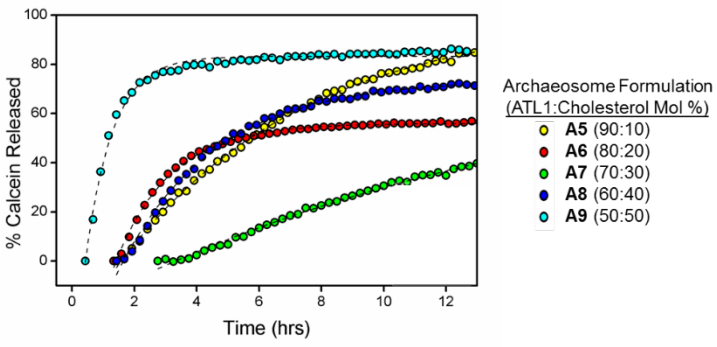

Figure 4.2: Calcein release assay for the optimization of ATL1 lipid/cholesterol formulation screen.

Among all five formulations, **A9** archaeosomes showed the greatest percent of released calcein. In less than 2 hours, **A9** showed leakage up to 80%. The high mole percentage of cholesterol suggests that too much cholesterol may cause **A9** to exhibit high permeability. As we decrease the percentage of cholesterol, we see less calcein leakage for **A5-8**. **A5**, **A6**, and **A8** showed similar release profiles with comparable rates of release within 4 hours. Over the course of the incubation, **A5** & **A8** reached over 80% & 60% leakage respectively, while **A6** reached roughly 50% leakage. Despite all formulations showing 50% calcein leakage or higher,

only **A7** showed less than 50% leakage. Although the release profile for **A7** begins just after 2 hours, we observed a slow and gradual release over 9 hours. **A7** shows calcein release up to 40% demonstrating that ATL1-based archaeosomes containing 30% cholesterol decrease the rate of calcein leakage. Overall, the release profiles of **A5-7** suggests that cholesterol helps slow that release of calcein and should be incorporated within archaeosome formulations to prepare less permeable liposomes.

4.2.3 Thermostability

After conducting the cholesterol screen and finding the optimal archaeosome formulation, we investigated the thermostability of calcein-encapsulated liposomes **L5** and **A7**. Recall that **A7** contains 30% cholesterol while **L5** contains 25% cholesterol. **L5** and **A7** were incubated at variable temperatures ranging from 0-65°C for 24 hours shown in **Figure 4.3**. In comparing the two liposomes, **L5** overall showed greater stability at variable temperatures. At 4°C and 22°C, **L5** released less than 20% calcein. At 37°C, we see an increase in release of calcein at 40%. As the temperature increases to 50°C and 65°C, we observe leakage of 65% and 100% respectively. At low temperatures, **L5** show stability while increasing the temperature increases the percent of leakage.

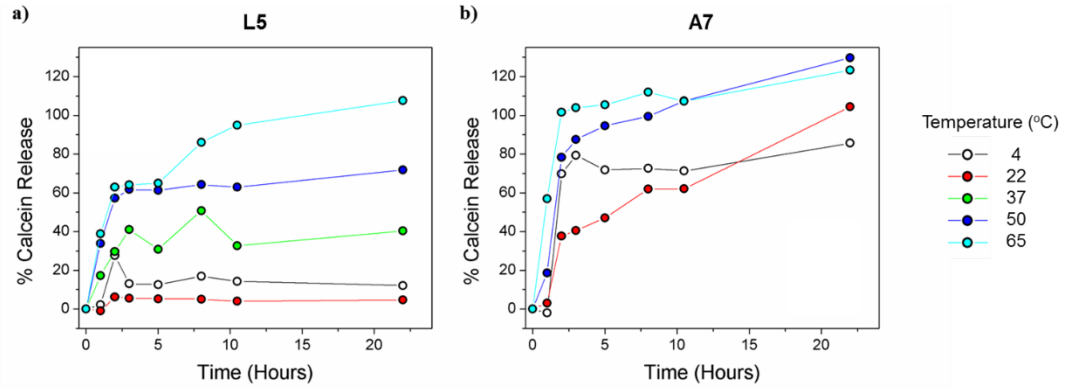

Figure 4.3: Thermostability assay of calcein leakage of liposomes. a) **L5** liposomes release profile. b) A7 archaeosomes release profile.

In contrast, **A7** archaeosomes exhibit high calcein release profiles at all temperatures. Incubation of **A7** at 37ºC was not obtained. At 4ºC, **A7** had already leaked 70% calcein in just 2.5 hours. Despite the increase in temperature to 22ºC, **A7** leaked less than 40% in that same timespan. The slow release at 22ºC cannot be explained as one would expect a slower release at lower temperatures. At 50ºC and 65ºC, we see over 80% of calcein released. Over the course of 24 hours, **A7** reaches 100% leakage in almost all cases with the exception at 4ºC. Through these studies, we continue observe high calcein leakage for our archaeosome formulations compared to conventional liposomes.

4.3 Temperature Dependence Studies

Archaeosomes have shown high stabilities towards drastic changes in temperature. Even at high temperatures, archaeosomes are do not exhibit leakage comparable to conventional liposomes and maintain their mophology. To test the structure stability of our archaeosomes, we conducted various temperature dependence experiments by DLS. Here, we discuss the stability of archaeosomes with respect to temperature.

4.3.1 Temperature Dependence

We questioned whether the structure of archaeosomes would be dependent on temperature and would form kinetically trapped aggregates at high temperatures. To confirm the stability of archaeosomes from the previous cholesterol screen experiments, we used DLS to measure the hydrodynamic diameter at increasing and decreasing temperatures. Although **A7** showed reduced membrane permeability with respect to calcein, we wanted to see how the structures would be affected by changes in temperature such as possible agglomeration. **Figure 4.4** shows the incremental DLS measurements of archaeosomes **A5-7** and **L5** as heat was gradually ramped up from 25ºC to 95ºC and back down to 25ºC. **A5** archaeosomes increased

in size as the temperature increased and decreased as the particles were cooled down shown in **Figure 4.4a**. Due to the variability in diameter, **A5** showed to be an unstable formulation. In contrast, **A6-8** demonstrated stable structures shown in **Figure 4.4b-c**. The diameters of **A6-8** were relatively consistent showing that the diameter does not increase not decrease as the heat is ramped up and down.

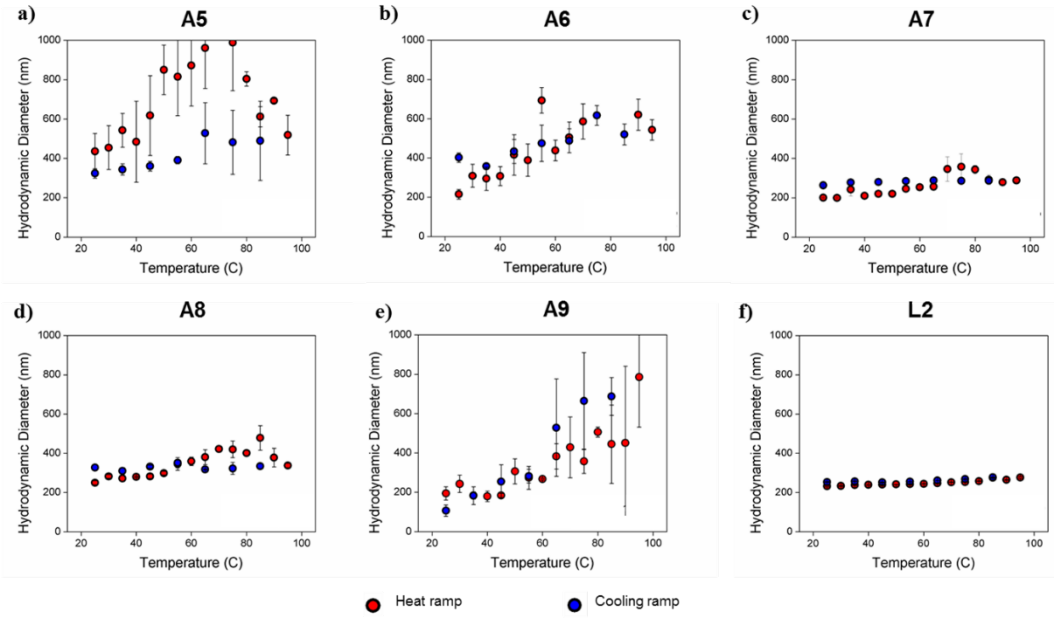

Figure 4.4: Temperature dependence analysis of liposome formulations (lipid/cholesterol mol %) via DLS measurements. a) **A5** (90:10) formulation. b) **A6** (80:20) formulation. c) **A7** (70:30) formulation. d) **A8** (60:40) formulation. e) **A9** (50:50) formulation. f) **L2** (75:25) formulation.

As a control and comparison, we carried out the same experiment using **L2** shown in **Figure 4.4f**. Among all formulations, **L2** demonstrated the highest stability. Regardless of the temperature whether ramping up or down, the diameter of **L2** liposomes were steadily maintained. Again, this was consistent with the calcein leakage assays for this formulation mixture. Our results, suggests that are our archaeosomes are not as stable as we had anticipated.

4.4 Blood Serum Assay

Although our archaeosomes have not yet shown to significantly reduce membrane permeability, we focused our efforts to test the stabilities of our materials in biological environments. **L5** and **A7** liposomes were incubated in various blood serum concentrations for 19 hours at 37ºC shown in **Figure 4.5**. At all blood serum percentages, **L5** showed higher fluorescence within 2 hours compared to **A7**. With 20% blood serum, only L5 showed less fluorescence compared to all other percentages, however, we observe high fluorescence within the first hour. Although we relatively observe higher fluorescence for **A7**, the rate of increase in fluorescence is much slower compared to **L5** liposomes. We see maximum fluorescence within 5 hours, whereas, L5 liposomes reach maximum fluorescence within 1 hour. At 0% we would expect A5 to show less fluorescence and higher fluorescence at 100% blood serum. We are unable to explain this outcome, however, the proteins in blood serum may be binding to the archaeosome coagulating all together. Through this initial study, we observe greater stability for archaeosomes compared to DPPC-based liposomes.

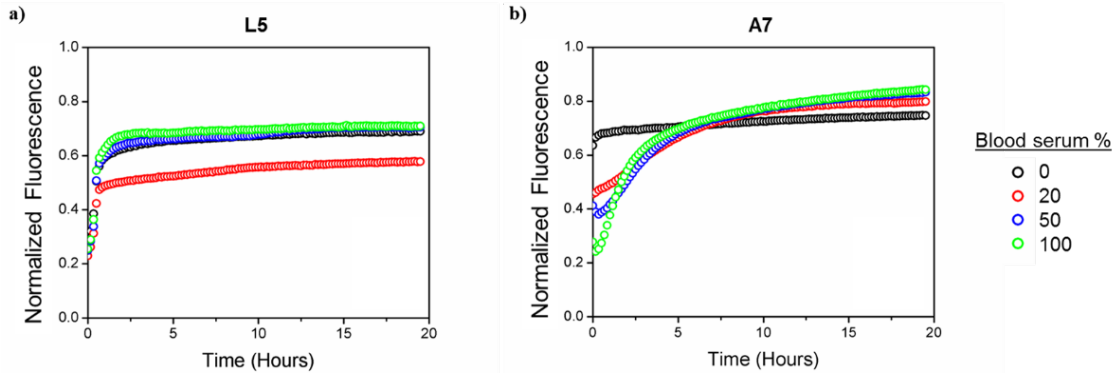

Figure 4.5: Liposome stability in blood serum. a) **L5** calcein release profile. b) **A7** calcein release profile.

4.5 Conclusions

In this chapter, we have discussed the morphological stability and membrane permeability of **A5-9**. Despite our aim to generate stable systems from archaeal-inspired materials, we have shown that our archaeosomes do not show significant advantages as we had desired. Comparing our archaeosomes to conventional liposomes, we show that our materials are not as stable to DPPC-based liposomes. Without the presence of cholesterol, **A2** showed increase fluorescence compared to **L5** suggesting that cholesterol was necessary to form more stable archaeosomes. Through release studies, we observed **A7** to have an optimum lipid/cholesterol formulation. This was also confirmed by our DLS heat ramp and cooling experiments showing that the diameter is not affected by changes in temperature. Although DPPC-based liposomes show greater stabilities, we observe greater archaeosome stability in blood serum. Overall, despite showing significant archaeosome stabilities, we believe that our synthesis allows for the facile modulation for obtaining new lipids that may provided enhanced properties.

4.6 Experimental

4.6.1 General Methods/Instrument Details

All regents were purchased from commercial sources. Calcein was purchased from Avanti Polar Lipids, Inc. Water was purified by MiliQ water filter (Irvine, CA) and autoclaved prior to use. Sonication was achieved using a Branson ultrasonic ¾ Benchtop Cleaner bath or probe sonicator. The hydrodynamic radius was determined by DLS on a DynaStarPro Nanostar provided by Wyatt Technologies. Electron electron microscopy images were obtained by Spherea for dry stain TEM and Polara for cryo-em.

4.6.2 General Purification Procedures

To separate free calcein from calcein-loaded liposomes, the liposome mixtures were purified by size-exclusion chromatography using Sephadex G-100. 200 μL of liposome solution was loaded onto the column and the fractions were collected. The calcein-encapsulated liposomes were visible by a dark orange band running off through the column, while free calcein fluoresced to a bright yellow-green color. The fractions were then analyzed by DLS to confirm the presence of calcein- loaded liposomes.

4.6.3 General Calcein Release Study Procedures

After purification, the percent of calcein release was analyzed by a 96-well plate reader. Liposome samples (5μL) were placed in wells containing buffer (95μL) and incubated over time at various temperatures. To determine maximum percentage of release, liposome samples (5μL) were placed in buffer (95μL) containing 2.5% Triton x-100, a surfactant used to completely lyse the membranes. The release of calcein was monitored by absorbance and fluorescence at the excitation and emission wavelengths of 495/515 nm, respectively.

4.7 References

1. Gliozzi, A., Relini, A. & Chong, P. L. G. Structure and permeability properties of biomimetic membranes of bolaform archaeal tetraether lipids. *J. Memb. Sci.* **206,** 131–147 (2002).

2. Réthoré, G., Montier, T., Le Gall, T., Delépine, P., Cammas-Marion, S., Lemiègre, L., Lehn, P. & Benvegnu, T. Archaeosomes based on synthetic tetraether-like lipids as novel versatile gene delivery systems. *Chem. Commun. (Camb).* 2054–6 (2007). doi:10.1039/b618568a

3. Liposome, M., Faneca, H. & Lima, M. C. P. De. Liposomes. **606,** 209–232 (2010).

4. Tenchov, B., Vescio, E. M., Sprott, G. D., Zeidel, M. L. & Mathai, J. C. Salt tolerance of archaeal extremely halophilic lipid membranes. *J. Biol. Chem.* **281,** 10016–10023 (2006).

5. Koyanagi, T., Leriche, G., Onofrei, D., Holland, G. P., Mayer, M. & Yang, J.

Cyclohexane Rings Reduce Membrane Permeability to Small Ions in Archaea-Inspired Tetraether Lipids. *Angew. Chemie - Int. Ed.* **55,** 1890–1893 (2016).

6. Le Gall, T., Barbeau, J., Barrier, S., Berchel, M., Lemi??gre, L., Jefti??, J., Meriadec, C., Artzner, F., Gill, D. R., Hyde, S. C., F??rec, C., Lehn, P., Jaffr??s, P. A., Benvegnu, T. & Montier, T. Effects of a novel archaeal tetraether-based colipid on the in vivo gene transfer activity of two cationic amphiphiles. *Mol. Pharm.* **11,** 2973–2988 (2014).

7. Jacquemet, A., Lemiègre, L., Lambert, O. & Benvegnu, T. How the stereochemistry of a central cyclopentyl ring influences the self-assembling properties of archaeal lipid analogues: Synthesis and cryoTEM observations. *J. Org. Chem.* **76,** 9738–9747 (2011).

8. Zavec, A. B. edina, Ota, A., Zupancic, T., Komel, R., Ulrih, N. P. & Liovic, M. Archaeosomes can efficiently deliver different types of cargo into epithelial cells grown in vitro. *J. Biotechnol.* **192,** 130–135 (2014).

9. Febo-Ayala, W., Morera-Félix, S. L., Hrycyna, C. A. & Thompson, D. H. Functional reconstitution of the integral membrane enzyme, isoprenylcysteine carboxyl methyltransferase, in synthetic bolalipid membrane vesicles. *Biochemistry* **45,** 14683–14694 (2006).

10. Barbeau, J., Cammas-Marion, S., Auvray, P. & Benvegnu, T. Preparation and Characterization of Stealth Archaeosomes Based on a Synthetic PEGylated Archaeal Tetraether Lipid. *J. Drug Deliv.* **2011,** 1–11 (2011).

11. Chang, H. I. & Yeh, M. K. Clinical development of liposome-based drugs: Formulation, characterization, and therapeutic efficacy. *Int. J. Nanomedicine* **7,** 49–60 (2012).

Chapter 5 : Future Outlook

5.1 Activation of Archaeosomes

Towards our overarching goal to develop stable and robust materials, we successfully synthesized archaeal-type lipids **ATL1-5**. Utilizing click chemistry, we developed a facile and modular approach for the synthesis of a myriad of archaeal-type lipids using a single synthetic scheme. Our design proved to be highly efficient in 11 synthetic steps our less compared to other reported synthetic routes. Here we showed that we can incorporate chemical features of archaeal lipids to generate archaeal-type lipids.

In regards to our future work, we aspire to add new archaeal-type lipids to our library that have function. Incorporating dye as the linker would provide a strategy for the labeling and fluorescence of liposomes. This would serve as a great tool for the visualization of archaeosomes within macrophage uptake assays as well as *in vivo* targeting. Furthermore, we plan to generate stimuli-responsive archaeosomes that release its cargo upon physical or chemical activation. Towards this idea, we seek to synthesize an archaeal-type lipid with an azobenzene moiety in the hydrophobic core that would isomerize from *trans* to *cis* upon ultra-violet activation. Upon activation, the membrane would exhibit high permeability in a controlled fashion. Incorporating functionality within the linker of the archaeosome membrane would then provide greater utility as a lipid material.

5.2 Polar Head Group Modification

Towards our future work of generating new archaeal-type lipids, we plan to install different hydrophilic head groups. Within our lipid library, we specifically incorporated phosphatidylcholine as the head groups for our archaeal-type lipids as they are known to

stabilize liposomes, however we plan to append biomolecules as the hydrophilic head groups. To this regard, we plan to attach peptides for targeting and activation. Using peptides specific for matrix metalloproteinases (MMPs), we can generate archaeosomes that are respond to MMP activity. Incorporating cleavable peptide sequences, we envision that we can develop materials that aggregate at cancerous tissues upon enzymatic cleavage. Furthermore, to extend the functionality of biomolecules, we also aspire to conjugate single stranded DNA as head groups. Incorporating DNA as the head groups would potentially increase the cellular uptake of archaeosomes within macrophages. Additionally, single stranded DNA could serve as a transfection agent or potentially an inhibitor to knockdown the expression of a gene. Given the installation of the biomolecules as hydrophilic head groups, we can design bio-responsive and stimuli-responsive archaeosomes may potentially serve as targeting agents.

5.3 Modify Design Strategy

From the synthesis of archaeal-type lipids, we proved that archaeal-type lipids are capable of assembling into discrete and well-defined liposomes. Specifically, we showed that archaeosomes composed of lipid **ATL1** form liposomes with or without the presence of additives such as cholesterol or DSPE-PEG. Although we have extensively characterize our archaeosome formulations, we observe leakage properties comparable to DPPC-based liposomes. The high calcein permeability of our archaeome formulations proved to be less stable and robust compared to our DPPC controls. We hypothesized that the leakage may be attributed to the heteroatoms in the triazole rings. Despite our intention for using this facile strategy, the triazole rings may be the cause of such high permeability. To address this issue, our future work aims to employ different conjugation methods such as olefin metathesis or Heck coupling to avoid the triazole formation. By modifying our chemistry, we can preserve our design strategy to develop more stable archaosomes.

5.4 Enzyme Stability

As a potential drug delivery system, we aimed to develop liposomes stable under biological environments. In the blood serum assay, we demonstrated that archaeosomes exhibit a slower release profile compared to the DPPC liposome control. We plan to continue this study and extend this towards lipase treatment. Our future work aims to demonstrate that archaosomes are resistant to phospholipases and various non-specific enzymes. This aims to further support that archaosomes are not easily degraded by enzymes.

5.5 Conclusions

In this thesis, we describe the facile and modular synthesis of archaeal-type lipids and their assembly into well-defined archaeosomes. Although these materials are not as stable as we had intended, we have developed a process to efficiently generate a library of lipids. Our future work is to continue synthesizing new archaeal-type lipids that prove to be thermostable, chemically stable, and biologically stable. Towards this goal, we intend to tune our strategy to achieve stable and robust archaeosomes that reduce membrane permeability.